Modelling of the dynamics of atomic clusters in intense laser fields

By

GAURAV MISHRA

PHYS01201004003

Bhabha Atomic Research Centre, Mumbai

A thesis submitted to the
Board of Studies in Physical Sciences

In partial fulfilment of requirements

for the Degree of

DOCTOR OF PHILOSOPHY

of

HOMI BHABHA NATIONAL INSTITUTE

November, 2014

HOMI BHABHA NATIONAL INSTITUTE[1]

Recommendation of the Viva Voce Committee

As members of the Viva Voce Committee, we certify that we have read the dissertation prepared by Gaurav Mishra entitled Modelling of the dynamics of atomic clusters in intense laser fields and recommend that it may be accepted as fulfilling the thesis requirement for the award of Degree of Doctor of Philosophy.

Chairman-		Date
Guide/Convener-		Date
Co-guide/Convener-	(if any)	Date
Member-1		Date
Member-2		Date
Member-3		Date

Final approval and acceptance of this thesis is contingent upon the candidates submission of the final copies of the thesis to HBNI.

I/We hereby certify that I/we have read this thesis prepared under my/our direction and recommend that it may be accepted as fulfilling the thesis requirement.

Date:

Place:

Co-guide(if applicable) Guide

[1]This page is to be included only for final submission after successful completion of viva voce.

STATEMENT BY THE AUTHOR

This dissertation has been submitted in partial fulfilment of requirements for an advanced degree at Homi Bhabha National Institute (HBNI) and is deposited in the Library to be made available to borrowers under rules of the HBNI.

Brief quotations from this dissertation are allowable without special permission, provided that accurate acknowledgement of source is made. Requests for permission for extended quotation from or reproduction of this manuscript in whole or in part may be granted by the Competent Authority of HBNI when in his or her judgement the proposed use of the material is in the interests of scholarship. In all other instances, however, permission must be obtained from the author.

Gaurav Mishra

DECLARATION

I, hereby declare that the investigation presented in the thesis has been carried out by me. The work is original and has not been submitted earlier as a whole or in part for a degree / diploma at this or any other Institution / University.

Gaurav Mishra

List of publications arising from the thesis

Journal

1. "Molecular dynamic simulation for laser−cluster interaction", Amol R Holkundkar, Gaurav Mishra, & N K Gupta, **2011**, Phys. Plasmas, *18*, 053102-1-7.

2. "Effect of laser pulse time profile on its absorption by Argon clusters", Gaurav Mishra, A. R. Holkundkar & N K Gupta, **2011**, Laser Part. Beams, *29*, 305-313.

3. "Molecular dynamic studies on anisotropy of atomic cluster explosions driven by few-cycle intense lasers", Gaurav Mishra & N K Gupta, **2011**, Europhys. Lett., *96*, 63001-p1-p6.

4. "Molecular dynamic studies on anisotropic explosion of laser irradiated Xe cluster", Gaurav Mishra & N K Gupta, **2012**, Phys. Plasmas, *19*, 093107-1-5.

5. "Carrierenvelope phase effects on ionization dynamics of atomic clusters irradiated by intense laser pulses of a few cycles", Gaurav Mishra & N K Gupta, **2013**, J. Phys. B: At. Mol. Opt. Phys., *46*, 125602-1-6.

6. "Laser induced neutron production by explosion of the deuterium clusters", A. R. Holkundkar, Gaurav Mishra, & N K Gupta, **2014**, Phys. Plasmas, *21*, 013101-1-6.

Conferences

1. "Anisotropic ion emission in coulomb explosion of argon cluster driven by few cycles laser pulse", Gaurav Mishra, A. R. Holkundkar & N K Gupta, **2010**, DAE-BRNS National Laser Symposium (NLS-19), RRCAT Indore, (1 Dec – 4 Dec).

2. "Effect of Pulse Duration on Coulomb Explosion of Laser Irradiated Ar Clusters", Gaurav Mishra & N K Gupta, **2010**, 3^{rd} International Symposium on material chemistry (ISMC-2010), BARC Mumbai, (7 Dec – 11 Dec).

3. "Effect of self generated electric field on spatial anisotropy of ions ejected from laser irradiated Xe clusters", Gaurav Mishra & N K Gupta, **2013**, DAE-BRNS National Laser Symposium (NLS-21), BARC Mumbai, (6 Feb – 9 Feb).

4. "Modeling of Intense Ultra Short Laser Interaction with Atomic Clusters", N K Gupta & Gaurav Mishra, **2013**, IFSA2103 Nara, Japan, (8 Sep – 13 Sep).

5. ”Investigation of neutron generation in laser-cluster interaction”, Gaurav Mishra, A. R. Holkundkar & N K Gupta, **2014**, DAE-BRNS National Laser Symposium-22 (NLS-22), Manipal University, Manipal, (8 Jan – 11 Jan).

Gaurav Mishra

To my parents

Ramakant Mishra and *Pushp Lata Mishra*;

without their blessings, hard work and support

it was never possible to reach at this stage of my life

ACKNOWLEDGEMENTS

I am deeply indebted and grateful to my guide Dr. N. K. Gupta for his whole-hearted support, encouragement and guidance. He persuaded me to register for Ph.D. and inspired me continuously to finish it in proper time. He provided me enough freedom to explore the field but kept an eye so that I didn't drift much away from the subject.
I am also very grateful to Dr. L. J. Dhareshwar (ex Head, Laser & Neutron Physics Division, BARC) to allow me to register for Ph. D. I am also extremely thankful to my friend and ex-colleague Dr. Amol R. Holkundkar (BITS, Pilani) for fruitful discussions on various research problems. I explored a lot about linux and other open source softwares in his company.
I acknowledge to Dr. G. M. Petrov (NRL, Plasma Physics Division, Washington, DC) for the various inputs at the time of writing the MD code.
I am extremely grateful to Prof D. Mathur (TIFR) for suggesting the problems of anisotropy and carrier-envelope (CE) phase for my research work.
I sincerely acknowledge the support and guidance from all doctoral committee members (Dr. L. 1. Dhareshwar, Dr. N. K. Gupta, Dr. B. N. Jagtap & Dr. M. Krishnamurthy).
Special thanks to Dr. D. Biswas and Dr. Raghwendra Kumar to help me to sort out various problems related with computers. I am also thankful to Dr. Aditi Ray, Dr. Kondayya Gundara and Dr. Karabi Ghosh for various discussion on both professional and personal fronts. I am also grateful to Dr. S. Degwekar for his peaceful company during the lunch and tea time.
My deepest thanks to my friends Mr. K. C. Gupta, Mr. Anek Kumar and Mr. Arun Singh, their suggestions and words of appreciation have always been extremely encouraging.
Finally, I sincerely acknowledge the support of my family here in Mumbai: my wife, my brother and my daughter for their invaluable support.

Contents

SYNOPSIS

1. Introduction: The development of chirped pulse amplification (CPA)[1] and Kerr-lens mode-locking has enabled researchers all over the world to generate routinely high intensity ($> 10^{14} W/cm^2$) and short ($< 1ps$) laser pulses. This invention has revived the field of laser matter interaction. In the last decade, a new kind of material, namely atomic/molecular clusters, has drawn a world wide attention to be used as a target for the generation of dense plasma by irradiation of laser light. These clusters are produced by the isentropic expansion of a high pressure gas through a nozzle[2]. After passing through the nozzle, the gas becomes supersaturated due to the drop in the temperature and clusters are formed as a result of nucleation. These targets, intermediate to to gases and solids, contain both the advantages of solids and gaseous targets. For instance, energy absorption efficiency of laser light by clusters is comparable to solid target plasmas[3] yet the particle emission from cluster is debris free much like as in gases. The high local density of atoms ($n_l \sim 10^{22} atoms/cm^3$) inside a cluster, lack of thermal dissipation and collective effects (cluster sizes are much smaller than the wavelength of incident laser light) are responsible for enhanced energy absorption by clusters compared to the solids. The absorbed energy is redistributed among MeV ions, KeV electrons and KeV X-rays. While considering the cluster charging dynamics, the concept of inner and outer ionization is very useful. Inner ionization refers to the removal of electron from parent atom yet confined in the cluster due to coulomb force of residual ions. On the other hand outer ionization refers to the removal of electrons form cluster itself as the these electron achieve sufficient energy to overcome the coulomb barrier of the cluster. The heating of the cluster plasma is mainly governed by the inner electrons as a outcome of inverse bremsstrahlung and collective resonance effects. The cluster plasma expands depending on the population of inner electron. If the space charge is strong enough it retains most of electrons inside the cluster, then cluster plasma expands due to pressure of electron gas. This mode of cluster expansion is known as hydrodynamic expansion. On the other hand, if most of the electrons leave the cluster immediately then cluster explodes due to the repulsion among remaining positive charges of ions in the cluster. This is called Coulomb explosion. Laser-driven particle acceleration, coherent and incoherent X-ray generation, nuclear fusion in deuterium clusters, production of efficient

plasma wave-guides and high-order harmonic generation are few of the important application of laser-cluster interaction.

Theoretical modelling of the intense laser pulse interaction with rare-gas clusters is a challenging subject involving the non-linear, nonperturbative response of many ions and electrons. As noted above, the laser-cluster interaction proceeds through three sub-processes: *viz...* laser induced ionization of atoms, further absorption of laser energy, and expansion of cluster. In order to investigate these processes and explain the observed experimental results, several models have been put forward. Among them the earliest is the so-called nanoplasma model, which treats the cluster as a spherical plasma ball with assumption of uniform radial plasma density[4]. It may be noted that nanoplasma model and its further improved versions are essentially fluid models which can not provide experimental results beyond average values. To get more insight, various particle models like particle-mesh, in particular particle-in-cell (PIC), and particle-particle like molecular dynamics (MD) were developed. They are more appropriate as cluster is essentially a collection of particles rather a fluid. The limited number of particles in a cluster ($10^3 - -10^5$), combined with the numerous advantages of grid-less calculations gives preference to MD simulations for laser cluster interaction. In view of this, we have developed a three dimensional time dependent relativistic MD code and validated it against theoretical and experimental results. After a brief introduction of the rich field of laser-cluster interaction in chapter 1, we describe the details of MD model and its validation in chapter 2. Chapter 3 essentially deals with the energetics of the cluster nanoplasma under the influence of various experimental parameters like laser pulse duration and cluster density. Anisotropic ion emission from laser irradiated clusters is discussed in chapter 4. Effects of carrier-envelope phase on ionization dynamics of laser driven xenon clusters are studied in chapter 5. The problem of neutron generation from deuterium clusters is investigated in chapter 6. Finally the the thesis is concluded in chapter 7 along with future direction.

2. Molecular dynamic simulation model and its validation: We have developed a three dimensional time dependent relativistic molecular dynamic code to study the interaction dynamics of the intense laser with atomic clusters. For computation purposes, a three dimensional simulation box is considered. A single spherical cluster is assumed to be at the center

of the simulation box. The size of the simulation box is considered to be equal to the distance between two neighbouring clusters(R_{IC}). The number of atoms in a cluster is calculated as $N_{Atoms} = (R_0/R_W)^3$ where R_0 is initial radius of the cluster and R_W is the Wigner-Seitz radius of the cluster material. The initial arrangement of the atoms inside the cluster is done randomly. One of the main problems associated with MD simulations is the calculation of binary Coulomb forces among charged particles which becomes increasingly time consuming for cluster sizes $> 15\mathring{A}$. In order to avoid this problem, lumping of particles into pseudo macro-particles (N_{Macro}) is done such that each macro-particle consists of n ($n = N_{Atoms}/N_{Macro}$) identical particles with a charge qn and mass mn (q and m are the charge and mass of the individual particle) . The presence of neighbouring clusters is mimicked by applying periodic boundary condition at the face of simulation box. Our code also facilitates the option of open boundary condition (for very low cluster density) and mixed boundary conditions. As the dimensions of the simulation domain are small as compared to the laser wavelength, only the time variation in laser pulse intensity and electric field is taken into account. The amplitude of the laser pulse intensity and electric field will remain constant in simulation domain for a given time instant. We have used mainly Gaussian time profile of incident laser unless stated explicitly. The ionization of the cluster atoms is carried out by optical field and collisional ionization using MonteCarlo method. For the optical field ionization (OFI) we calculate the OFI rate ν_{ofi} as a function of laser field strength by using Ammosov-Delone-Krainov (ADK) tunnel ionization formula[5]. Once a sufficient number of electrons are accumulated in the system, they further create more electrons by inelastic collisions with other atoms and ions. The collisional ionization rate ν_{ci} is calculated from the best fitted data[6] on the ionization rates for the atomic species of the cluster with $Z < 28$. For atomic species with atomic number greater than 28, e.g. Xe in our results, Lotz formula is used for calculations of ν_{ci}[7]. All the particles are subjected to laser electromagnetic force plus the coulomb force of other particles. After the calculation of the force, each particle is advanced to its new position according to the relativistic equations of motion. The phase-space of all particles is stored after certain time steps, which is later post-processed in order to calculate the particle (electron + ion) energy distribution function.

The present MD code is validated against various published theoretical and experimental re-

sults. For example, we have studied the interaction of 125 fs, 800 nm laser pulse with peak intensity of $10^{16} W/cm^2$ with deuterium ($R_0 = 100\mathring{A}$), argon and xenon ($R_0 = 50\mathring{A}$) clusters. For all these studies, we have used periodic boundary condition with simulation box size (R_{IC}) of $20R_0$. As the atomic number of cluster material increases, the average degree of ionization also increases. It is found to be 12 and 8 from Xe and Ar clusters respectively which is close to the published results. Similar trend is observed for mean ion kinetic energies calculated for various species of cluster material. The effect of cluster material on cluster expansion is also studied. It has been found that expansion velocity is maximum for lightest materiel i.e. deuterium(D) and minimum for heaviest material *i.e.* xenon(Xe). It can be explained by the fact that expansion velocity of cluster depends upon the charge to mass ratio which decreases monotonically as the cluster material is changed from D to Xe. We have also calculated the the ion energy distribution function for all three cluster species. These results are in good agreement with the studies of *Petrov et al*[8]. The existing MD code is also validated against direct experimental results of laser-cluster interaction. For this, we have investigated the anisotropy of ion emission from laser irradiated clusters in longer pulse duration of 100 fs. Relatively large argon clusters Ar_{400000} were irradiated by laser of peak intensity in this experiment[9] and more energetic ions were detected along laser polarization direction than perpendicular to it. Our simulation results not only predict the ion energies observed in the experiment of ~ 200 KeV but also shows asymmetry along the laser polarization direction.

3. Energetics of cluster nanoplasma : Effect of laser pulse duration and cluster density: Possibly, the huge attention devoted to the field of laser-cluster interaction, is due to the unique nature of the energetics of the cluster nanoplasma, created after the irradiation by short laser pulses. We investigate the effects of various experimental parameters (laser pulse duration and cluster density) on the energetics of the cluster nanoplasma. Various theoretical models are proposed to explain the experimentally observed strong laser energy absorption (90%)[3] by clusters. *Dimire et al*[4], in the framework of nanoplasma model, suggested linear resonance to be responsible for high energy absorption that occurs during the expansion of the cluster after laser irradiation. Assuming cluster to be a dielectric sphere in the presence of static electric field of $\mathcal{E}_0$, the electric field inside the cluster is given as $\mathcal{E} = 3\mathcal{E}/|\epsilon + 2|$. The dielectric constant

of the cluster plasma is calculated as $\epsilon = 1 - \left(\omega_p^2/\omega\left(\omega + i\nu\right)\right)$, where $\omega_p = \sqrt{(4\pi e^2 n_e/m_e)}$ is the plasma frequency and ν is the electron-ion collision frequency. During the time of cluster expansion, a resonance occurs at the electron density of $n_e = 3n_c$ which is characterized by a minimum in $|\epsilon + 2|$ leading to enhancement of electric field and energy absorption inside the cluster. It is important to note that nanoplasma model assumes spatially uniform electron density during the time of expansion. Literature also supports the idea of non-linear resonance where the ions and electrons separately as charged spheres, oscillate around their common center of mass under the action of laser light. Energy is absorbed resonantly when the normalized effective oscillation frequency becomes unity. There are, however, simulation results that contradict this perception and completely reject the idea of resonance absorption. The above discussion reflects that the reason responsible to the high energy absorption inside the cluster is still not clearly understood.

We have used MD simulations to show the existence of linear resonance Assuming linear resonance to be responsible for enhanced energy absorption in cluster, energy absorbed by the cluster will be a function of laser pulse duration due to the difference between peak of the laser pulse and timing of resonance condition ($n_e = 3n_c$). Our simulation parameters are Ar cluster of radius ($R_0 = 30\mathring{A}$), a laser pulse of intensity $8 \times 10^{16} W/cm^2$ with FWHM pulse duration varying from 10 fs to 120 fs. Both mean kinetic energy of ions and energy absorbed by the cluster have shown an optimum value at a pulse duration of 25 fs. For this optimum pulse duration, both peak of laser pulse and resonance condition, are in closest vicinity to each other. Moreover, the presence of optimum pulse duration is diminished when the temporal profile of incident laser pulse is changed from Gaussian to second order super-Gaussian (nearly flat top). Thus, we conclude that the presence of an optimum pulse duration is a clear indication of existence of linear resonance during the cluster expansion.

Further, we also observe in our MD results that the cluster density plays an important role to affect the energetics of cluster nanoplasma. The effect of varying cluster density in the simulation results can be mapped by changing the inter-cluster distance which is same as the size of the simulation box used in the simulations. We find that just by increasing the size of the cluster, it is not possible to increase the the mean kinetic energy of ions after explosion. In

fact, the shielding of the ions due to electrons of neighbouring cluster is more effective when the smaller value of inter-cluster distance is used for larger sized clusters. Further, we also compare our MD results of distribution of various ionic species with the earlier experimental results[10] which are in good agreement for appropriately chosen inter-cluster distance consistent with the experiments.

4. Anisotropic ion emission from laser irradiated clusters : Breakdown of spherical isotropy in few-cycles pulse duration limit: As mentioned previously, the heating of the cluster and its subsequent evolution can be explained by two models namely Coulomb explosion and hydrodynamic expansion depending upon the number of inner electrons present inside the cluster. Both of these extreme cases lead to isotropic emission of ions from the cluster. When the laser irradiated clusters consist of intermediate population of inner electrons, ion emission is observed to be anisotropic due to the combined action of laser and radial field inside the cluster. This anisotropy depends upon the direction of laser polarization: more energetic ions are emitted along the laser polarization direction (0^o) than the perpendicular direction (90^o) to it. This kind of anisotropy, termed as normal anisotropy, was observed in experiments with Ar[9] as well as Xe[11] clusters in long pulse duration limit. Recent experiments[12] with few cycle laser pulses have revealed that the nature of anisotropy reverses i.e. the ion yield is higher along perpendicular direction of laser polarization than parallel to it. The physical reason for this change of nature of anisotropy is not understood completely. In order to understand the physical processes responsible for it, we have performed detailed MD studies on this kind of anisotropy termed as atypical anisotropy on various sized Ar clusters ($16-58\mathring{A}$) driven by laser of intensities varying from $5 \times 10^{14} W/cm^2$ to $3 \times 10^{16} W/cm^2$. The FWHM laser pulse duration is varied from 5 to 100 fs. For a fixed cluster size of $58\mathring{A}$ and laser intensity of $4.5 \times 10^{15} W/cm^2$, we observe an optimum pulse duration of 10-20 fs for which the atypical anisotropy manifests itself prominently. For this optimum pulse duration, the well-developed electron cloud oscillates with the laser frequency and strictly follows the laser electric field. Consequently, inner electron charge gets smeared more along the the direction of the laser electric field rather than the perpendicular direction. This elongation of electron cloud effectively shields the ions more along 0^o compared to 90^o. This initial shielding effect finally results in the ion anisotropy of

the Coulomb explosion. At the time of explosion, more ions will emerge along the perpendicular direction of laser polarization rather the parallel direction due to this shielding. For many-cycle pulse durations *e.g.* 100 fs, simultaneous presence of higher-charge states and reduced directed motion of the electron cloud diminishes the observed atypical anisotropy. For the case of shortest pulse duration of 5 fs used in above simulations, this anisotropy again diminishes as the pulse duration is too small to create a sufficiently sized inner electron cloud. We have also investigated the effect of laser intensity ($5 \times 10^{14} W/cm^2 - -3 \times 10^{16} W/cm^2$) on the optimum pulse duration of 10 fs achieved in the above simulation results and found an optimum value of intensity of $4.5 \times 10^{15} W/cm^2$. Further we have varied the size of cluster from 16 to $58 \mathring{A}$ for the optimized values of pulse intensity and pulse duration. As the size of the cluster is increased , the atypical anisotropy increases.

5. Carrier envelope phase effects in the regime of few cycles laser pulses: With the rapid development of of femtosecond laser technology in the last decade, it has become routinely possible to generate intense laser pulses of few cycles[13]. For these ultra short pulses, the initial phase(phi) of the carrier wave with respect to the envelope, so called carrier-envelope (CE) phase, is an important parameter to completely describe the electric field ($\mathcal{E}(t) = \mathcal{E}_0(t)\cos(\omega t + \phi)$)[14]. For such ultra-short pulses with stabilized CE phases, the strong dependence of the probability of tunnelling on the instantaneous electric field dictates the release time of the electron. For case of isolated atoms, the tunnel-ionized electron follows the laser field and may return to the parent ion. In the vicinity of the parent ion, this field-liberated electron can lead to high harmonic generation (HHG) by recombination, above-threshold ionization (ATI) by elastic scattering or non-sequential double ionization (NSDI) by inelastic scattering with it. All these processes depend upon the temporal variation of incident laser electric field which in turn is a function of CE phase. We have tried to see the effect of CE phase in two different laser pulse duration regimes namely few cycles ($\tau_1 = 2T_0$ with T_0 as one laser cycle) and many cycles ($\tau_2 = 8T_0$) for cluster targets. In particular, Xe_{400} clusters are irradiated by incident laser pulse with electric field profile for two different values of CE phase ($\phi = 0$ and $\phi = \pi/2$) at peak intensity of $1.0 \times 10^{16} W/cm^2$. For these studies, we have used a conventional model of an n-cycle laser pulse, the sin^2 pulse $\mathcal{E}(t) = \mathcal{E}_0 sin^2(\omega t/2n) cos(\omega t + \phi);\ \ 0 < t < nT$, for tem-

poral variation of a laser electric field at frequency ω and time period T. To accommodate the effect of the CE phase (ϕ), the amplitude of the electric field is replaced by the absolute value of the time-dependent electric field ($|\mathcal{E}(t)|$) in the conventional cycle averaged ADK rate[5] for all calculations performed in this study, following the work of *Bauer*[15]. It is also noteworthy that the collisional ionization implemented in our code automatically accounts for collisions with parent atoms as well as with other atoms due to the fact that we strictly follow the particle trajectories in our MD simulation model. When cycle averaged ionization rates are used, we do not observe any difference in the fractional ionization yield of various ionic species for the two values of CE phase when using few cycles laser pulse for irradiation. The situation does not change even if the pulse duration is changed from few cycles to many cycles. On the other hand, we observe a significant difference in ionic yields for $\tau_1 = 2T_0$ when modified ADK rates (electric field amplitude replaced by $|\mathcal{E}(t)|$) are used. This difference for the two values of CE phases is due to the different electric field variations. If we change the pulse duration of laser from few cycles to many cycles ($\tau_2 = 8T_0$), we no longer see the difference in ionization yield for the two values of CE phases. We further confirmed above findings by comparing the average degree of ionization (Z_{avg}) for $\phi = 0$ and $\phi = \pi/2$ which differs for $\tau_1 = 2T_0$ and remains same for $\tau_2 = 8T_0$. We have also studied the effect of phase dependent collisional ionization on the ionization dynamics of the cluster, in addition to the modified tunnelling ionization. The difference between Z_{avg} for $\phi = 0$ and $\phi = \pi/2$ reduces when the collisional ionization is artificially switched off for the case of $\tau_1 = 2T_0$. As expected we do not observe any difference for $\tau_2 = 8T_0$. Finally, it is concluded that both tunnel ionization and collisional ionization depend upon the CE phase of the incident laser pulse of few cycles (~ 2) pulse duration.

6. Neutron production from laser driven clusters: The possibility of laser driven deuterium or/and tritium cluster neutron source[16] prompted us to investigate theoretically this problem. In particular, we have studied the effect of laser intensity, cluster radius and inter-cluster distance on the neutron production by D-D or D-T reaction by using our MD code. For the calculation of neutron yield, a one dimensional beam energy deposition model is coupled with existing MD code in which high energy deuterium ions ejected from the cluster interact with

deuterium or tritium containing compound and slows down via various processes like ionization, excitation etc. The slowing down of energetic ions is characterized by stopping power which is calculated by SRIM[17](Stopping Range of Ions in Matter). The simulation parameters for these studies lie in two categories : medium sized cluster ($80 - 200\mathring{A}$) and very large clusters or nano-droplets ($20 - 200nm$). At fixed intensity of $10^{18}W/cm^2$ and pulse duration of 50 fs, we observed that the amount of laser energy absorbed increases as $\sim R^5$ whereas average kinetic energy of ions goes as $\sim R^2$ for medium sized clusters. It has been also found that the maximum kinetic energy of the ions is 5/3 times the average ion kinetic energy, which is also in excellent agreement with the theoretical prediction by Last and Jortner[18]. It is found that the neutron yield per joule is more for tritium target than deuterium target due to the increased fusion cross section of D-T reaction than D-D. The number of neutrons per unit joule of absorbed energy goes as $\sim R^3$ for for medium sized clusters ($R = 80 - 200\mathring{A}$). To study the effect of inter-cluster distance (R_{IC}) on neutron production, we have simulated the interaction dynamics of $100\mathring{A}$ deuterium cluster irradiated with 50 fs, 800 nm laser of peak intensity $10^{18}W/cm^2$ by varying R_{IC} in multiple of cluster radius. It is observed that average kinetic energy of ions increases as R_{IC}^3 while energy absorption by cluster remains nearly independent of R_{IC}. The neutron yield also increases as the value of R_{IC} increases due to the increased value of kinetic energy. The effect of laser intensity is also studied for these laser and cluster parameters by changing the value of intensity from 10^{15} to $10^{18}W/cm^2$. It is found that the laser intensity does not play very prominent role after some threshold value of $\sim 10^{16}W/cm^2$. For very moderate intensities also, the cluster is fully ionized and afterwards the dynamics is more or less independent of the laser intensity. We have also investigated the role of larger clusters or nano-droplets on neutron generation from deuterium clusters. We have observed a quadratic and linear dependence of absorbed energy per particle on cluster radius for medium size ($80 - 200\mathring{A}$) clusters and name-droplets ($20 - 200nm$), respectively. For medium size clusters, the cluster outer ionization is complete before the cluster explosion so we observe a quadratic dependence of absorbed energy on cluster radius. For nano-droplets, the outer ionization is never complete due to their large size and thus, coulomb explosion in the regime of incomplete outer ionization leads to the linear dependence of absorbed energy on cluster size.

6. Conclusions and future directions: Finally the thesis is summarized with main conclusions. The future direction of the present work in also discussed in this chapter. **References**

1. D. Strickland and G. Mourou, *Opt. Commun.*, **56**, 219, (1985).

2. 2. O. F. Hagena and W. Obert, *J. Chem. Phys.*, **56**, 1793, (1972).

3. T. Ditmire et al, *Phys. Rev. Lett.*, **78**, 3121, (1997).

4. T. Ditmire et al, *Phys. Rev. A*, **53**, 3379, (1996).

5. 5. M. V. Ammosov, N. B. Delone, and V. P. Krainov, *Sov. Phys. JETP*, **64**, 1191, (1986).

6. G. S. Voronov, *At. Data Nucl. Data Tables*, **65**,1, (1997).

7. W. Lotz, *Z. Phys.*, **216**, 241, (1968).

8. G. M. Petrov and J. Davis, *Phys. Plasmas*, **15**, 056705, (2008).

9. V. Kumarappan, M. Krishnamurthy, and D. Mathur, *Phys. Rev. Lett.*, **87**, 085005, (2001).

10. C. Prigent et al, *Phys. Rev. A* , **78**, 053201, (2008).

11. V. Kumarappan, M. Krishnamurthy and D. Mathur, *Phys. Rev. A* , **66**, 033203, (2002).

12. D. Mathur et al., *Phys. Rev. A* , **82**, 025201, (2010).

13. M. Nisoli et al, *Opt. Lett.*,**22**, 522, (1997).

14. T. Brabec and F. Krausz, *Rev. Mod. Phys*, **72**, 545, (2000).

15. D. Bauer, *Laser Part. Beams*, **21**, 489, (2003).

16. T. Ditmire et al., *Nature* **398**, 489, (1999).

17. J. F. Ziegler, M. D. Ziegler, and J. P. Biersack, *Nucl. Instrum. Methods B* **268**, 1818, (2010).

18. I. Last and J. Jortner, *J. Chem. Phys.*, **121**, 3030, (2004).

19. S. Ron, I. Last, and J. Jortner, *Phys. Plasmas* **19**, 112707, (2012).

List of Figures

CHAPTER 1

Introduction

This thesis presents the theoretical studies on the interaction of ultra-short, intense laser pulses with atomic clusters. We have made an attempt to improve the current understanding of the dynamics of laser irradiated clusters and also reported some new features found in this work. This chapter introduces some basic terminolgy used in the field of ultra-short, intense lasers and plasma physics. We have also made an overview on the subject of laser-cluster interaction in this chapter.

The technological advancements made in the last two decades have completely revolutionized the field of ultra-short, intense lasers [1, 2]. Due to this progress, it has become routinely possible to operate the table top lasers with terawatt peak powers. The availability of these terawatt laser systems accelerated the research in the fields of atomic physics (multi-photon ionization, above threshold ionization, harmonic generation etc.), high temperature-high density plasmas and inertial confinement fusion [3]. The underlying principles for the generation of ultra-short, intense laser pulses are described in section 1.1. A majority of the research community has put a significant amount of effort to use either a low density (10^{19} atoms/cm^3) in the form of individual atoms or a high density (10^{23} atoms/cm^3) in the form of solid as a target for these lasers. For gaseous targets, various atomic processes in the presence of these kind of laser fields and their outcome as a result of this interaction is discussed in section 1.2.4. The physics of laser-matter interaction completely changes when gas targets are replaced by solids. The emergence of plasma is realized as a result of this interaction. Basic terminology used in plasma physics along with various laser absorption processes in plasmas are discussed in section 1.3. We have also discussed the applications of laser produced solid plasmas in this section. Atomic clusters, intermediate to to gases and solids, contain both the advantages of solids and gaseous targets. The high

local density of atoms in clusters is solid like whereas the average atomic density is similar to that found in gaseous targets. Apart from that lack of thermal dissipation effects, emergence of collective behaviour are such properties which present the clusters as a very unique target of laser irradiation. Laser irradiated clusters show a huge number of promising applications. A detailed survey of laser-clusters interaction including various theoretical models, experimental findings and their applications are discussed in section 1.4. Rest of the outline of the thesis is presented in section 1.5.

1.1 Generation of ultra-short, intense laser pulses

Before describing the generation of ultra-short, intense laser pulses, we have to define the limits on the pulse duration and intensity of laser light to be counted in this category. Generally the label ultra-short applies to pulses with durations less than tens of picoseconds (often in the range of femtoseconds). The term "intense" is defined as the intensity of laser pulse approaching to the value of $10^{15} W/cm^2$. At this intensity level, the electric field ($10^9 V/cm$) of the laser pulses becomes comparable to coulomb field in hydrogen atom. The generation of ultra-short, intense laser pulses have become possible due to two very important discoveries namely kerr-lens mode locking (KLM)[4] and chirped pulse amplification (CPA)[5, 6] made in this field. Most of the ultra-short lasers employ titanium-doped aluminium oxide (Ti : Sapphire - Ti^{3+} : $Al_2\ O_3$) oscillator due to certain important features like excellent thermal conductivity, large gain bandwidth and wide tunable range[7].

1.1.1 Laser longitudinal modes and process of mode locking

Before describing the method of kerr lens mode locking, a brief introduction of longitudinal modes and process of mode locking in a laser cavity is required. Longitudinal modes are nothing but various standing wave patterns which develop in the laser cavity (a combination of mirrors with a gain medium in between) along the axial direction

of the laser at frequencies as given below

$$\nu = n\,(c/2\eta d) \tag{1.1}$$

In multi-mode regime of laser operation, the time distribution of output intensity necessarily depends upon the inter-phase relationship of various longitudinal modes. For example, if the initial phases are chosen randomly, the output intensity shows random fluctuation in time. On the other hand, if there exists a constant phase relationship among the all participating longitudinal modes, the output intensity will be a repetitive pulsed time profile due to the constructive interference of participating modes. This concept is back bone for mode-locking which is used to generate the shorter pulse duration. In mode locking, all longitudinal modes (locked with a constant phase relationship) are allowed to interfere each other to produce a train of evenly spaced light pulses. If (2n+1) longitudinal modes with equal amplitude E_0 exist in the laser cavity with the phase relationship $\phi_l - \phi_{l-1} = \phi$, then total electric field is given by

$$\begin{aligned} E(t) &= \sum_{-n}^{+n} E_0 \exp\{j(\omega_0 + l\Delta\omega)t + l\phi\} && (1.2)\\ &= A(t)\exp(j\omega_0 t) && (1.3) \end{aligned}$$

where ω_0 is the central frequency,$\Delta\omega$ is the frequency difference between two consecutive modes and $A(t)$ can be written as follows

$$A(t) = \sum_{-n}^{+n} E_0 \exp\{jl(\Delta\omega)t + l\phi\}. \tag{1.4}$$

Transforming the time such that $\Delta\omega t' = \Delta\omega t + \phi$, we get from the above equation following result for A(t)

$$\begin{aligned} A(t') &= \sum_{-n}^{+n} E_0 \exp\{jl\Delta\omega t'\}. && (1.5)\\ &= E_0 \frac{\sin\{(2n+1)\Delta\omega t'/2\}}{\sin(\Delta\omega t'/2)} && (1.6) \end{aligned}$$

By plotting the output intensity ($I(t) \propto A^2(t')/E_0^2$) against time, one can show that output from the laser will be a repetitive pulsed train. The pulse will appear at

$$\Delta\omega t'/2 = n\pi \quad \text{with n=0,1,2....}\pi \tag{1.7}$$

so the time difference between two consecutive pulse can be written as

$$t' = 2\pi/\Delta\omega = 1/\Delta\nu. \tag{1.8}$$

The full width at half maximum(FWHM) pulse duration is approximately equal to t'_p which comes at the next zero of $I(t')$ i.e.

$$(2n+1)\Delta\omega t'_p/2 = \pi \tag{1.9}$$

$$t'_p = 2\pi/(2n+1)\Delta\omega = 1/\Delta\nu_L = 1/\text{Total gain bandwidth} \tag{1.10}$$

It is important to see that gain medium with larger gain band leads to shorter pulse duration via mode-locking. This is the reason why Ti : Sapphire is most widely used oscillator for generation of short laser pulses.

In time domain, mode locking means selection of a noise pulse and allow it to amplify while suppressing other noise pulses such that the former one is getting amplified. This is equivalent to locking of longitudinal models in the frequency domain as described earlier.

There are mainly two methods to achieve mode-locking : active mode locking and passive mode locking. The former is the result of external modulation of cavity losses by external source like acoustic-optical modulator while the latter is achieved by insertion of a intensity dependent saturable absorber. We will only describe Kerr-lens mode locking which is used in the widely available laser system such as Ti : Sapphire laser.

1.1.2 Kerr Lens Mode Locking

The discovery of self-mode-locking[4] which produced 60 fs pulse from a Ti : Sapphire without a saturable absorber, completely revolutionized the field of ultra-short laser pulse generation. Initially it was termed as magic mode locking but sooner it was explained by the self focusing[2] of the laser beam due to Kerr non-linearity of the gain medium[8]. Consider the propagation of a spatial Gaussian profile beam in optical Kerr medium. Due to the optical kerr effect ($n = n_0 + n_2 I$), the refractive index is more along the axial direction of laser medium in the center of the beam compared to its value at the periphery. Consequently the beam is slower in the center than in the outer parts of the medium which leads to the self focusing of the beam towards to the center. It means that stronger intensity part of the Gaussian beam will be strongly focused than the lesser intensity part where the focusing will be negligible. Clearly, the central part of the beam will be subjected to less cavity losses than the outer part of the input beam which leads to the amplification of higher intensity portion of the pulse at the expense of the suppression of lower intensity portion of the pulse. This is nothing but the self-mode-locking of the modes in the time domain. One can enhance the self-locking process of the modes by putting a thin aperture ahead of the optical medium such that in passes the stronger intensity portion of the beam and blocks the lower intensity part of the beam. A slit can be placed inside the cavity to help the self-locking process since it increases the difference between the losses undergone by the weak intensities and those undergone by the intensity maxima. Till now we have only explained that how the pulsed regime is favoured over continuous regime in a mode locked laser. We have to also explain the pulse shortening achieved in this kind of mode locking technique. Actually, along with self focusing of laser pulse inside the optically active medium, there also exists non linear Kerr effect due to time dependent intensity profile (self phase modulation) of the laser beam which broadens the frequency spectrum of the pulse. This allows the pulse to be further shortened which could have not been obtained by the normal mode locked lasers.

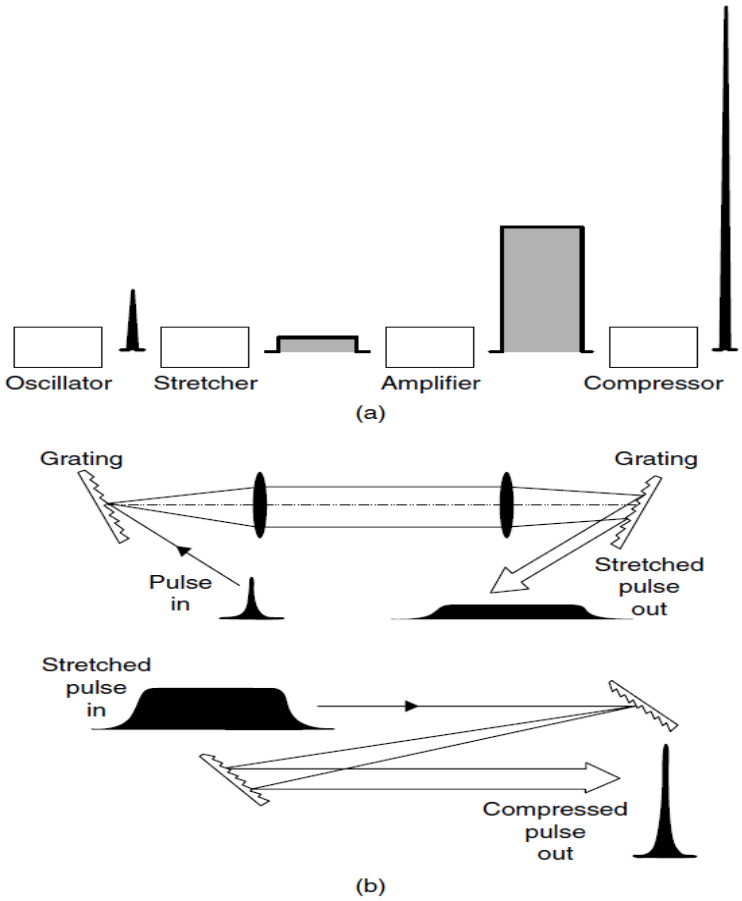

Figure 1.1: *Schematic of chirped pulse amplification (CPA) method (a), matched stretcher and compressor of the CPA technique (b) (taken from Ref. [9]).*

1.1.3 Chirped pulse amplification

Many interesting applications of ultra-short pulses require high peak powers which are not available from the conventional mode-locked oscillator. Historically femtosecond pulses were amplified dye cells but it was only possible to get millijoule energy of pulse due to the lower saturation fluence. With the advent of novel solid state gain medium in the 1980, it became possible to extract more energy due to high saturation fluence few joule/cm^2. However, amplification of femtosecond pulses lead to the beam distortions and optical damage at higher intensities due to intensity dependent non linear effects like self focusing and self phase modulation long before the level of saturation fluence is reached.

In 1985, Strickland and Mourou[5, 6] discovered a new technique called "chirped

pulse amplification" for amplification of femtosecnd pulses. The triumph of this technique was that one can reach upto very high intensities without inducing significant self focusing and self phase modulation which could otherwise lead to catastrophic optical damage. Nearly all high peak power lasers system with ultra-short pulse duration employ the technique of CPA in combination with the technique of optical compression. A schematic of this technique is presented in Fig. 1.1. In CPA[10], first a mode-locked laser pulse is generated with energies of $10^{-9}J$ and pulse duration in the range of $10^{-12} - 10^{-14}$ fs. These ultra-short pulses are passed through a stretcher (optical fibre or diffraction grating arrangement) to stretch the pulse to typically $100ps$ so that their power is reduced by nearly three orders of magnitude. Now the energy content of these stretched pulses can be safely increased upto six to nine orders of magnitude by passing through one or more stages of laser amplifiers. Once the sufficient amplification is achieved by maximum possible extraction of energy from the laser amplifiers, these pulses are further re-compressed back to femtosecond duration by a use of optical compressor (another pair of diffraction grating arrangement). The output pulse after the compression is a very short pulse with high peak powers. When these high power, ultra-short pulses are focussed onto a small area, intensities of the order of atomic unit of intensity ($10^{16}W/cm^2$) are readily achieved.

1.1.4 Generation of intense, few cycles laser pulses

Till now we have seen the working principles of generation of intense laser light with femtoseconds pulse duration. With the advancements made in the field of ultra-short laser systems, it has become possible to generate the intense light pulses with pulse durations consisting only a few optical cycles where one laser period is defined as $T = 2\pi/\omega$[11]. The generation of few cycles laser light pulses works on the two principles : Self-phase modulation creates extra frequencies in the original pulse through a Kerr medium and optical compression by group velocity dispersion squeezes that extra bandwidth to narrower pulse width. The interplay between SPM and GVD is the basis of all pulse compression techniques till today. To understand the process of SPM, we consider the propagation of light pulse with Gaussian time profile ($I(t) = \exp(-\Gamma t^2)$

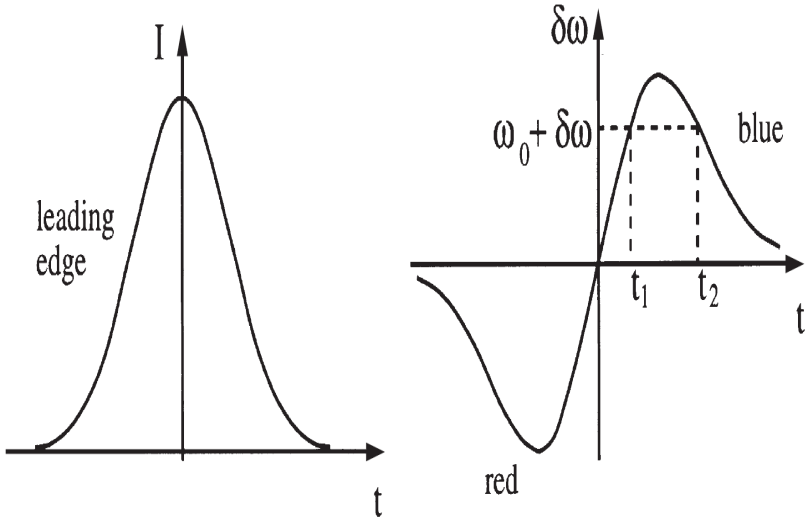

Figure 1.2: ***Left*** *Temporal variation of a Gaussian light pulse;* ***Right*** *new frequencies as a result of SPM (figure taken from Ref. [2]).*

through a Kerr medium. The non-linear index of refraction can be expressed as

$$n = n_0 + \frac{1}{2} n_2 I(t), \tag{1.11}$$

For simplicity, if only plane electromagnetic wave is considered to be propagating in the nonlinear medium

$$E(t,x) = E_0 exp\{j(\omega_0 t - kx)\}, \quad \text{with k=} \frac{\omega_0}{c} n(t) \tag{1.12}$$

Now the time dependent frequency can be defined as

$$\omega(t) = \frac{\partial(\omega_0 t - kx)}{\partial t} = \omega_0 - \frac{\omega_0}{c} \frac{\partial n(t)}{\partial t} x \tag{1.13}$$

Above relation suggests that new low frequencies are generated in the leading edge of the pulse ($\partial I(t)/\partial t = +ive$) and high frequencies are produced in the trailing part of the pulse ($\partial I(t)/\partial t = -ive$). SPM offers a way to further shortening of the pulse by introducing a spectral broadening of the pulse. Further compression of the pulse is achieved by passing through either a fibre with anomalous dispersion or a dispersive element like combination of diffraction gratings. The mechanism lies in the fact the

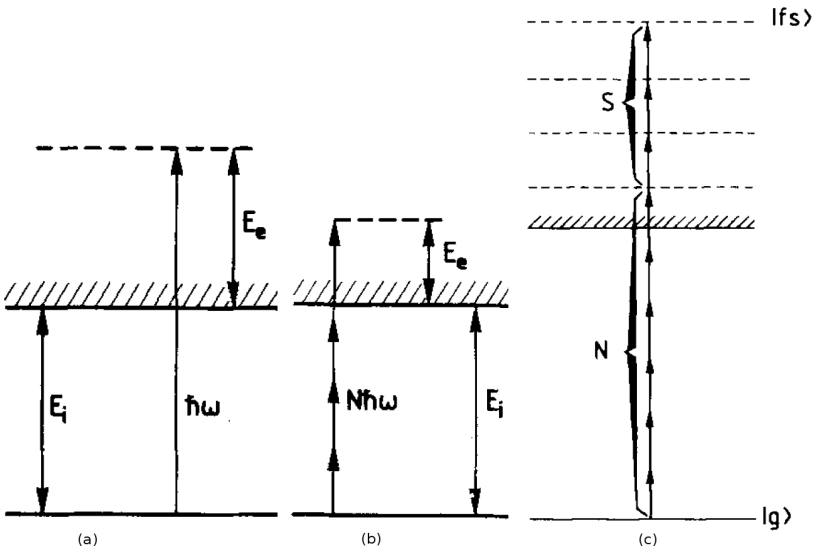

Figure 1.3: *(a)Photo ionization (b)Multi-photon ionization (c)Above threshold ionization (figure taken from Ref. [14])*

redder part of the pulse becomes slower and bluer part of the pulse becomes faster due to negative group velocity dispersion (For $\omega_2 > \omega_1$, $\Delta\tau = -ive$) experienced in the medium. A technique based on using hollow fibre filled with noble gases for SPM and a pair of quartz prism for negative GVD is used to obtain the pulse duration as close to 10fs[12]. Another technique, using the self guiding or filamentation of intense laser pulse propagation in a transparent noble gas, demonstrated 5.7 fs laser pulse with an excellent spatial beam profile[13].

1.2 Behaviour of atoms under strong light fields : transition from weak to strong light intensity regime

1.2.1 Photoelectric effect

The way light couples to the matter is a strong function of laser intensity. At low light intensity, atom can be photo-ionized (Fig. 1.3(a)) by absorbing a single photon from electromagnetic radiation provided the energy of the photon is greater than or equal to the ionization energy of the atom (Einstein's law of photo-electric effect)[15]. As evident that photoelectric effect is a consequence of the idea that the light exchanged energy with the matter in discrete quantities called 'photons'. The response of the

atoms in this weak intensity regime is a linear function of the intensity.

1.2.2 Multi-photon ionization : non-linear photoelectric effect

When the intensity of light is increased further to interact with the atoms, multi-photon ionization (MPI) of atoms start playing significant role. MPI, a further generalisation of photoelectric effect, is a consequence of simultaneous absorption of more than one photons (Fig. 1.3(b)). MPI was theoretically studied long ago in thirties[16] but its experimental demonstration[17, 18] became only possible with the invention of intense source of the light such as laser. MPI is a non-linear interaction as it fulfils the condition, $\hbar\omega < I_p$, where $\hbar\omega$ is the energy of single photon and I_p is the ionization potential of the electron in the atom. MPI is the demonstration of non-linear character of Maxwell's equation *i.e.* dependence of dielectric constant (and magnetic permeability) on the electric field strength which is observable at sufficiently high intensities. The non-linear response of matter in the field of electric field can be described as

$$P = \chi\colon E + \chi\colon EE + \chi\colon EEE + ... \tag{1.14}$$

where the first term is linear susceptibility, second term, the lowest order non-linear susceptibility and so on. For instance, the first demonstration of MPI[17] (I_p=12.13 eV and $\hbar\omega$=1.78 ev) can be explained as a effect generated by the polarization at frequency ω created by the fifth-order non-linear susceptibility. This interpretation is analogous to that fact the ionization is outcome of absorption of six photons[14]. Typically intensities of $10^{10}W/cm^2$ are the minimum requirement for the observation of MPI in atoms. These intensity values are still much lower than the atomic value of intensity ($I_{atm} = 3 \times 10^{16}W/cm^2$) that means that perturbative approaches are adequate to study the MPI at these intensities. By using lowest order (non-vanishing) perturbation theory (LOPT), the n-photon ionization rates are given by[19]

$$\Gamma_n = \sigma_n I^n \tag{1.15}$$

where n is the minimum number of photon needed for the ionization,σ_n is the generalized cross section and I is the intensity of the incident light. The energy conservation law reads for this non-linear photoelectric effect/MPI as

$$E_e = n\hbar\omega - I_p, \tag{1.16}$$

where E_e is energy of the ejected electron. Note that the above equation is the generalisation of Einstein's law and kinetic energy of electron is less than the energy of single photon. Consequently, if we plot the electron energy distribution function, we observe a single photon peak at energy $n\hbar\omega - I_p$. This picture prevails at weak laser intensity.

1.2.3 Above threshold ionization

At sufficiently high intensities ($I > 10^{11}W/cm^2$), the ejected electron can absorb photons in excess of the minimum number required for the ionization to occur (Fig. 1.3(c)). This process is called "Above threshold ionization (ATI)". This phenomenon was observed in an experiment on 6-photon ionization of xenon atom performed at $10^{12}W/cm^2$, which showed, in addition to the expected electron peak, a second one separated from the first by a photon energy[20]. The field induced distorted atomic potential is responsible for the absorption of more photons than required for ionization. Despite being the difficulties with LOPT, the generalisation of perturbation theory led to the following result

$$\Gamma_{n+s} \propto I^{n+s}, \tag{1.17}$$

where n is the minimum number of photons required for ionization and s is the excess number of photons absorbed by the atom. Once again the the energy conservation comes from the generalised Einstein equation

$$E_e = (n+s)\hbar\omega - I_p. \tag{1.18}$$

At laser intensity of ($I = 10^{13}W/cm^2$), it is observed that first peak of ATI spectrum

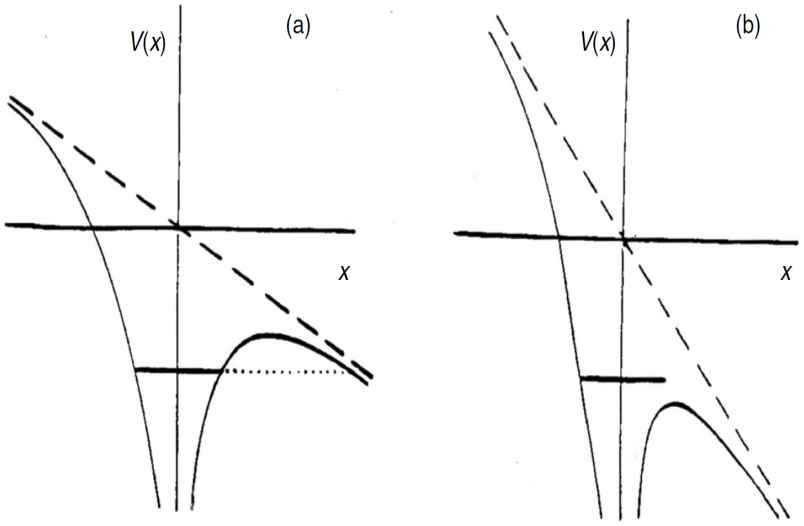

Figure 1.4: *(a)Tunnel ionization (b)Over the barrier ionization (figure taken from Ref. [22]).*

is smaller than the peaks observed at higher electron energy and higher peaks do not follow the usual power law described by the LOPT[21]. Moreover, the first peak gradually disappears as the intensity is further increased. This observation clearly reveals the breakdown of perturbation theory. This peak suppression is explained by the fact that AC starc shifts in the presence of external laser field are small for lowest bound states whereas they are of the order of electron ponderomotive energy (U_p)[1] for Rydberg and continuum states.Consequently the there is a corresponding increase in the intensity dependent ionization potential such that $I_p(I) \simeq I_p + U_p$. If this increase is such that $n\hbar\omega < I_p + U_p$, then ionization by n photons is energetically forbidden. However, the experiments involve use of smoothly varying intensity pulse so the atoms will be exposed to range of intensities and the corresponding peaks in the photo-electron spectrum will not completely vanish.

1.2.4 Tunnel ionization and over the barrier ionization

At low incident photon energy and sufficiently intense ($< 10^{15} W/cm^2$) laser field, the atomic potential is distorted by the incident field such that the electron can tunnel

[1] U_p is the cycle averaged oscillatory energy of electron in electromagnetic field. In non-relativistic case, the value of $U_p(eV)$ amounts to be equal to $(e^2\mathcal{E}_0/4m_e\omega^2) \approx 9.33 \times 10^{-14} I(W/cm^2)\lambda^2(\mu m)$, where $\mathcal{E}_0, I, \omega$ and λ are electric field, intensity, angular frequency and wavelength of incident laser electromagnetic field. For typical value of laser intensity of $10^{16} W/cm^2$ and wavelength of 800 nm, U_p comes about to be 600 eV, which is quite huge compared to the single photon energy of 1.54 eV.

through the effective potential barrier formed by adding the atomic potential and instantaneous laser field (Fig. 1.4(a)). This method of ionization is termed as optical field ionization (OFI) or tunnel ionization (TI). It was the pioneering work of Keldysh[23] who introduced a Keldysh adiabaticity parameter(γ) to define a transition from multiphoton ionization ($\gamma \gtrsim 1$) to tunnel ionization ($\lesssim 1$). The inherent assumption in Keldysh [23] and keldysh type[24–26] theories to describe TI is quasi-static or adiabatic approximation which means that the atom behaves at every instant of time as if the electric field component of laser field were static. In other words, ionization is adiabatic if time taken by the electron to tunnel through the barrier ($\tau_{tunnel} = \sqrt{2I_p}/\mathcal{E}_0$) is shorter than time during which the electric field changes significantly. Mathematically this condition reads as

$$\gamma = \omega\tau_{tunnel} \lesssim 1. \tag{1.19}$$

As described earlier, denoting $U_p = \mathcal{E}_0^2/4\omega^2$ as ponderomotive energy of electron, one can alternatively define γ as

$$\gamma = \sqrt{\frac{I_p}{2U_p}}. \tag{1.20}$$

The use of adiabatic approximation facilitates the calculation of ionization rate in terms of cycle averaged of the rate of ionization $W_{static}\left[\mathcal{E}(t)\right]$ by a static electric field $\mathcal{E}$ whose instantaneous value at time t is $\mathcal{E}(t)$. The static tunnelling rate for ground state of hydrogen atom is given as[**?**]

$$W_{static}(\mathcal{E}) \simeq \frac{4}{\mathcal{E}} \exp\left(-\frac{2}{3\mathcal{E}}\right). \tag{1.21}$$

More generally, for a hydrogenic positive ion of nuclear charge Z initially in its ground state,

$$W_{static}(\mathcal{E}) \simeq \frac{4Z^5}{\mathcal{E}} \exp\left(-\frac{2Z^3}{3\mathcal{E}}\right). \tag{1.22}$$

The tunnelling formulae given in previous equations can be generalised for arbitrary bound states and non-hydrogenic systems to give following rate formula

$$W_{static}(\mathcal{E}) = A_{n^*l}B_{l,m}I_p\left(\frac{2(2I_p)^{3/2}}{\mathcal{E}}\right)^{2n^*-|m|-1}\exp\left(-\frac{2(2I_p)^{3/2}}{3\mathcal{E}}\right). \tag{1.23}$$

The coefficient $A_{n^*,l}$ comes from radial part of the wave function at $r \gg 1/\sqrt{2I_p}$ depends upon the effective principal quantum number n^* and orbital angular momentum number l. The coefficient $B_{l,m}$ comes from the angular part of the wave function and depends upon the orbital angular momentum and its projection m on the laser polarization vector. The values of $A_{n^*,l}$ and $B_{l,m}$ are calculated as

$$A_{n^*,l} = \frac{2^{2n^*}}{n^*\Gamma(n^*+l+1)\Gamma(n^*-l)} \tag{1.24}$$

$$B_{l,m} = \frac{(2l+1)(l+|m|)!}{2^{|m|}|m|!(l-|m|)!}, \tag{1.25}$$

where $\Gamma(x)$ is the gamma function. The coefficient $A_{n^*,l}$ can be further simplified using the Ammosov, Delone and Krainov(ADK)[26] approximation as

$$A^{ADK}_{n^*,l^*} = \frac{1}{2\pi n^*}\left(\frac{4e^2}{n^{*2}-l^{*2}}\right)^{n^*}\left(\frac{n^*-l^*}{n^*+l^*}\right)^{l^*+1/2}, \tag{1.26}$$

where e is 2.718... and l^* is the effective angular momentum number. For $n^* \gg l^*$,

$$A^{ADK}_{n^*,l^*} \simeq \frac{1}{2\pi n^*}\left(\frac{4e^2}{n^{*2}}\right)^{n^*}. \tag{1.27}$$

Using adiabatic approximation, the result for ionization in slowly varying laser electric field ($\mathcal{E}(t) = \mathcal{E}_0\cos(\omega t)$) can be obtained by taking average of the static ionization rate given by equation1.23 over a complete laser cycle. The final result is given by

$$\begin{aligned} W_{ad} &= \left(\frac{3\mathcal{E}_0}{\pi(2I_p)^{3/2}}\right)^{1/2} W_{static}(\mathcal{E}_0) \\ &= \left(\frac{3\mathcal{E}_0}{\pi(2I_p)^{3/2}}\right)^{1/2} A_{n^*l}B_{l,m}I_p\left(\frac{2(2I_p)^{3/2}}{\mathcal{E}_0}\right)^{2n^*-|m|-1}\exp\left(-\frac{2(2I_p)^{3/2}}{3\mathcal{E}_0}\right) \end{aligned} \tag{1.28}$$

The ionization rate result given by equation 1.28 is known as Perelomov, Popov and Terent'ev (PPT) rates[24, 25]. Once the coefficient $A_{n^*,l}$ is replaced by $A^{ADK}_{n^*,l^*}$ as calculated by ADK, the final ionization rated are termed as ADK rates[26]

$$W_{ad} = \left(\frac{3\mathcal{E}_0}{\pi(2I_p)^{3/2}}\right)^{1/2} A^{ADK}_{n^*,l^*} B_{l,m} I_p \left(\frac{2(2I_p)^{3/2}}{\mathcal{E}_0}\right)^{2n^*-|m|-1} \exp\left(-\frac{2(2I_p)^{3/2}}{3\mathcal{E}_0}\right). \tag{1.29}$$

The ADK rate given by equation 1.29 is a rather a simple form which can be easily computed.

When the intensity is further increased upto $10^{15}W/cm^2$, the interaction potential between the laser field and atom becomes strongly enough to distort the effective potential barrier to a large extent (Fig. 1.4(b)). Consequently, the barrier becomes smaller and lower until the ground state remains no longer bound and the electron simply passes over the barrier so the process is known as "over the barrier ionization(OTBI)"[19]. The critical field can be obtained by equating the maximum of the combined potential (Coulomb plus laser) to the ionization potential of the atom or ion so that the electron escapes without tunnelling. This critical field is given by

$$\mathcal{E} = I_P^2/4Z, \tag{1.30}$$

where I_p is the ionization potential and Z is the charge state of the relevant atom or ion. The threshold intensity corresponding to this critical field is

$$I_{th} = I_P^4/16Z^2. \tag{1.31}$$

$$I_{th}(W/cm^2) = 4 \times 10^9 I_P^4(eV)/Z^2. \tag{1.32}$$

1.3 Laser solid target interaction

As mentioned earlier, the response of matter to intense laser light is a strong function of density. Till now, we have seen the interaction of independent atoms (in a gaseous form) to the laser field which gives rise to information about fundamental ionization processes and light interactions with free electrons. On the other hand, when high density solid targets are exposed to incident laser electromagnetic field, the interaction changes significantly. Various density effects like collisional ionization, recombination and collective effects start playing important roles other than the fundamental ionization processes and a soup of ions and electrons so called plasma is formed. These high density and high temperature laser produced plasma is different than the conventional plasma sources. Below we describe in short about the basic terminology used in plasma physics

1.3.1 Introductory concepts of plasma physics

The plasma state of the matter is a gaseous mixture of positive ions and electrons which show a collective or cooperative behaviour to external stimulus. Due to long range coulomb forces (r^{-2}) compared to the neutral gas (r^{-6}), each plasma particle interacts simultaneously with a large number of particles[27]. Thus, plasmas show a collective response of many plasma particles to an external perturbation. Following are the certain conditions which need to be fulfilled by any mixture of charged particles to be called as a plasma.

1.3.1.1 Debye shielding

The most important characteristic of a plasma state is to to effectively screen or shield the electric field of any charge imbalance (external or internal) created. This property naturally maintains the quasi-neutral character of a plasma state. Consider an extra positive charge $+Q$ into an infinitely homogeneous plasma, which originally has equal charge densities of electrons and singly charged positive ions $n_{e0} = n_{io}$. It is naturally expected that electrons will quickly surround the the positive charge and ions are

repelled by the presence of extra positive charge. Consequently, the net electric field of $+Q$ charge will significantly reduce after a characteristic length the so called Debye length λ_d due to the screening as explained. The expression for λ_d is given as follows

$$\frac{1}{\lambda_d^2} = \frac{e^2 n_{e0}}{\epsilon_0 k_B T_e} + \frac{e^2 n_{i0}}{\epsilon_0 k_B T_i}. \tag{1.33}$$

The potential $\Phi(r)$due to +Q charge is given by the following expression

$$\Phi(r) = \frac{Q}{4\pi\epsilon_0 r^2} \exp(-r/\lambda_d). \tag{1.34}$$

It may be noted from the expression of Debye length that it is a function of temperature and particle density. More the temperature, shielding length will be more and more the particle density, shielding length will me small. Thus for effective shielding one requires the high particle density and low temperature of plasma. We can also conclude from the spatial dependence of potential that a cloud of electron and ions will behave as a plasma on scale lengths much larger than the Debye length($d \gg \lambda_d$).

1.3.1.2 Quasineutrality

One of the definitive property of plasma is to maintain its quasi-neutrality i.e. the plasma macroscopically almost neutral but there can be significant charge imbalances on microscopic level. As mentioned in the discussion of Debye length, the effect of charge imbalance does significantly dies away several lengths of $|lambda_d$. This means that plasma maintains its quasi-neutral character for distances $d >> \lambda_d$ whereas the distances less than λ_d are the regions of breakdown of charge neutrality condition. So one can define the quasi-neutrality condition for distances greater than λ_d as

$$\left| \sum_j Z_j e n_{i0,j} - n_{e0} e \right| \ll n_{e0} e, \tag{1.35}$$

where j stands for the ion species j of charge number Z_j. For singly charged ionic species, this condition turns out to be as $n_{i0} \approx n_{e0}$

1.3.1.3 Plasma parameter

Plasma parameter N_d is defined by the number of particles in the Debye sphere of radius λ_d. Its value has to be $\gg 1$ so the statistical concept of Debye shielding remains valid. Mathematically, one can write for electron Debye sphere as

$$N_{de} = \frac{4}{3}\pi n_e \lambda_d^3 \gg 1. \tag{1.36}$$

1.3.1.4 Response time and plasma frequency

As mentioned earlier that the Debye shielding is consequence of collective effects in spatial domain. In the time domain, the collective effects are designated by the response time of electron after which they achieve a shielded equilibrium. If the potential perturbation is small enough ($e\Phi \ll k_B T$), the electron energy is slightly deviated from its thermal value. Consequently, one can safely write the electron velocity as $v_e \approx \sqrt{k_B T_e/m_e}$. For the establishment of new shielded equilibrium, the electron must be able acquire its new position at a typical distance of λ_d in a response time of $\tau \approx \lambda_{de}/v_e$. The reciprocal of this response time τ is called the electron plasma frequency ω_{pe}

$$\omega_{pe} = v_e/\lambda_{de} = \sqrt{\frac{n_e e^2}{\epsilon_0 m_e}}. \tag{1.37}$$

It means that collection of oppositely charged particles qualifies to be called as a plasm on time scales much greater than the inverse of electron plasma frequency ($T \gg \omega_{pe}^{-1}$).

1.3.1.5 Electrostatic response of a plasma

In general, plasma motion induced by an electric field produces an electromagnetic field. In many cases of interest, the field produced by the plasma motion can be represented solely by an electric field, without being accompanied by magnetic field perturbations. In this situation, the plasma response is electrostatic. One of the example is Debye shielding as discussed in the earlier section. In following we will consider the oscillatory electrostatic response or electrostatic waves in the plasma in the absence of magnetic field. As mentioned earlier that plasma oscillation are electrostatic in na-

ture, but they are stationary oscillations of electrons around a mean position. In the presence of a finite temperature, these plasma oscillations start to propagate. Electrons streaming into adjacent layers of plasma with thermal velocities will carry information about what is happening in the oscillating region. The plasma oscillation can then be called as *electron plasma wave*. The dispersion relation for the electron plasma wave, known also as plasmon:

$$\omega^2 = \omega_p^2 + 3k^2 v_{th}^2, \tag{1.38}$$

where ω_p and $v_{th} = \sqrt{k_B T_e/m_e}$ represent the plasma oscillation frequency and thermal velocity of electrons, respectively.

Plasmas also support *ion-acoustic wave* or *ion sound wave* in which ions play an important role. Here ions form regions of compression and rarefaction just as in ordinary sound wave in a gas. But the difference is that ordinary sound waves would not occur in absence of collisions whereas ions can still transmit the vibrations to each other because of their charge. Since the motion of massive ions will be involved, these will be low frequency oscillation. The dispersion relation for ion-acoustic wave reads as

$$\omega = \sqrt{\frac{T_e + \gamma_i T_i}{m_i}} k \equiv c_s k, \tag{1.39}$$

where γ_i, T_i, m_i and c_s represent specific heat ratio, ion temperature, ion mass and ion acoustic speed, respectively.

1.3.1.6 Ponderomotive force in plasma

The ponderomotive force per unit volume is related to the gradient of the radiation pressure P_l. The radiation pressure due to the laser hitting at a sharp boundary in the vacuum can be written as $P_l = I_l(1 + R)/c$, with R as reflection coefficient at the boundary. However, determination of radiation pressure in a plasma is not so straight forward, it requires the knowledge of electromagnetic field inside the plasma. Thus, one expects dependence of ponderomotive force on the electromagnetic fields in the plasma[28]. Rather than attempting a rigorous derivation of ponderomotive force, let us consider a simple non-relativistic ($v/c \ll 1$) case of a single electron osccilating near

the center of a focused laser beam[29]. The equation of motion for the electron in the linearly polarized laser $\vec{\mathcal{E}}_y(r) = \hat{y}\mathcal{E}_y(r)\cos(\omega t - kx)$ can be written as

$$\frac{\partial v_y}{\partial t} = -\frac{e}{m}\mathcal{E}_y(r). \tag{1.40}$$

The laser is assumed to propagate along $+ve$x direction and has a spatial intensity dependence along $y-$direction as shown in the figure. Expanding the electric field via taylor method gives electric field to be as

$$\mathcal{E}_y(r) \simeq \mathcal{E}_0(y)\cos\phi + y\frac{\partial \mathcal{E}_0(y)}{\partial y}\cos\phi + ..., \tag{1.41}$$

where $\phi = \omega t - kx$. To lowest order, we can get

$$v_y^{(1)} = -v_{osc}\sin\phi; y^{(1)} = \frac{v_{osc}}{c}\cos\phi, \tag{1.42}$$

where $v_{osc} = e\mathcal{E}_0(y)/m\omega$. Substituting back into equation of motion for electron yields

$$\frac{\partial v_y^{(2)}}{\partial t} = -\frac{e^2}{m^2\omega^2}\mathcal{E}_0\frac{\mathcal{E}_0(y)}{\partial y}\cos^2\phi. \tag{1.43}$$

Multiplying by m and taking the cycle-average yields the ponderomotive force on the electron

$$f_p \equiv \langle m\frac{\partial v_y^{(2)}}{\partial t}\rangle = -\frac{e^2}{4m\omega^2}\frac{\partial \mathcal{E}_0^2}{\partial y}. \tag{1.44}$$

Above equation suggests that ponderomotive force acts in the opposite direction of intensity gradient of laser i.e. this force will push electrons away from regions of higher local intensity. It is important to note that this force is independent of the charge of the species.

For its physical realisation, one considers the motion of free electron in the E field with decreasing amplitude along y- direction[30] as shown in Figure1.5. A free electron is shifted by the E-field from its original position y_0 to y_1. From there it is then accelerated to the right until it has passed y_0. Now the electron is decelerated in the forward direction as the electric field is reversed and it stops at position y_2. If y_0' des-

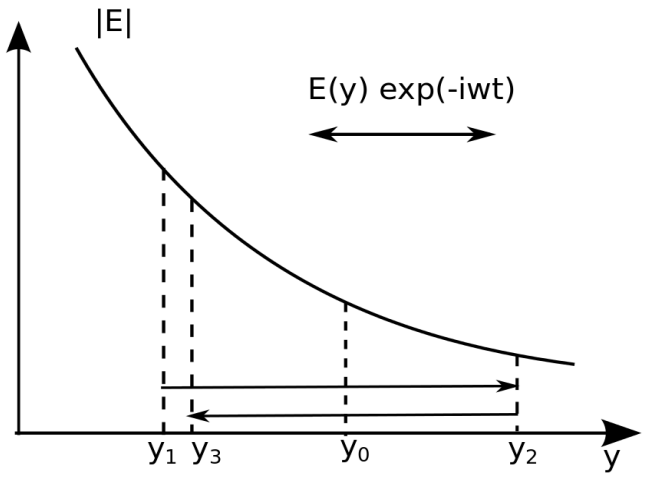

Figure 1.5: *Schematic representation of drift of charged particle due to ponderomotive force along the decreasing field amplitude.*

ignates the position at which the field reverses its direction ($y_0' > y_0$), the declaration interval in right ($y_2 - y_0'$ is more than that acceleration interval in left ($y_0' - y_1$). This is due to the reason that electric field is weaker in the right side and therefore a longer distance is required to take away the energy gained in the former quarter period of oscillation. On its way back the electron is stopped at the turning point y_3 which is shifted away from its earlier position y_1 in the direction of decreasing electric field amplitude. Since this consideration is based energy and work so the drift along the decreasing field amplitude is independent of the charge of the species (electron or positron).

1.3.1.7 Landau damping

Landau damping is a phenomena of wave damping without energy dissipation by collision. It was first discovered by Landau as a complete mathematical concept but sooner it was demonstrated experimentally also. The physical reason behind this method of energy dissipation is wave-particle interaction in which the particles with velocities closer to wave phase velocity do not observe the fluctuating electric field of wave and thus able to exchange the energy with the wave. Particles with velocities slightly less than the wave phase velocity are accelerated by the wave electric field,

gaining energy from the wave while the particles with velocities slightly greater than the wave phase velocity are decelerated by the wave electric field, losing energy to the wave. In Maxwellian plasma, there are more number of electrons with velocities slower than the phase velocity of wave ($v_p = \omega/k$ is the phase velocity of the wave) than that of electrons with velocities faster than v_p. Consequently, there will be more number of electrons gaining energy from the wave than losing to the wave. Ultimately, the wave will be damped and the process is termed as Landau damping.

1.3.2 Laser absorption in plasmas

1.3.2.1 Inverse bremsstrahlung

Inverse bremsstrahlung is the simplest mechanism by which incident laser energy is absorbed in the plasma. As it is a well known fact that bremsstrahlung or braking radiation is the radiation emitted by a charge particle when it encounters collisions with other particles. Inverse bremsstrahlung or collisional absorption is the reverse process in which an electron absorbs a photon while colliding with ions present in the plasma. To understand it physically, we consider the free electron oscillating in the laser electric field (ions, being heavy, serve as a neutralising environment). The directed energy of electron motion is randomized and hence converted into heat energy by collisions with ions. Alternatively, incident laser field drives electron current and the resistivity produced by electron-ion collisions lead to "Joule heating" of plasma[**?**]. A detailed investigation which includes the solution of electron equation of motion in presence of damping term due to collisions and Maxwell's equation, yields the following dispersion relation for laser light propagating the plasma:

$$k^2 = \frac{\omega^2}{c^2} - \frac{\omega_p^2 \omega}{c^2(\omega + i\nu_{ei})} \tag{1.45}$$

,where ω_p and ν_{ei} are plasma oscillation frequency and electron ion collision frequency. For the case of plasma corona ($\nu_{ei} \ll \omega$), a first order Taylor expansion of this equation

yields

$$k^2 \simeq \frac{\omega^2}{c^2}\left(1 - \frac{\omega_p^2}{\omega^2} + \frac{i\nu_{ei}\omega_p^2}{\omega^3}\right). \tag{1.46}$$

Solving this equation for k, by expanding the square root of the right-hand side of above equation in the limits $\nu_{ei}/\omega \ll 1$ and $\omega^2 - \omega_p^2 \gg (\nu_{ei}/\omega)\,\omega_p^2$, one gets

$$k \simeq \frac{\omega}{c}\sqrt{\left(1 - \frac{\omega_p^2}{\omega^2}\right)}\left\{1 + i\left(\frac{\nu_{ei}}{2\omega}\right)\left(\frac{\omega_p^2}{\omega^2}\right)\frac{1}{1-\omega_p^2/\omega^2}\right\}. \tag{1.47}$$

The index of refraction can be calculated with the help of real part of above equation1.47, which reads as

$$\eta \equiv Re\left\{\frac{kc}{\omega}\right\} = \left[1 - \left(\frac{\omega_p}{\omega}\right)^2\right]^{1/2}. \tag{1.48}$$

This equation suggests that η becomes imaginary for $\omega_p > \omega$ *i.e.* the light can not propagate in the plasma for $\omega_p > \omega$. Since $\omega_p \sim n_e^{1/2}$, where n_e is electron density, that means light incident from the under dense region can only propagate up to the density at which $\omega_p = \omega$. This limit is called *critical density* $\left(n_{ec} = \epsilon_0 m\omega_0^2/e^2\right)$, where ω_0 is the frequency of incident laser light. Now one can calculate the spatial damping rate of the laser energy by inverse bremsstrahlung

$$\kappa_{ib} = 2Imk = \left(\frac{\nu_{ei}}{c}\right)\left(\frac{\omega_p^2}{\omega^2}\right)\left(1 - \frac{\omega_p^2}{\omega^2}\right)^{-1/2}. \tag{1.49}$$

Using the definition of critical density and spitizer formula for electron-ion collision frequency at critical density $\left(\nu_{ei} = 4\left(2\pi\right)^{1/2} Z_i^2 e^4 n_i \ln\wedge/3\left(k_B T_e\right)^{3/2} m_e^{1/2}\right)$, one get the absorption coefficient

$$\kappa_{ib} \propto \frac{Z_i n_e^2}{T_e^{3/2}}\left(1 - \frac{n_e}{n_c}\right)^{-1/2} \tag{1.50}$$

The dependence of κ_{ib} on n_e/n_c reflects the fact that a large fraction of the inverse bremsstrahlung absorption occurs near the critical density. It is important to note that inverse bremsstrahlung absorption is efficient only if enough number of collisions take place. But $\nu_{ei} \sim T_e^{-3/2}$, which means that this process becomes less significant at

higher temperature or high laser intensity. At high laser intensity, other processes for absorption of laser energy comes into the picture which will be described in the next section.

1.3.2.2 Resonance absorption

Resonance absorption is an alternate mechanism of laser energy absorption at high intensities and high temperature where IB becomes insignificant. When a p-polarised[1] light is incident at an angle other than zero from normal incidence on a spatially inhomogeneous electron density profile, electron plasma waves are excited. This occurs due to the condition that the component of laser electric field becomes parallel to the plasma density gradient. Near the critical density the electric field becomes very large and will resonantly excite these electron plasma waves. The damping of these waves (either collisional or collision-less such as Landau damping) eventually transfers the electromagnetic energy into thermal energy, thus heating the plasma. This whole process of conversion of laser energy into plasma heating via generation of electron plasma waves and their damping, is termed as *resonance absorption*. This process is impossible for s-polarised EM wave due to the absence of any component of electric field parallel to density gradient of electrons.

Consider the laser propagation in the y-z plane at angle θ_0 to the normal of the vacuum-plasma interface ($z = 0$) with the linear variation of electron density on the plasma side (Figure1.6). The dispersion relation characterizing the light wave is

$$\omega^2 = \omega_p^2 + \left(k_y^2 + k_z^2\right) c^2. \tag{1.51}$$

Since the variation of electron density is along z-direction, k_y is constant and can be written as $k_y = \omega \sin\theta_0/c$. Since the reflection of EM wave occurs at the surface where $k_z = 0$, so one find the following realizations

$$n_e = n_c \cos^2\theta_0, \omega_p = \omega\cos\theta_0, z = L\cos^2\theta_0. \tag{1.52}$$

[1]For p-polarised electromagnetic wave, the electric field of the wave lies in the plane of incidence.

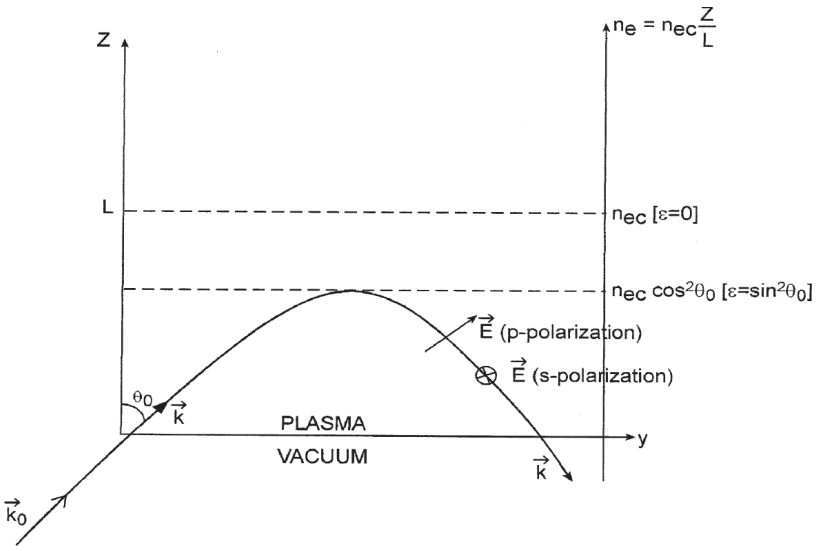

Figure 1.6: *Propagation of linearly polarized laser in the y-z plane (figure taken from Ref. [28]).*

Even though an obliquely incident light wave reflects at a density less than the critical density, its field still tunnels into the critical density region and excites the resonance. If the angle of incidence θ is too large, the light will be turned away far from the the critical density and the incident wave has to tunnel through too large distance to reach $n = n_c$. If the angle θ is too small, the component of the electric field at the turning point will be too small. In both these cases, resonance absorption will be small. The optimum angle of incidence for which absorption will be maximum is given as $\sin\theta \simeq 0.8\,(c/\omega L)^{1/3}$, where L is the density scale length. It is important to note that RA is larger than IB for parameters like high laser intensity or high plasma temperature; longer laser wavelength i.e. lower value of n_c; and short plasma scale length L. It has been shown that absorption due to RA can approach up to about 50% at sufficiently high laser intensities for correct value of laser polarization and angle of incidence.

1.3.2.3 Other mechanisms

Various other mechanisms for laser energy absorption exist in the laser solid plasma. We will briefly discuss about them. *Vacuum heating*, proposed by Brunel(1987)[31], is one of the important mechanism which works in for femstosecond interactions in

steep plasma density gradient. Electrons near the edge of a sharp vacuum-plasma boundary is able to see directly the laser field. Indeed, a thermal electron arriving near the edge at the right moment in the laser cycle may be dragged out violently into the vacuum well beyond the Debye sheath. As the field reverses its direction, this same electron will return to the vacuum-plasma interface and accelerated back into the plasma. Electric field of the laser can not penetrate more than the skin depth of the plasma, so the propagation will be unaffected from the laser electric field and eventually dump its energy into the plasma through collisions.

Another phenomenon similar to vacuum heating is $j \times B$ heating mechanism which becomes important for normal incidence and relativistic quiver velocities[32]. Only difference from vacuum heating lies in the driving term which for this case, is the high-frequency $v \times B$ component of Lorentz force operating at twice of the laser frequency. Actually, the longitudinal force due to linearly polarised electromagnetic wave of frequency ω consists of two parts: first is usual DC ponderomotive force which pushes the electron density profile inwards and the second, high frequency term leads to the heating in a similar fashion to the component of a p-polarised electric field parallel to the density gradient.

Incident laser light is also capable of coupling with the natural collective modes of the plasma like electron plasma wave or ion-acoustic wave through the *parametric excitation*[1] processes such that these modes grow and becomes unstable until they saturate in a turbulent state[**?**]. If we can define a matching condition among frequency and wave-numbers such as $\omega_0 = \omega_1 + \omega_2, \mathbf{k}_0 = \mathbf{k}_1 + \mathbf{k}_2$, where $(\omega_0, \mathbf{k}_0)$ is frequency and wave number for pump wave that decays into two waves $(\omega_1, \mathbf{k}_1)$ and $(\omega_2, \mathbf{k}_2)$, one can define various parametric processes in laser produced plasmas as following[**?**]: For example, if $\omega_0 \approx \omega_p$ and ω_1 and ω_2 corresponds to plasmon and an ion wave, the process is called *decay mode* which results into the absorption of laser. This effect occurs close to critical density $n_e \approx n_c$. If the pump wave with frequency $\omega_0 > 2\omega_p$ decays into a photon and a plasmon, leading to laser scattering, the process is called *stimulated*

[1] A parametric excitation process is defined as a non-linear phenomena where a periodic variation in the medium induces growing oscillation at different frequency.

Raman scattering (SRS). This instability reduces the laser absorption, $\omega_0 > 2\omega_p$ implies the occurrence of this process at $n_e < n_c/4$. The laser pump with frequency $\omega_0 > \omega_p$ can also decay into ion wave and backscattered photon and thus reduces the laser absorption. The process is termed as *stimulated Brillouin scattering (SBS)*. $\omega_0 > \omega_p$ implies that this instability occurs at $n_e < n_c$. It is also possible that laser pump wave with frequency $\omega_0 = 2\omega_p$ may decay into two plasmons, inducing laser absorption. This phenomena is known as *two plasmon decay or* $2\omega_p$ instability and occurs at $n_e = n_c/4$.

1.4 Laser-cluster interaction

The advent of high intensity ($10^{15} W/cm^2$) and short pulse ($\leq 1ps$) laser has revolutionized the field of laser matter interaction. We have already seen the two extremes states of matter : high density solid target and low density gas target which interact with the laser field. One of the important applications of these studies is to produce the particles (electron and ions) and photons that have energies far beyond the single incident photon energy. As far as gas targets are concerned, they have appeared as a promising target for conversion of laser energy into conversion of bright, coherent soft x-rays through harmonic generation and x-ray lasers[33, 34]. Moreover, these targets do not produce any debris. However, their use is limited due to poor absorption of laser light into the gaseous atoms that ultimately turns into a reduced conversion efficiency of laser photons into x-ray photons. On the other hand, if gas targets are replaced by solid targets, laser energy is strongly absorbed due to the various mechanisms such as IB, RA, and various parametric instabilities as mentioned in the previous section. The enhanced absorption of laser energy is reflected into energetic photons as well particles with energies in the range of MeV[35, 36]. The problem with the solid targets is generation of debris which is detrimental to optics and vacuum present in the laser plasma experiments.

Now here comes the clusters which are uniquely placed in between the gaseous and solid targets and contain both the advantages of solid and gaseous targets (Fig.1.4). For instance, energy absorption efficiency of laser light by clusters is more than that

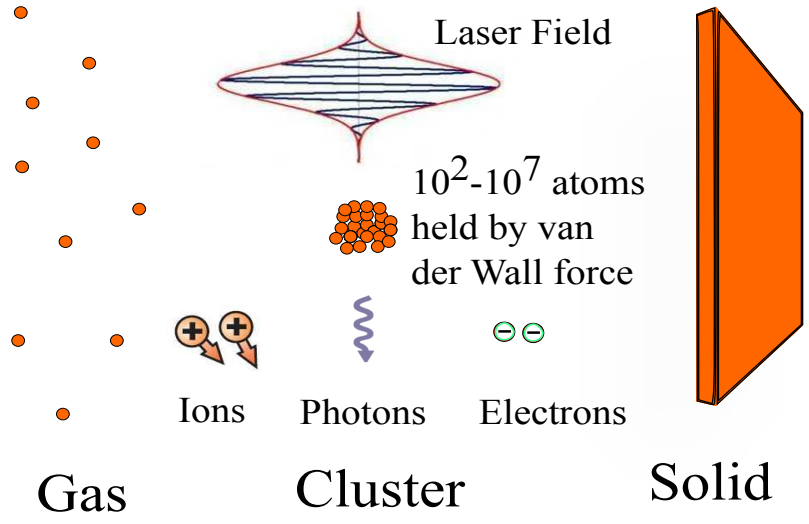

Figure 1.7: *Clusters intermediate to gas and solid target gives rise to the emission of energetic particles after the irradiation by short and intense laser fields*

of solid target yet the particle emission from cluster is debris free much like as in gases. The high local density of atoms ($n_l \sim 10^{22}$ atoms/cm^3) inside a cluster, lack of thermal dissipation and collective effects (cluster sizes are much smaller than the wavelength of incident laser light) are responsible for enhanced energy absorption by clusters compared to the solids. The low average density of atoms ($n_a \sim 10^{15}$ atoms/cm^3) in the clustered beam leads to the debris free emission of particles from cluster explosion. It has been shown experimentally that clusters absorb more than 90% of incident laser energy[37]. The outcome of this enhanced absorption of incident laser energy translates into ejection of highly-charged ions[38] with energies upto MeV[39], KeV electrons[40] and emission of x-rays ranging from Kev[41] to hundreds of eV ($< 500eV$)[42, 43]. Laser-driven particle accelaration[44], coherent and incoherent X-ray generation[45], nuclear fusion in deuterium clusters[46], production of efficient plasma wave guides[47] and high orders harmonic generation[48] are few of the important application of laser-cluster interaction.

These clusters are produced by the isentropic expansion of a high pressure gas with sufficiently large polarizability through a nozzle into the vacuum[49]. The decrease of temperature due to the isentropic expansion process allows the weak Van der Waals interaction to take effect between the gaseous atoms that leads to the forma-

tion of near-solid state density droplets, so-called clusters, embedded in a low density surrounding gas. All of the clusters thus formed are not of a single size, but they have a distribution known as long normal distribution. Hagena obtained a empirical relationship for a parameter so called Hagena parameter which charaterizes the average size of the clsuter. The Hagean parameter is defined as:

$$\Gamma^* = k \left[\frac{d(\mu m)}{tan\ \alpha}\right]^{0.85} \frac{p_0(mbar)}{T_0^{2.29}(K)} \tag{1.53}$$

where d is the jet throat diameter, α is the jet expansion half angle, p_0 is the backing pressure, T_0 is the stagnation temperature and k is a constant that depends on the particular atomic species (k = 5500 for Xe, 2890 for Kr, 1650 for Ar, 180 for Ne, and 4 for He [50]). Most studies suggest that clustering begins when this parameter exceeds 300 where the average size of the cluster varies as $(\Gamma^*)^{2.0-2.5}$ [49]. The average size of the cluster in terms of number of atoms per cluster can be written in terms of Hagena parameter as

$$N_c \cong 33 \left[\frac{\Gamma^*}{1000}\right]^{2.35} \qquad (\Gamma^* \leq 10^4) \tag{1.54}$$

$$N_c \cong 100 \left[\frac{\Gamma^*}{1000}\right]^{1.8} \qquad (\Gamma^* > 10^4)\ . \tag{1.55}$$

Eq. (1.55) is the modified scaling law given by Dorchies et al. [51] which is valid when Hagena parameter is of the order of 10^4 or more.

Once the clusters are formed, the next question comes how do they interact with the laser field. In general, the laser-cluster interaction proceeds through three subprocesses: viz. ionization of atoms, absorption of laser energy, and expansion of cluster. While considering the interaction process, one has to clearly differentiate between the inner and outer ionized electrons. Inner ionization refers to the removal of electron from parent atom yet confined in the cluster due to coulomb force of residual ions. On the other hand outer ionization refers to the removal of electron form cluster itself as the electron achieve sufficient energy to overcome coulomb barrier of cluster. The heating of the cluster plasma is mainly governed by the inner electrons as a outcome of inner ionization via inverse bremsstrahlung and collective resonance effects.

The cluster plasma expands depending on the population of inner electron. If the space charge is strong enough t retain most of electrons inside the cluster, then cluster plasma expands due to pressure of electron gas. This mode of cluster expansion is known as hydrodynamic expansion. On the other hand, if most of the electrons leave the cluster immediately then cluster explodes due to the repulsion among remaining positive charges of ions in the cluster. This is called Coulomb explosion. Theoretical modelling of the intense laser pulse interaction with rare-gas clusters is a challenging subject involving the nonlinear, nonperturbative response of many ions and electrons. Recent review[52] provide the overall status of the subject. Below we describe certain theoretical models to completely explain the each process in detail.

1.4.1 Coherent electron motion (CEM) model

This model, the earliest one, was put forward to explain the anomalous x-ray line emission from Kr and Xe clusters driven by high intense ($0.5 - 80 \times 10^{17} W/cm^2$), 248-nm laser with pulse duration $\sim 300 fs$[41, 53]. These were the first experiments which opened up a new and fascinating era of laser-cluster interaction which surprisingly gave rise to x-ray photons with energies far beyond the conventional atomic counterparts. According to this model[54], the rare-gas cluster is considered as a spherical group of atoms held together by weak van der Wall forces and characteristic dimension of the cluster has to be smaller than skin depth. The initial ionization of atoms is due to the optical field ionization. In the presence of strong electromagnetic field and sufficiently large cluster, these tunnel ionized electrons are accelerated by the external optical field and collide with the other atoms or ions within the same cluster to create further ionization. Thus the production of inner-shell excited species can give rise to the prompt x-ray emission. This model was further generalised to match with the experimental findings[55]. The most important one was the coherent or ordered motion of the (Z) field-ionized electrons induced by the external driving field. The collection of coherently driven electrons behaves like a quasi-particle with a charge Ze and mass Zm_e which greatly enhances the coupling between the atom/ion and quasi-particle. It was also proposed to allow the process of multiple electron ejection from a inner-shell,

to account for the high-charge states of the ionic species. Experimental findings were greatly accounted for by inclusion of these considerations.

1.4.2 Nanoplasma model

Experiments by Ditmire et al[43] on laser driven clusters revealed very efficient absorption of laser light and similar strong x-ray emission as observed by McPherson et al. The difference was that the emission from these interactions was long lived ($\sim 1ns$), contrary to the results of McPherson et al where the x-ray emission was observed to be prompt ($\sim 100 - 1000fs$) after excitation by laser[]. To explain these results, it was suggested that incident short pulse laser interacts with the cluster which is nothing but a small ball of high-density plasma, and so the name nanoplasma. The clusters serve only to absorb the laser energy, with the bulk of the x-ray emission occurring after the cluster has expanded in to a underdense plasma. There are two important length scales: one is Debye length of cluster plasma $\lambda_d = \sqrt{\epsilon_0 n_e e^2/kT_e} = 5\mathring{A}$ (for a solid density, 1000 eV plasma) and the other is laser wavelength ($\lambda = 800nm$). The typical cluster sizes ($\sim 100\mathring{A}$) lies in between two extreme limits so that assumption of small plasma ball of cluster plasma is justified. The smallness of cluster plasma allows to ignore the spatial variation of laser field across the cluster and all of the atoms and/or ions see the spatially uniform optical field of incident laser. There are two important assumptions made in this model[43]: one is high degree of collisionality in the cluster (for the attainment of Maxwellian electrons distribution) and second is the uniform density within the cluster throughout the cluster expansion.

The ionization of the cluster atoms is due to both tunnel ionization and electron impact ionization. Both thermal electrons and laser driven oscillating electrons contribute to electron impact ionization rate. Incident laser primarily deposits its energy into the free electrons in the cluster and that this energy deposition is through collisional inverse bremsstrahlung. Assuming the cluster as dielectric sphere, the heating rate averaged over a laser time cycle can be written as:

$$\frac{\partial U}{\partial t} = \frac{\omega}{8\pi} Im\left[\epsilon\right]\left[\mathcal{E}\right]^2 \tag{1.56}$$

The electric field calculation inside the cluster is similar to find out the field within the uniform dielectric sphere surrounded by a constant electric field[56]. Thus the E-field inside the cluster is given as

$$\mathcal{E} = \frac{3}{|\epsilon + 2|}\mathcal{E}_0, \tag{1.57}$$

with $\mathcal{E}_0$ as field outside the cluster. Substitution of electric field from equation 1.57 in equation 1.56, gives the heating rate as

$$\frac{\partial U}{\partial t} = \frac{9\omega}{8\pi}\frac{Im\left[\epsilon\right]}{|\epsilon + 2|^2}|\mathcal{E}_0|^2. \tag{1.58}$$

The expression for dielectric constant ϵ is calculated by the Drude model[57]:

$$\epsilon = 1 - \frac{\omega_p^2}{\omega\left(\omega + i\nu_{ei}\right)}, \tag{1.59}$$

where ω_p and ν_{ei} represent the plasma frequency and electron-ion collision frequency. It is instructive to see that both electric field and heating rate goes to a maximum when $|\epsilon + 2|$ goes to a minimum, which is a clear indication of resonance. The minimum value of $|\epsilon+2|$ corresponds to plasma frequency $\omega_p = \sqrt{3}\omega$ or in terms of electron density $n_e = 3n_c$, where ω and n_c represent the laser frequency and critical density, respectively. Initially the cluster plasma is overcritical i.e. $n_e \gg 3n_c$ but as the plasma expands the electron density reduces and resonance occurs at $n_e = 3n_c$. The expansion of the cluster plasma occurs in the combined action of hydrodynamic pressure ($P_e = n_e k T_e$) of heated electron gas and Coulomb pressure ($P_{Coul} = Q^2e^2/8\pi r^4$) from a charge build-up on the cluster resulting from outer ionization of cluster. It is important to note that for small clusters Coulomb force is important through $1/r^4$ scaling law. Once the cluster expands, however, the hydrodynamic force will begin to dominate since the hydrodynamic pressure scales as $1/r^3$ (through electron density n_e).

1.4.3 Ionization ignition model

As mentioned earlier that nanoplasma model does not consider the local coulomb field within the cluster for calculating the ionization rate. *Rose-Petruck et al* first pointed

out in their classical trajectory monte carlo (CTMC) simulation model that local field strengths are sufficient to further field ionize the atoms in the cluster[58]. In their model, the initial ionization was due to classical over the barrier ionization and further ionization was facilitated by the electron impact ionization. The relativistic classical equations of motion for all of the electrons and nuclei were then integrated over the duration of the laser pulse. When the ionization starts, the atoms/ions are still very much confined in the cluster where as electrons are substantially heated by the collisional processes and quickly removed from the cluster by the laser field. The high charge density of ions along with the fast fluctuations of the electric field due to electrons further enhances the ionization of the ions. This subsequent ionization proceeds very quickly and can have the appearance of an ionization ignition once the threshold intensity for single ionization is reached. The result of this ionization ignition leads to higher charge states produced in the laser driven cluster compared to the isolated atoms.

1.4.4 Modifications to nanoplasma model

As mentioned in the previous section that nanoplasma model is a uniform radial density model where radial electron density remains uniform during the cluster expansion. The outcome of this assumption leads to resonance condition at electron density of $n_e = 3n_c$. One of the main implications of this model a narrow resonance time interval[59] which is given as:

$$\delta t_{res} = \frac{2}{3}\frac{\nu}{\omega}\left(\frac{n_e}{3n_c}\right)^{1/3}\frac{R}{c_s} \tag{1.60}$$

for a cluster of radius R and electron density n_e, where c_s is the plasma sound speed, and ν/ω is the normalized collision frequency at $n_e = 3n_c$. Model calculations suggest that this time interval (δt_{res}) is $6fs$ and $40fs$ for clusters of radii $100\mathring{A}$ and $600\mathring{A}$ but the pump-probe and variable pulse width experiments suggested a much longer time interval (severals of picoseconds) for these resonance[60]. This discrepancy was resolved by *Milchberg et al* by considering the radial non-uniformity of cluster expan-

sion in self-consistent one dimensional radial Lagrangian plasma hydrodynamic[59]. They found that even for smaller clusters, radial non-uniformity of electron density is important and its inclusion results into *long-time resonances* at the critical density plasma layer n_c in stead of $3n_c$. This resonance is maintained throughout the pulse duration as long as the cluster plasma does not expand below critical density. A significant result of this is that the ponderomotive force, which is enhanced at the critical density surface, can be large enough to strongly modify the plasma hydrodynamics, even at laser intensities as low as $10^{15}W/cm^2$ for 800 nm laser pulses.

The use of quasi-static dielectric constant as given by Drude's model ($\epsilon = 1 - \omega_p^2/\omega\,(\omega + i\nu_{ei})$ overestimates the enhancement of electric field in clusters. In fact, calculation of ϵ by this model is not suitable to describe the laser energy absorption due to the rapid change in the electron density and plasma temperature resulting from the resonant heating and expansion of clusters. In stead of this, *Liu et al*[61] modified the Ditmire's nanoplasma model by inclusion of an effective plasma dielectric constant ($\epsilon_{eff} = \epsilon + i\epsilon/\omega$), which is obtained by solving the Maxwell's equations for a rapidly expanding plasma. It can be shown that the electric field calculated by using ϵ_{eff} is much smaller than that by using ϵ. At the resonance point, the rapid change of electron density and temperature results in the rapid change of the plasma current density associated with the free electrons. This plasma current density will produce an electric field that to some extent weakens the resonance enhancement of the electric field inside the cluster.

In the framework of nanoplasma model, the electric field ($\mathcal{E} = \sqrt{1 + (\omega/\nu_{ei})^2}\mathcal{E}_0$) and rate of heating ($\partial U/\partial t = 3\omega^2 I_0/c\nu_{ei}$) at the resonance ($\omega_p = \sqrt{3}\omega$) strongly depend on the value of electron-ion collision frequency. Both of them may approach to very large values if ν_{ei} becomes very small. In fact, the ν_{ei} is known to be inversely proportional to the cube root of the electron velocity[43] except for the slowly varying Coulomb logarithm term. So near the plasma resonance, both the laser intensity and quiver velocity ($v_q = e\mathcal{E}/m\omega$) of electron increases. This reduces the collision frequency and consequently, the electric field increases inside the cluster. This feedback loop continues and leads to significantly small value of ν_{ei} and enhanced value

of $\mathcal{E}$ inside the cluster. The enhancement of the heating when the collision frequency tends towards zero seems paradoxical. *Megi et al*[62] suggested that the consideration of other damping mechanism like electron cluster surface collision effects can resolve this issue. In fact, the damping effect can be accounted for by an effective collision frequency, $\nu_{eff} = \nu_{ei} + Av/R$, where v is the effective velocity of electron defined as vector sum of electron thermal velocity and electron quiver velocity. The second term in ν_{eff} signifies the contribution from collisions with cluster surface. Now near the resonance, ν_{ei} reduces as mentioned earlier but the surface term increases with the electron velocity and thus prevents the total collision frequency dropping and the electric field inside the cluster diverging.

The original nanoplasma model of Ditmire et al[43] only takes into account first-order ionization processes in which a valence electron is directly promoted from the ground state to the continuum. This original nanoplasma model by Ditmire et al can not explain the experimental results on laser driven Ar clusters performed by Micheau et al[63]. In that experiment, a prominent population of charge states with $q \geq 14$ were observed whereas the nanoplasma model only suggests charge states upto Ar^{13+}. These results can be explained by improving the nanoplasma model to include the high-order ionization transitions involving intermediate excited states[63]. The effect of lowering of ionization potential in the dense cluster environment was studied by *Hilse et al* using a modified nanoplasma model[64]. In the regime of the dense non-ideal nanoplasma, the bound state properties can be strongly affected by the interaction with the surround- ing particles. An important effect is the ionization energy suppression which was treated by *Hilse et al* using the Stewart-Pyatt approach[65]. The main result was the appearance of considerable higher ionic charge states if non-ideal rates are used in the model.

1.4.5 Particle-particle/particle-mesh models

It is important to note that the nanoplasma model and its different variants are fluid models *i.e.* they follow a statistical continuum picture. Due to this limitation, they can not describe the interaction dynamics of laser-cluster interaction in microscopic

manner. For example, fluid models can only account for the average values like average kinetic energy, average charge state etc. It is unable to predict correctly about distribution of ion energies and various charge states which is generally achieved in experiments. To gain more insight into the dynamics of laser cluster interaction, particle models were developed. These models are basically of two types : one is particle-particle also knows molecular dynamics (MD)[66–73]and the other one is particle-mesh typically know as particle-in-cell (PIC)[74–77] in the literature.

Inner ionization of clusters is due to optical field. The contribution from optical field is either over the barrier or tunnel ionization. The ionization due to impact of electrons with atoms/ions is considered by using semiempirical Lotz cross section[78, 79]. Once inner ionized, both MD and PIC use classical equations of motion to advance the particle in time domain. The difference lies in the calculation of total force appearing in the equation of motion. In MD, the force on each particle is the sum of all two-body Coulomb forces from other charged particles which scales as $O(N^2)$ for N number of particles in the cluster plasma. The force due to the laser electromagnetic field is also added to this force. In the PIC, the field is computed on a grid of cells, and the force on the particles is calculated from the interpolated fields at the particle position. The computation time scales as $O(N)$ for N number of particles. PIC methods are less time consuming than MD methods due to linear dependence of computation time on number of particles. Similarly, MD methods are grid-less calculations compared to their PIC counterparts. The grids become difficult to handle in three dimension whereas MD does not offer this kind of complexity, so easily extendible to three dimension. If the size of the cluster is not large ($10^3 - 10^5$), MD methods are favourable than PIC methods but for large sized clusters one has to choose the PIC methods. It is noteworthy to mention that N^2 problem of MD calculations can be improved by using Barnes and Hut algorithm[80] in which the computation time scales as $O(N \log N)$.

1.4.6 Non-linear Models

Till now all models which are used to explain the enhanced energy absorption by lasers, are based upon the linear resonance model used by Ditmire et al. Energy of the laser is efficiently absorbed at the linear resonance condition $n_e = 3n_c$ or equivalently $\omega_t = \omega_p/\sqrt{3} = \omega$[1]. It was argued by Mulser et al[81] that this model of linear absorption does not work for ultra-short laser pulse duration or during the early-cycles of a long-pulse laser cluster interaction. The reason is the much higher electron density compared to critical electron density or equivalently $\omega_t \gg \omega$ so that the condition of linear resonance is never achieved. To account for the laser energy absorption in this regime due to the absence of so called linear resonance, idea of non-linear resonance (NLR)[81] *i.e.* lowering of the eigenfrequency or resonance frequency with increasing oscillation amplitude was proposed and also verified in the PIC simulation results[82]. To explain NLR, a rigid sphere model of two interpenetrating spheres (RSM) of positive charge (ions) and sphere of negative charge (electron) was considered. The potential between two spheres for small energy of excitation is harmonic with eigenfrequency $\omega_t \gg \omega$. As the amplitude of oscillation increases, the potential becomes anharmonic and the restoring force becomes weaker than that of the linear oscillator. Consequently, the eigenfrequency decreases and at some exciation energy it may become equal to laser frequency leading to the resonance, the so called "non-linear resonance.

1.5 Outline of the thesis

In thesis, we describe the various features of interaction of van der Wall bonded atomic clusters with high intensity lasers with pulse durations limited to hundreds of femtoseconds. In chapter 1, we mention briefly about femtosecond lasers. Atomic clusters , an intermediate between gases and solids, when irradiated by femtoseconds

[1]The condition of resonance can also be achieved by modelling the motion of inner electron cloud along the laser polarization direction by a driven and damped harmonic oscillator[69]. The eigenfrequency ($\omega_t = \sqrt{Q_{ion}}/R(t)^3 = \omega_p/\sqrt{3}$) of this oscillation is determined by charge and size of the cluster. The condition of resonance is achieved when this eigenfrequency (ω_t) matches with the laser frequency (ω) due to the electron emission and cluster expansion

laser demonstrate the experimental results which are advantageous than using gases or solid, alone. Clearly, the ionization dynamics and further heating of the cluster plasma is entirely different in laser driven clusters if compared to the laser driven solids or gases targets. Keeping this transition in mind, we have introduced a general introduction in chapter 1 which covers the lase atoms interaction along with the laser driven solid target plasma. In the end of this chapter, we mentions the general features of laser driven clusters and various models to describe this interaction.

In chapter 2, we describe our three dimensional relativistic molecular dynamic model for studying the laser-cluster interaction. After the detailed description of the code, the code is validated against various theoretical and experimental results.

Chapter 3 deals with the problem of enhanced energy absorption by laser driven clusters. Although various models such as linear resonance predicted by nanoplasma model, non-linear resonance model are used to explain this, but literature also supports the idea of no-resonance. In this chapter, we have used MD simulations to show the existence of linear resonance for laser driven Ar clusters by varying the pulse duration of laser.

Chapter 4 deals with the distribution of ions, in energy as well as number, ejected from the Ar and Xe clusters when irradiated by the laser of pulse duration ranging from hundreds of femtosecond to few laser time cycles. Clear revelation of this anisotropy is observed that changes with the duration of laser pulse.

In chapter 5, we mention about the effect of few-cycles lase pulses on the ionization dynamics of Xe cluster. For these ultra short pulses, the initial phase(ϕ) of the carrier wave with respect to the envelope, so called carrier-envelope (CE) phase, is an important parameter to completely describe the electric field. We have tried to see the effect of CE phase in two different laser pulse duration regimes namely few cycles ($\tau_1 = 2T_0$ with T_0 as one laser cycle) and many cycles ($\tau_2 = 8T_0$) for cluster targets.

The possibility of using laser driven deuterium or/and tritium cluster as a neutron source, poses this problem of laser-cluster fusion to be studied in chapter 6. In particular, we study the effect of laser intensity, cluster radius and inter-cluster distance on the neutron production by D-D or D-T reaction by using our MD code.

Finally the thesis is summarized with main conclusions in chapter 7. The future direction of the present work in also discussed in this chapter.

CHAPTER 2

Molecular dynamic simulation model and its validation

As mentioned in the previous chapter1, the interaction of high-intense laser with atomic clusters proceeds through three sub-processes : ionization of atoms via tunnel ionization, absorption of energy by collisional processes augmented by plasma resonance and further expansion of cluster by Coulomb explosion or hydrodynamic expansion. Theoretical modelling of these processes is quite demanding as these processes are nonlinera and nonpeturbative. In spite of that, various models have been put forward. Among them, the most widely used model is Ditmire's Nanoplasma model. Due to its limitation of treating the cluster in statistically continuum fashion, various particle models such as molecular dynamic and particle in cell models are developed to study the interaction process in more detail. In this chapter 2, we will describe our molecular dynamic (MD) model and validate it against various earlier theoretical and experimental results.

2.1 Numerical model

We have developed a time dependent three dimensional relativistic particle-particle (molecular dynamic abbreviated as MD for further usage) simulation model to study the interaction dynamics of rare-gas clusters driven by femtosecond laser pulses. In general, MD methods are employed to investigate the equilibrium properties or transport properties of a system close to the equilibrium. We have used MD methods to determine the temporal dynamics of a system, consisting of thousands of particles, driven by strong fields which is far away from thermal equilibrium.

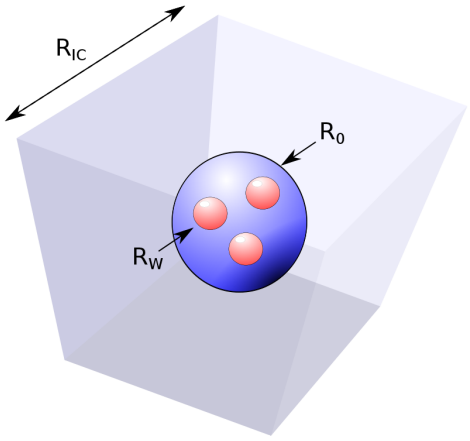

Figure 2.1: *Initial configuration of cluster inside the simulation box of size R_{IC}. R_0 is the radius of the cluster and R_W represents the Wigner-Seitz radius of the constituent atoms.*

2.1.1 Description of the initial configuration

We consider a rare gas cluster as a tightly bound system with N number of constituent atoms. The initial structure of rare gas cluster is assumed to be spherical with radius R_0. If the tightly bound cluster is assumed to be a spherical drop of liquid with density ρ, then number of atoms in the cluster can be calculated by dividing the total volume $(4/3\pi R_0^3)$ of the cluster by volume occupied by a single atom $(4/3\pi R_W^3$, where R_W is the Weigner-Seitz radius[1] of the atom. This description of cluster geometry as a spherical drop of liquid is analogous to the liquid drop model used in nuclear physics[83, 84]. Thus the total number of constituent atoms is written as

$$N = \left(\frac{R_0}{R_W}\right)^3. \tag{2.2}$$

In our simulation model, the single cluster is assumed to be located at the origin of

[1] R_W is equal to the radius of a sphere whose volume is equal to the mean volume per atom in the system under consideration.

$$\begin{aligned} \frac{4}{3}\pi R_W^3 &= \frac{V}{N} = \frac{1}{n} \\ R_W &= \left(\frac{3}{4\pi}\frac{1}{n}\right)^{1/3} \\ &= \left(\frac{3}{4\pi}\frac{M}{\rho N_a}\right)^{1/3}, \end{aligned} \tag{2.1}$$

where M is the molar mass, ρ is the mass density, n is the number density and N_a is the Avogadro's number. For example R_W is $1.70, 2.02, 2.40$, and $2.73\mathring{A}$ for deuterium, neon, argon, and xenon clusters, respectively[73].

coordinate system inside a three dimensional simulation box extending from $-R_{IC}/2$ to $+R_{IC}/2$ along all three coordinate axes x, y and z. The cluster is situated exactly in the center of the simulation box. Actually the size of the simulation box is equal to the distance between two cluster *i.e.* an identical cluster is placed at distance R_{IC} along all six directions $(+x, +y, +z, -x, -y, -z)$. This distance between two cluster is taken to be, in general, an integral multiple of cluster radius $R_{IC} = n \times R_0$. The parameter n depends upon the density of clusters *i.e.* the cluster density is more, the distance between two clusters will be less and so the number n. Opposite occurs when cluster density is less. In general we have chosen this number to be approximately equal to 20 following the earlier simulations[71, 72]. In general, the volume occupied by the single cluster is very small roughly $\approx 1\%$ compared to total volume of the simulation box. The space between between the cluster and surfaces of the box is assumed to be empty. Strictly speaking, for initial distribution of atoms inside the cluster, one should choose according to the lowest energy configuration[85] assuming the inter-atomic potential to be of the form Lennard-Jones ($V_{LJ} = 4\epsilon \left\{(\sigma/r)^{12} - (\sigma/r)^{6}\right\}$), where σ is the depth of the potential well and ϵ is the characteristic length) type. These techniques are used for position determination of atoms within the cluster consisting of hundred of atoms. Since we are dealing with clusters consisting of several thousand of atoms, one has to go for approximate methods. One of them is the random placement of atoms inside the cluster of radius R_0. We have used this technique for initial atomic configuration. Further we assume that all atoms in the cluster are initially stationary. This is due to the fact that initial motion of atoms in the cluster is insignificant compared to the final highly energetic motion of particles (ions as well as electrons) as a outcome of cluster explosion under intense laser irradiation.

This single rare gas spherical cluster of radius R_0 is irradiated by a high intensity near infra-red ($\lambda = 800nm$) laser pulse propagating along y-direction and polarized in the x-direction. This kind of laser propagation leads to the variation of electric and magnetic fields along parallel to x and z axes, respectively, *i.e.*, $\mathcal{E} = [\mathcal{E}_x, 0, 0]$ and $\mathcal{B} = [0, 0, \mathcal{B}_z]$. The coupling of the laser pulse to an electron at position $\vec{r}$ is considered

in the dipole approximation such that that the interaction potential can be written as

$$V_{las}\left(\vec{r},t\right)=e\vec{\mathcal{E}(t)}\cdot\vec{r}. \tag{2.3}$$

This treatment is well justified in our case as the typical sizes of the cluster are much smaller than the wavelength of the shining laser. Consequently, the spatial variation of laser electric field is ignored across the dimensions of the cluster and only temporal variation of the electric field is worth-considering. In our simulations, we have used mainly Gaussian time profile for laser intensity, unless otherwise stated. The expression for temporal profile of laser intensity reads as

$$I(t)=I_0\exp\left\{-2.77\left(\frac{t}{\tau}-1.6)\right)^2\right\}\ W/cm^2, \tag{2.4}$$

where $I_0(W/cm^2)$ and τ represent the peak laser intensity ans full width at half maximum (FWHM) pulse duration, respectively. Clearly, the peak of the laser pulse is shifted from origin and is placed at $t=1.6\tau$. This pulse is similar to the pulses used previous experiments and simulations[43, 73]. The time dependent electric and magnetic fields are related with intensity as

$$\mathcal{E}(t)=\mathcal{E}_0(t)\cos(\omega t) \tag{2.5}$$

$$\mathcal{E}_0(t)=3\times10^4\sqrt{8\pi I(t)10^5/c}\quad V/m \tag{2.6}$$

$$\mathcal{B}(t)=\mathcal{E}(t)/c,\quad T \tag{2.7}$$

where ω is laser frequency and $c(m/s)$ is the velocity of light.

2.1.2 Ionization mechanisms for laser driven clusters

2.1.2.1 Optical field ionization

As mentioned earlier, the choice of cluster material in our simulation studies is mainly rare gas (Ar, Kr, Xe) clusters and typical intensities of irradiating laser are $\sim 10^{16}W/cm^2$

at near infrared wavelength ($\lambda = 800nm$). As described in the previous chapter 1, the Keldysh parameter $\left(\gamma = \sqrt{I_p/2U_p}\right)$ which decides the mode of initial ionization (tunnel or multi-photon[23]) due to the incident laser, turns out to be much smaller than 1 for the laser and cluster parameters used in our studies. For example, γ is equal to 0.10078 for Xe cluster with first ionization potential as $I_p = 12.13eV$ and laser ponderomotive potential as [1] $U_p = 5.9712 \times 10^2 eV$. Similar trends follow for other clusters ($I_p = 13.999, 15.759eV$ for Kr and Ar) at typical laser intensities of $\sim 10^{16} W/cm^2$. This simple calculation of Keldysh parameter suggests that initial ionization mechanism of atoms commences due to tunnel or optical field ionization in the presence of intense laser fields[24–26]. Due to the complexity of Perelomov-Popov-Terentev (PPT) tunnelling rate, we use Ammosov-Delone-Krainov (ADK) rates for tunnel ionization. It is important to note that ADK rates are easier to compute and can be easily attached with a online code which repetitively calculates these rates as time progresses. The ADK rate formula W_{ad} for optical field ionization (OFI) as a function of laser field strength reads as[**?**],

$$\begin{aligned} W_{ofi} = & \left(\frac{3\mathcal{E}_0 n^{*3}}{\pi Z^3}\right)^{1/2} \frac{(2l+1)(l+|m|)!}{2^{|m|}(|m|)!(l-|m|)!} \\ & \times \left(\frac{2e}{n^*}\right)^{2n^*} \frac{1}{2\pi n^*} \left(\frac{2Z^3}{\mathcal{E}_0 n^{*3}}\right)^{2n^*-|m|-1} \\ & \times \left(\frac{Z^2}{2n^{*2}}\right) exp\left(-\frac{2Z^3}{3n^{*3}\mathcal{E}_0}\right) \frac{1}{2.4 \times 10^{-17}} \quad s^{-1} \end{aligned} \tag{2.8}$$

where $\mathcal{E}_0 = \sqrt{2 \times 10^4\, I/(c\, \varepsilon_o)}/5.14{\times}10^{11}$ is the electric field in atomic units, $I(W/cm^2)$ is the intensity of laser light and c is the speed of light in SI units, ε_o is the permittivity of free space, Z is the degree of ionization, $n^* = Z/\sqrt{2I_p}$ is the effective quantum number, I_p is the ionization potential in atomic units, e is the charge of electron, l and m are the orbital and magnetic quantum numbers of outer electron respectively. Ionization rate is calculated for each value of m and averaged over it. It is important to note that the ADK rate formula used in Eq. 2.8 reverts back to the ADK rate introduced in Eq. 1.29 of chapter 1 when the value of n^* is put as equal to $Z/\sqrt{2I_p}$ in this Eq. 2.8.

[1] $U_p = 9.33 \times 10^{-14} eV \times I_0[W/cm^2] \times [\lambda(\mu m)]^2$

It is important to note that ionization ignition model of laser driven small rare gas clusters described in chapter 1, considers the electric field of neighbouring ions while calculating the ionization due to the incident laser pulses. The consideration of the field of neighbouring ions can be very significant in certain situations like, (1) the density of atoms in cluster is too high, which manifests small internuclear distance between atoms, and (2) the interaction of very short but high intensity laser pulse, which will result in quick ionization of cluster atoms to higher charge states without any significant motion. In our simulation studies, we have not considered the situations in which the above mentioned conditions meet. Also, the ADK rates used in our model are derived only for harmonic electromagnetic field variations where as the inter-cluster fields are highly irregular. Thus it would be an over-simplification to replace the laser electric field appearing in the ADK rate Eq. 2.8 by a resultant electric field which is sum of laser electric field and inter-cluster field in situations mentioned above. To account for these possibilities, one has to calculate directly the tunnel integral in the combined potential of laser and other particles which further leads to calculation of tunnelling rate[86]. Furthermore it should be noted that even though at later stage we achieve some higher charge states, but by that time the cluster will expand enough to lower the possibility of ionization due to the field of the neighbouring ions.

2.1.2.2 Impact ionization

As mentioned earlier, tunnel ionization is initiating mechanism for cluster atoms under the intense laser field irradiation. Due to high density of atoms/ions in the cluster, possibility of impact ionization of atoms/ions can not be ruled out. Moreover, it has been experimentally pointed out that collisional ionization is a very important mechanism for further creating the high charge states due to high energy electrons achieved as a results of gigantic resonance in the cluster plasma[43]. As the sufficient number of electrons gets accumulated in the system, they further create new charge states due to their inelastic scattering to atoms/ions. Knowledge of impact cross-section is an essential ingredient to calculate the impact ionization rate. If σ_{ei} denotes the impact

cross section for an individual electron with ionization potential I_p due to the impacting electron with energy ($E > I_p$), the sub-shell cross section for all q_i equivalent electrons will be q_i times σ_{ei}. Now the total impact cross section (σ) of the atom with N sub-shell with corresponding sub-shell cross sections $\sigma_i = q_i\sigma_{ei}$ can be written as

$$\sigma = \sum_{i=1}^{N} \sigma_i. \tag{2.9}$$

Lotz[78] proposed an empirical formula for calculations of σ from the ground state that can be written as

$$\sigma = \sum_{1=1}^{N} a_i q_i \frac{\log(E/I_p)}{EI_p} \left\{1 - b_i \exp\left[-c_i(E/I_p - 1)\right]\right\}; \;\; ; E \geq I_p, \tag{2.10}$$

where i=1 is the outermost shell, i=2 is the next inner sub-shell, etc. In this equation, a_i,b_i and c_i are individual constants, which have to be determined by experiment, theory or reasonable guess work. Generally the b_i and c_i are much smaller than value of a_i and one can take value of $a_i = 4.5 \times 10^{-14} cm^2(eV)^2$ and $b_i = 0$ for four times and higher ionized ions as mentioned by Lotz[79]. So we ignore the values of b_i and c_i in comparison of a_i. Further, formula2.10 can be clubbed togther with a Maxwelian elecron distribution at tmeperature T

$$\frac{dn}{n} = \frac{2}{kT}\left(\frac{E}{kT}\right)^{1/2} \exp(-E/kT)dE \tag{2.11}$$

and yields the rate of impact ionization (s^{-1})

$$W_{ci} == 6.7 \times 10^{-7} \frac{n_e \; a \; q}{I_p\sqrt{kT_e}} \int_{I_p/kT_e}^{\infty} \frac{e^{-x}}{x} dx \qquad s^{-1} \tag{2.12}$$

where a is given in $10^{-14} cm^2(eV)^2$, and I_p and kT_e in eV. Here we have only considered the contribution from the outermost sub-shell ($i = 1$) and so removed the symbol of $\sum$ and subscript i.

The collisional ionization rates for neutral Xe (I_p = 12.49 eV), Xe^{25+} (I_p = 0.86 KeV) and Xe^{43+} (I_p = 3.33 KeV) as a function of electron energies are presented in

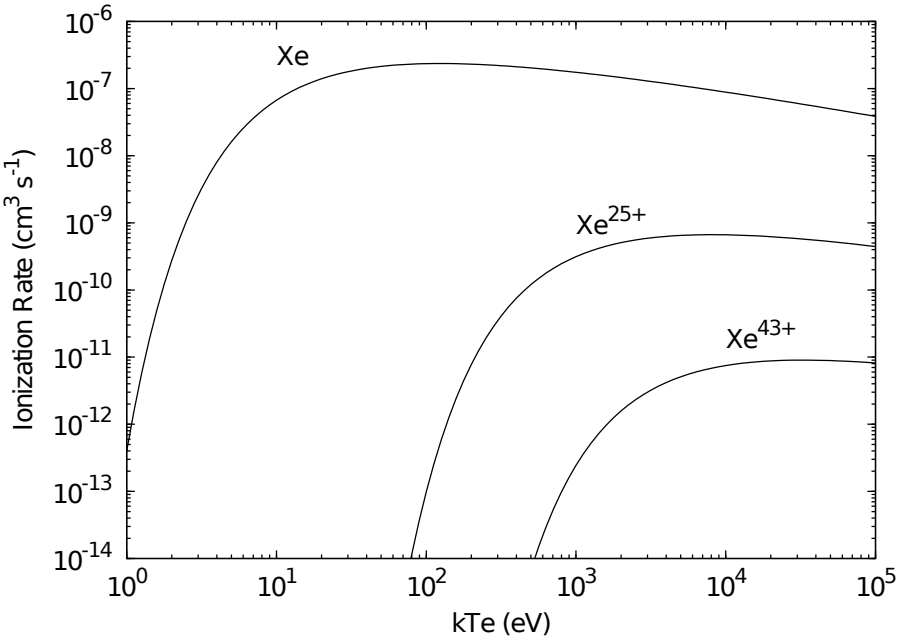

Figure 2.2: *Collisional ionization rates for Xe, Xe^{25+} and Xe^{43+} as a function of impact electron energies.*

Fig. 2.2. The results using this classic model are in excellent agreement with the one semi-relativistic configuration-average distorted-wave method presented by Loch et al. [87].

It is important to note that empirical cross-sections for impact ionization are not necessarily very practical from the point of view of users. As in our case, we deal with a large number of atoms with tens of ionized charge states and we have to calculate these rate coefficient again and again which makes their use a bit time consuming. Therefore, we look for some fitting formulas so that one time operation can solve the purpose. Voronov et al[88], suggested a fitting formula for the elements with atomic number ranging from 1 to 28

$$W_{ci} = n_e \, A \frac{(1 + P \, U^{1/2})}{(X + U)} U^K e^{-U} \quad s^{-1} \tag{2.13}$$

where $U = I_p/kT_e$, n_e, I_p and kT_e are electron density, ionization potential (eV) and

electron temperature (eV) respectively. P, A, K, X are adjustable parameters.

In our code, impact ionization rates are calculated by Voronov's fitting formula given by Eq. 2.13 for light element ($Z < 28$) clusters like Ar, Kr. For heavier element clusters like Xe, we have used the Lotz empirical collisional ionization rate given by Eq. 2.12.

It should be noted that the collisional ionization rates calculated by Eqns. 2.12 and 2.13 relies on the electron density, i.e. the assembly of thermal electrons, which is calculated by the knowledge of the number of electrons inside the cluster. It might be a matter of debate that the plasma formed by the cluster qualifies to be thermal so that the collisional ionization can be calculated by the Lotz formula. However, in previous studies the usage of this methodology is proved to be very efficient in predicting the charge states seen experimentally [43, 89].

2.1.2.3 Implementation of ionization

The final removal of electron with the atom is performed in Monte-Carlo fashion as our code is a particle-particle code *i.e.* we deal with the individual particles, not with the fluid. It is customary to use ionization rates directly in the rate equation dealing with the number of particles in hydro-codes. In our case, we have to decide whether a particular atom will be ionized or not *i.e.* either it is 0 or 1, nothing in between. In other words, hydro-codes involve the smooth evolution of charge states whereas particles codes rely on the method of jump (increase the charge by one). It is the reason Monte-Carlo decision making comes into the picture. Once we know the tunnel ionization rate (Eq. 2.8) and impact ionization rate (Eq. 2.12 or 2.13) as a function of time, total ionization rate $W = W_{ofi} + W_{ci}$ and ionization probability $W\Delta t$ are calculated for each ion and atoms after each time step Δt. A random number lying in between 0 and 1 is generated and if the number is less than the ionization probability then only the ion is ionized and one electron is created. The created electron is placed randomly in the spherical vicinity of radius $0.25R_0$, with parent atom be at the centre. This is mainly done to avoid the charge imbalance in the cluster.

Here we want to make couple of comments. We have not considered the recombi-

nation of electrons with ions in the present model as it is expected to be small for short pulse duration considered in our studies. In particular, the recombination is important when plasma cools from its hot state and this occurs at relatively longer time scale [43]. Furthermore, we have not accounted for the bound states explicitly. These bound states play an important role in the studies of x-ray emission from clusters. They can also influence the degree of ionization through two-step process *viz.* excitation followed by ionization [90]. However, we have ignored this two-step process following the earlier MD simulations [58, 67, 68].

2.1.3 Motion of charged particles

As it has been discussed in the previous section, charged particles (ions/electrons) are born as a result of tunnel or impact ionization. For the determination of movement of these charged particles, one has to calculate the total force that they experience. In the present case, charged particles experience two kinds of forces : one is the laser electromagnetic force ($\vec{F}_{Las}$) and the second is the Coulomb force ($\vec{F}_{Cou}$) due to the other charged particles present in the cluster. The total force ($\vec{F}_i$) acting on i^{th} particle at time t is given as,

$$\begin{aligned} \vec{F}_i &= \vec{F}_{Laser} + \vec{F}_{Coulomb} \\ &= q_i[\vec{E(t)} + \vec{v_i} \times \vec{B(t)}] + \sum_{\substack{k \\ i \neq k}} \frac{1}{4\pi\epsilon_0} \frac{q_i q_k \vec{r_{ik}}}{r_{ik}^3}. \end{aligned} \tag{2.14}$$

where, $\vec{v_i}$ and q_i is the velocity and charge of the i^{th} particle, r_{ik} is the distance between two particles with $\vec{E(t)}$ and $\vec{B(t)}$ being the laser electric and magnetic fields respectively.

Here, we want ot make an important point regarding the calculation of binary Coulomb force which goes as N^2 for say N number of particles. This is one of the main problems associated with MD simulations. This Coulomb force calculations becomes extremely time consuming for cluster sizes greater than $15\mathring{A}$. In order to avoid this problem, lumping of particles into pseudo macro-particles is done to reduce the

computational cost[71]. A macro-particle consists of n identical particles with a charge qn and mass mn (q and m are the charge and mass of the individual particle). The total number of macro-particles in the system N_{Macro} is obtained by dividing the total number of atoms N_{atom} as given by Eq. 2.2, to the number of particles per macro-particle n *i.e.* $N_{Macro} = N_{atom}/n$. The parameter n is carefully chosen. On one hand, it should be large enough so that the number of macro-particles in the system is not too big. On the other hand, n must be small enough to prevent macro-particles from attaining excessively large charge resulting in too strong binary Coulomb interactions. This leads to non-physical results[71]. For any calculations to take-off, one has to predefine the number of macro-particles (neutral atoms) at the beginning of the simulation. It is important to note that ionization of cluster atoms leads to generation of new electron macro-particles while the number of ion macro-particles remains same, in course of time.

As it can be seen from the total force Eq. 2.14, the Coulomb force ($\vec{F}_{Coulomb}$) has a singularity at a zero inter-particle separation. So, one has to regularize the Coulomb interaction at excessively short distances in order to achieve the stability of the classical Coulomb system and to avoid the classical ion-electron recombination. It is achieved by smoothing the Coulomb interaction either by inserting a cutoff[91] to the potential or attributing an effective width of size to the particle[71]. We have considered the finite size of the macro-particles, in view of this $r_{ik} \equiv \sqrt{|r_i - r_k|^2 + r_0^2}$, with r_0 being the smoothing term which is introduced in the definition of r_{ik} to avoid a steep increase in forces at very small distances.

After the calculation of the force, each particle is then advanced to its new position according to its relativistic equations of motion [71],

$$\frac{d\vec{p_i}}{dt} = \vec{F_i} \tag{2.15}$$

$$\vec{v_i} = \frac{\vec{p_i}/m_i}{\left(1 + \frac{|\vec{p_i}|^2}{(m_i c)^2}\right)^{1/2}} \tag{2.16}$$

$$\frac{d\vec{r_i}}{dt} = \vec{v_i}. \tag{2.17}$$

Here, $\vec{p_i}$, $\vec{v_i}$, $\vec{r_i}$ and m_i are relativistic momentum, velocity, coordinate and mass of the i^{th} particle. One may note that Eq. 2.16 can be easily obtained from the definition of relativistic momentum $\vec{p_i}$ and relativistic γ_i factor

$$\vec{p_i} = \gamma_i m_i \vec{v_i} \tag{2.18}$$

$$\gamma_i = \frac{1}{\left(1 - \frac{|v_i|^2}{c^2}\right)^{1/2}} \tag{2.19}$$

Substituting the value of $\vec{v_i}$ from Eq. 2.18 to Eq. 2.19 yields

$$\begin{aligned} \frac{1}{\gamma_i^2} &= 1 - \frac{|p_i|^2}{(m_i \gamma_i c)^2} \\ \frac{1}{\gamma_i^2}\left(1 + \frac{|p_i|^2}{(m_i c)^2}\right) &= 1 \\ \frac{1}{\gamma_i} &= \frac{1}{\left(1 + \frac{|\vec{p_i}|^2}{(m_i c)^2}\right)^{1/2}} \end{aligned} \tag{2.20}$$

Substituting the final value of $1/\gamma_i$ from Eq. 2.20 to Eq. 2.18 yields the same velocity ($\vec{v_i}$) Eq. 2.16 which is solely dependent on relativistic momentum ($\vec{p_i}$),

$$\begin{aligned} \vec{v_i} &= \frac{\vec{p_i}/m_i}{\gamma_i} \\ &= \frac{\vec{p_i}/m_i}{\left(1 + \frac{|\vec{p_i}|^2}{(m_i c)^2}\right)^{1/2}}. \end{aligned} \tag{2.21}$$

2.1.4 Boundary conditions

Once we have defined the equation of motion for charged particles in the laser electromagnetic field and Coulomb field of rest of the charged particles, we have to also mention about the appropriate boundary conditions to give a fruitful result. In our case, we can define any of the three boundary conditions : open, periodic or mixed boundary conditions, depending upon the nature of the problem under consideration. Sometimes, the density of the clusters is extremely low in laser cluster interaction regime such that each cluster does not feel the presence of the neighbouring clusters. In this situation, one can use the open boundary condition (OBC) *i.e.* the particle can

go anywhere in the space. When the experimental conditions demand that presence of neighbouring clusters can affect the interaction dynamics of cluster under consideration, one can use the option of periodic boundary conditions (PBC). To formally apply PBC, we have to define the extent of the three dimensional computational box of size R_{IC} (R_{IC} is equal to the inter-cluster distance) :

$$-R_{IC}/2 \leq x \leq +R_{IC}/2 \tag{2.22}$$

$$-R_{IC}/2 \leq y \leq +R_{IC}/2 \tag{2.23}$$

$$-R_{IC}/2 \leq z \leq +R_{IC}/2. \tag{2.24}$$

The PBC is imposed by demanding two conditions (a) any particle leaving the computational box along any direction reappears from the opposite direction in the computational box with the same velocity, and (b) the electromagnetic field produced by the charged particles from adjacent clusters is also added to the Coulomb and laser fields in the cluster under consideration. It has been shown by Petrov *et al*[72] using tree algorithm for large cluster driven by intense lasers that the Debye length is comparable to the cluster radius during the expansion of the cluster. This means that the electrostatic field of individual clusters is well shielded and has negligible effect on neighbouring clusters. Moreover their calculations even after adding this coulomb field does not the change the results like absorbed energy per cluster, electron and ions density etc. by few percent. This is the reason why we have only implemented the PBC in terms of particles, not in fields. The purpose of mixed boundary condition is to insure the fast ionization of cluster atoms via periodic boundary condition (as it will mimic the presence of neighbouring clusters) and the free flight of the particles will then be insured by the open boundary condition, where the presence of neighbouring cluster is not important.

2.1.5 Interpretation of the results

Once a typical computer experiment using the MD simulation model, as described in the previous section, is over, it generates a huge data consisting of information about

the positions, velocities and charge states of all the particles at each time step. We only store the data at selected time steps. It is difficult to interpret the results directly from this raw data. To get some useful information about the interaction dynamics of laser driven clusters using MD simulation methods, we have to define some global average parameters like radius of the cluster, average degree of ionization etc. One calculate either their time dependent behaviour or final result when the pulse is over.

A very important parameter which is associated with the outward motion of ions, is the time dependent cluster radius which is defined as mean standard deviation of all the ions from the origin. More specifically, one can write cluster radius (R) as

$$R(t) = \sqrt{2\sum_{i=1}^{N}[x_i^2(t) + y_i^2(t) + z_i^2(t)]/N}, \tag{2.25}$$

where the sum is over only atoms or ions. The factor of two is introduced to roughly match the the cluster radius at time $t = 0$.

In terms of cluster ionization, a very important concept introduced earlier, is concept of inner ionization and outer ionization. Defining the cluster boundary by $R(t)$, the electrons which are detached from their parent atoms but are still confined inside the cluster, are termed as inner electrons. Mathematically it is equivalent to call those electrons as inner electrons which satisfy the requirement $|r_k(t)| \leq R(t)$, where $r_k(t)$ is the distance of the k^{th} electron from the center of the coordinate system. Similarly, the electron which have overcome the Coulomb forces of ions and crossed the cluster boundary, are termed as outer electrons. The condition for outer electrons is defined as $|r_k(t)| \geq R(t)$, where $r_k(t)$ and $R(t)$ have been already defined. We can easily count the total number of inner and outer electron at each each instant of time which satisfy the above mentioned inequalities and can plot the time dependent variation of population of inner and outer electrons.

The other parameter of concern is average degree of ionization of cluster under consideration. This time dependent parameter is defined at each time step by dividing the the sum of all ion charges to the total number of ions. One can also have the information about distribution of charge states during the cluster expansion as well

as at the end of the laser pulse. Similarly one can define the average kinetic energy of ions and average kinetic energy of electrons.

Another important quantity of interest is energy distribution functions of ions as well as electrons. This parameter is directly obtained in the experiments, so it is of much interest to determine it via simulations. The electron and ions energy distribution function (EEDF and IEDF) is calculated as,

$$EEDF = \frac{n(\mathcal{E})}{\sqrt{\mathcal{E}}\ \Delta\mathcal{E}} \quad eV^{-3/2} \qquad IEDF = \frac{n(\mathcal{E})}{\Delta\mathcal{E}} \quad eV^{-1}$$

where, $n(\mathcal{E})$ are number of particles in energy range $\mathcal{E}$ and $\mathcal{E}+\Delta\mathcal{E}$, $\Delta\mathcal{E}$ is the energy bin size. For EEDF the $\Delta\mathcal{E}$ is taken as $1/50$ of maximum electron energy and for IEDF it is taken as $1/10$ of maximum ion energy. It is important to note that these distributions can be measured with angular resolution which has an application to tell the nature of the explosion of cluster *viz.* isotropic or anisotropic.

2.2 Validation of the code

Before using our MD code to study a new problem in laser driven clusters, we have to validate it against earlier theoretical as well as experimental results. In this section, we intend to present some essential physics aspects of laser cluster interaction. For all the results presented in this article we have used PBC (otherwise stated). So the particles upon arrival on any side of the cube, reappears with same velocity on opposite side.

2.2.1 Comparasion with earlier computational results

In this section, we have used our MD code to study the gross features of laser-cluster interaction. Moreover, we have compared our results with the earlier published computational results with the same input parameters so that we can verify our results.

2.2.1.1 General features of laser driven Ar clusters

We have studied the interaction of 125 fs, 800 nm laser pulse with peak intensity of 10^{16}W/cm^2 with Deuterium, Argon and Xenon clusters. Figure 2.3 presents results of the interaction of the above mentioned laser with Xenon clusters of radius 50 Å. The

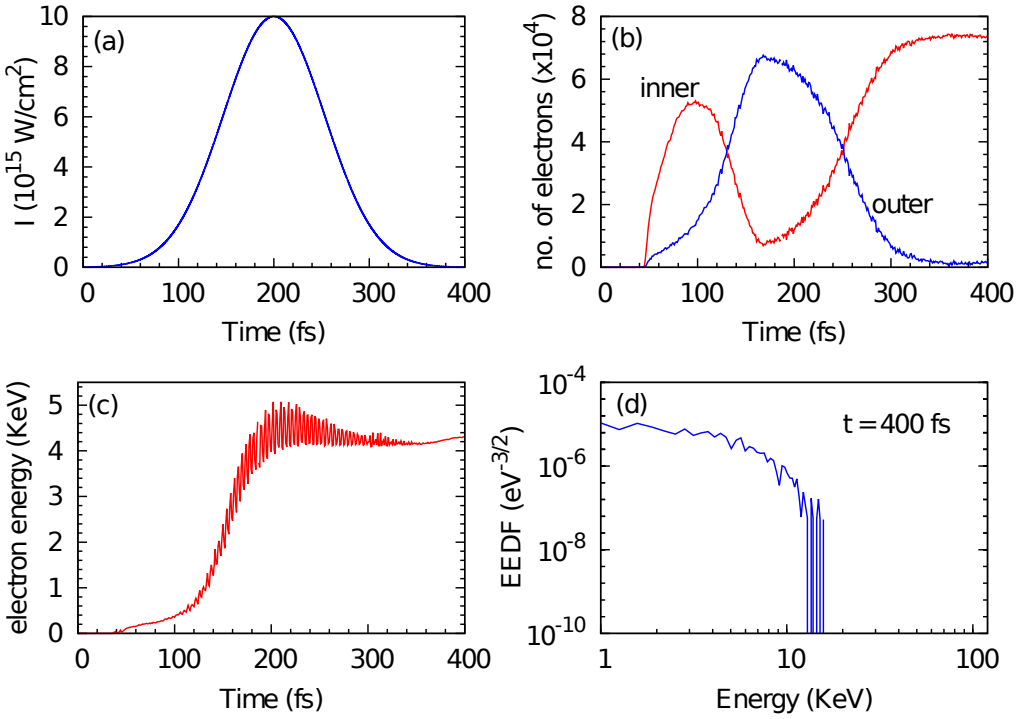

Figure 2.3: *Temporal profile of the laser pulse (a), inner and outer electrons (b), mean kinetic energy of electrons (c) and EEDF at 400 fs (d) are presented for 50 Å Xenon cluster.*

inter cluster distance (R_{IC}) in this case is considered to be $20R_0$. Typical laser pulse profile is shown in Fig. 2.3(a), however Fig. 2.3(b) shows the temporal evolution of inner and outer electrons. The time dependent population variation of electrons is a result of constant interplay of inner ionization, outer ionization and cluster expansion. Initially at time $t = 0$, all the particles in the cluster are neutral atoms and remain inside the cluster. It is quite obvious to see that both N_{in} and N_{out} are zero at time $t = 0$ due to the absence of any driving laser field. As the lase pulse is switched on, still we do not see any population increment in neither N_{in} nor N_{out} till time $\sim 40fs$. After this

time, tunnel ionization of cluster atoms start taking place at sufficient laser intensity. After some time, collisional ionization will also come into the picture to further create ionization due to inelastic collisions of electron with atoms/ions. Due to combined action of these ionization processes, the inner electron population quickly rises. The rate of increase of corresponding population of outer electrons is comparatively slower as the electrons have not gained sufficient energies to over come the Coulomb barrier of the cluster. The monotonous increment in N_{in} stops at time $t \sim 90fs$ whereas N_{out} continues to grow with increased rate from this time onwards. Moreover we observe from the Fig. 2.3(b) that N_{in} further decreases after this time. The opposite behaviour of the two populations is due to the reason that residual Coulomb field is not sufficient to hold the inner electrons further inside the cluster periphery. Consequently, N_{in} reduces whereas N_{out} increases with time. This behaviour continues till $t \sim 170fs$ and then reverses after this time *i.e.* inner population increases whereas outer population decreases. This reason is that cluster expansion due to the mutual repulsion of residual positive ions becomes effective after this time so that it acquires the outer electrons and convert them in the inner electrons. Finally the cluster completely disintegrates and all the outer ones become inner ones.

The temporal variation of electron mean kinetic energy (KE) in shown in Fig. 2.3(c). It is observed from this plot that mean KE of electrons first increases very slowly, suddenly at a time ($t \sim 100$) the slope of the increase of KE changes significantly. From this time onwards, the enhancement in the KE of electrons is quite rapid. Actually, the main contribution to mean KE of electrons is due to inverse bremsstrahlung heating and ponderomotive or oscillatory energy due to the oscillatory electromagnetic field of the incident laser. Initially both of these mechanisms of electron heating are small as the main production of electrons is due to the tunnelling only. After a significant time, when sufficient number of electrons are born, they start creating collisional ionization to further increase the population of electrons. This effect along with the increasing oscillatory laser amplitude gives rise to the increase in mean KE of electrons. Furthermore, one can observe the prominent electron oscillations in the laser electric field between 150 - 300 fs, Fig. 2.3(c). Once the laser cycle is over, the final KE of elecrtons

turns out to be 4.5 KeV which is in good agreement with the earlier MD simulations carried out by *Petrov et al [71] (Fig. 7e)* with the similar laser and cluster parameters. Sometimes, we are also interested in a parameter which describes how the various electrons are distributed with their energies. The corresponding parameter is known as electron energy distribution function (EEDF) and that is shown in Fig. 2.3(d) with log scales. It is observed that EEDF follows the Maxwell-Boltzmann distribution till a particular energy and then it suddenly drops with a cut off energy[1]. In our case the maximum or cut-off energy of electrons is found to be about 20 KeV.

2.2.1.2 Effect of cluster material on temporal dynamics of various types of clusters

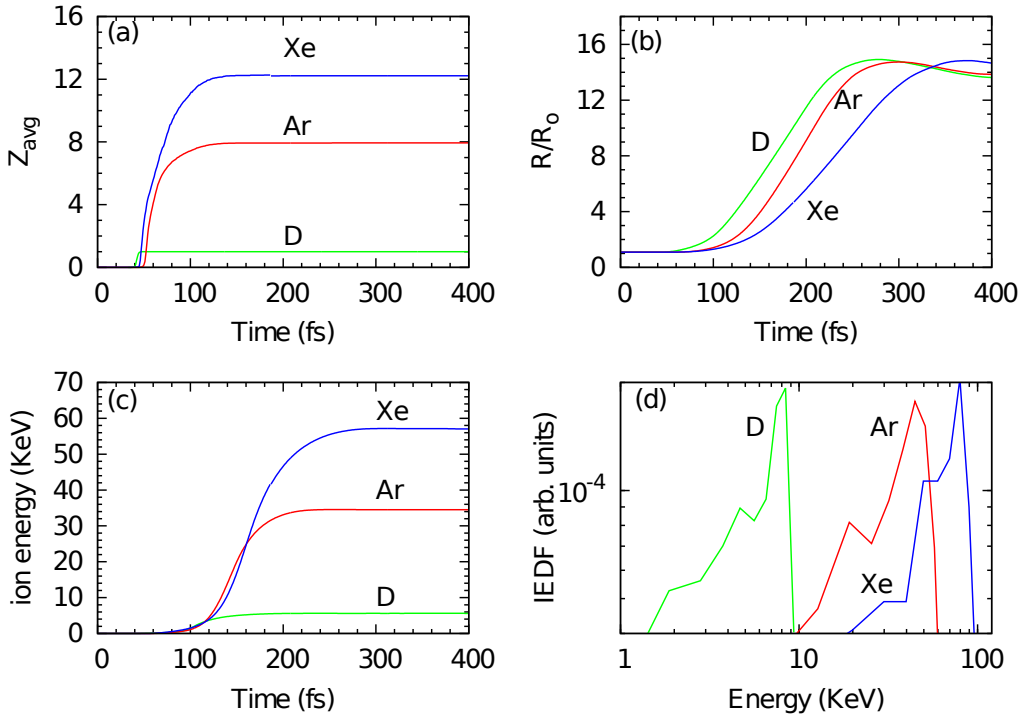

Figure 2.4: *Various physical quantities like average degree of ionization (a), temporal evolution of cluster radius (b), mean energy of ions (c) and IEDF (d) for Deuterium (green), Argon (red) and Xenon (blue) are presented.*

[1]For Maxwell-Boltzmann distribution to hold, one should get a straight line on the log scale when the number of electron lying in the energy range E and $E + dE$ is plotted against energy E.

Below we present some simulation results on clusters of different materials *Deuterium(D), Argon(Ar) and Xenon(Xe)* to determine how the change in type of cluster material affects the various global average parameters like average degree of ionization, cluster radius etc. For these results, we have used $100\mathring{A}$ Deuterium along with the $50\mathring{A}$ Argon and Xenon clusters. The peak intensity and FWHM pulse duration of irradiating laser are chosen as $10^{16}W/cm^2$ and $125fs$. The intercluster distance (RIC) in all these cases are considered to be $20R_0$, where R_0 is the initial cluster size. The variation of average charge per atom(Z_{avg}) for various clusters is presented in Fig. 2.4(a). It is important to see that ionization starts at different instant of time for different clusters. Since the ionization potential (IP) for D is smallest in all the elements, so its ionization starts at the earliest that follows for Xe and then Ar.[1]. Since the Deuterium atoms has only a single electron, so average charge per atom quickly saturates at 1. For other clusters, the ionization starts at near around $t \sim 40fs$ when the intensity of laser becomes sufficient to tunnel ionize the atoms. The initial quick rise in Z_{avg} at initial time is due to the tunnel ionization. Later, collisional ionization starts which is comparatively slower that leads to the change in the slope of plot between Z_{avg} and time t. Collisional ionization plays a major role in ionizing the cluster atoms, as can be seen from Fig. 2.4(a) that before the laser pulse peaks at 200 fs the atomic species attains the maximum charge states. This can be also validated using the short ($\sim$ 10 fs) laser pulses where most of the ionization took place after the completion of the laser pulse. Finally, the average charge per atom saturates at near about 12 and 8 for Xe and Ar clusters.

Next we describe the progress of cluster explosion in Fig. 2.4(b) where the temporal evolution of cluster radius ($R(t)$) is presented for all the species of cluster. As described in the upper paragraph where the average charge per atoms turns out to be maximum for Xe and minimum for D, one expects that the rate of cluster explosion has to be maximum for Xe and minimum for D. We obtain completely opposite of this in Fig. 2.4(b) where it is observed that D cluster expands at faster rate than Ar or Xe cluster. It suggests that consideration of ion charge only does not completely

[1] $IP_D < IP_{Xe} < IP_{Ar}$, where IP stands for the ionization potential.

explain the rate of expansion of cluster. One has to also consider the mass of the ion. Although Xe cluster shows the maximum Z_{avg} but it also has the maximum mass of the variuos types of ions under consideration. Consequently, its expansion velocity will be slower compared to the lightest Deuterium ion. Moreover, It was analytically shown by Krainov et al[92] that rate of expansion in case of Coulomb explosion can be written as

$$\begin{aligned} \frac{dR}{dt} &= \sqrt{\frac{2e^2N(Z-1)}{MR_0}}\left(1-\frac{R_0}{R}\right) \\ &\propto \sqrt{\frac{(Z-1)}{M}}, \end{aligned} \tag{2.26}$$

where R_0, M and $Z-1$ represent the initial radius, mass of the ion and average charge on the ion. Since the charge to mass ratio decreases monotonically from Deuterium ion to Xe ion, the rate of expansion also follows the same.

Fig. 2.4(c) represents the mean kinetic energy of ions for all clusters. It is important to note that the variation of the mean ion energy follows the same trend as obeyed by average degree of ionization as shown in Fig. 2.4(a). The mean kinetic energy of ions is found to be 58, 35 and 5 KeV for Xe, Ar and Deuterium clusters respectively. This can be explained easily by calculating the maximum ion energy(E_{max}) as $1/2M\,(dR/dt)^2$, where the value of dR/dt is taken from Eq. 2.26 as final or terminal velocity of ions. The final velocity of ions is found to be $\sqrt{2e^2N(Z-1)/MR_0}$ when R approaches to ∞. Thus the maximum energy of ions is obtained as $2e^2N(Z-1)/MR_0$, through which the average ion energy ($E_{avg} = 3/5E_{max}$) can be written as[73]

$$\begin{aligned} E_{avg} &= \frac{3}{5}\frac{N(Z-1)e^2}{R_0} \\ &\propto Z-1. \end{aligned} \tag{2.27}$$

It becomes clear from Eq. 2.27 that mean ion energy will be maximum for cluster species which possess the maximum charge per atom *i.e.* for Xe and on similar grounds will be minimum for D. The ion energy distribution function for all three cluster species is presented in Fig. 2.4(d). These results are in good agreement with

the studies of Petrov et al.[71–73].

2.2.1.3 Short pulse laser driven Xe clusters

We have also studied the interaction of comparatively short laser pulses with xenon clusters. For these studies, Xe_{2171} and Xe_{6100} are irradiated by $25fs$, $800nm$ laser pulses at peak intensities of 10^{15} and $2 \times 10^{16} W/cm^2$, respectively. These simulation

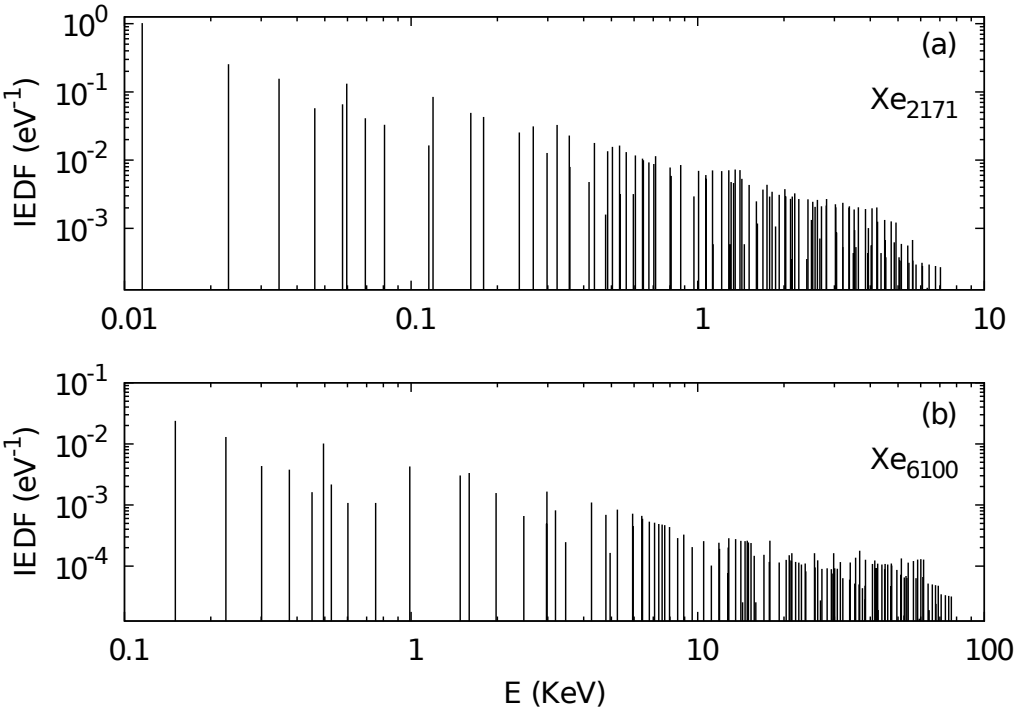

Figure 2.5: *Ion energies for Xe_{2171} (a) and Xe_{6100} (b) clusters are presented. The pulse duration of the laser pulse for both cases is 25 fs however the laser intensity is 10^{15} W/cm^2 for (a) and 2×10^{16} W/cm^2 for (b).*

parameters are same as used in recently published results of Heidenreich et al. [93, 94]. As the input parameter for cluster size in our code is cluster radius rather number of atoms in the cluster, the radius of the cluster ($R = N^{1/3}R_W$, with $R_W = 2.73\mathring{A}$ for Xe clusters) turns out to be equal to 35 and $50\mathring{A}$, respectively for Xe_{2171} and Xe_{6100}. Fig. 2.5 shows the ion energy distribution function (IEDF) for two clusters. The maximum energy for Xe_{2171} is found to be about 7 KeV, however the maximum energy for Xe_{6100}

is about 77 KeV. Our MD results show a good agreement with the results of Heidenreich et al. [93, 94]. They have also used MD methods to arrive upon these results. For the results presented in Fig. 2.5 we have used the open boundary conditions.

2.2.2 Comparasion with earlier experimental results

Although our MD results match well with the results of other computational methods with the same input parameters, the confirmation of any experimental findings using a simulation tool is a ultimate validation of the model used to investigate the problem. Keeping this in mind, we have also paid our attention to experimental aspect of laser-cluster interaction. We have investigated the interaction of 100 fs, 806 nm laser pulse of peak intensity 8×10^{15}W/cm^2 with Ar_{40000} clusters [95]. This experiment observed for the first time that energies of various ionic species after explosion of cluster depends upon the polarization state of the laser. Moreover, it was established that ion energy spectrum consists of two parts : higher energy portion which depends upon the laser polarization and low energy part which is completely isotropic. In the high energy part of IEDF, ion yield was more was more in the direction of laser polarization than perpendicular to it. The observed experimental results were explained on the basis of "charge flipping" model[95]. In this model, a net force starts acting on the ions along the laser polarization direction due to time dependent charge states arising from the continuous flipping of electrons from one pole to other and simultaneous emergence of higher charge states along this direction[77]. Consequently, the final energies of the ions also follow the same asymmetrical behaviour. The corresponding radius of the cluster turns out to be equal to $82\mathring{A}$ using equation $R = N^{1/3}R_W$, where $R_W = 2.4\mathring{A}$ and $N = 40000$ for Ar clusters. For a direct comparasion with experiments of *Kumarappan et al*, we have to determine the experimental observable which is nothing but the ion energy distribution function in this case. The IEDF is calculated along (0^0) and perpendicular (90^0) to the laser polarization directions at a virtual detector kept at distance of $10R_0$ from the center of the cluster. The corresponding IEDF along 0^0 and 90^0 is shown in Figure 2.6(a) while the fraction of different charge states at 50 and 350 fs are shown in Fig. 2.6(b). If we compare our MD results of IEDF with experimental

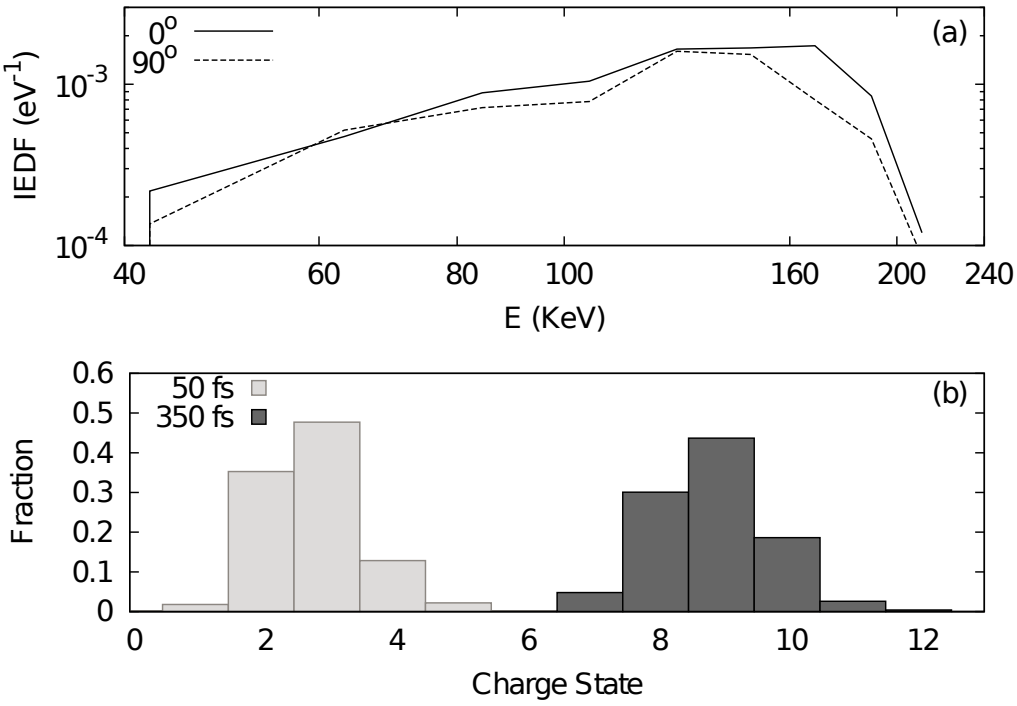

Figure 2.6: *The IEDF (a) for 82Å Argon cluster along (0^0) and perpendicular (90^0) to laser polarization direction is presented along with the fractional charge states at 50 and 350 fs (b).*

IEDF of *Kumarappan et al*, we find striking similarities in the two results. Our MD results correctly reproduces the experimental ion energies of $200KeV$. Moreover, the observed asymmetry along the laser polarization direction which was the essence of the experiment [95], is also verified in our results . As can be seen from Fig. 2.6(b) that in early stages most of the ions are doubly and triply ionized which due course of time enhanced to 8 and 9. The charge states so obtained are also in good agreement with the PIC study of same laser and cluster conditions [96].

As mentioned earlier, that the asymmetric explosion of the cluster is a result of charge-flipping process. We have tried to see this flipping of charges in our MD results. For that, we have plotted the positions of the electrons and ions at two consecutive laser half-cycles (Figs.2.7(a) and (c)) along with the charge state distribution in spatial $x - z$ cross section of the simulation domain (Fig.2.7(b) and (d)), where x and

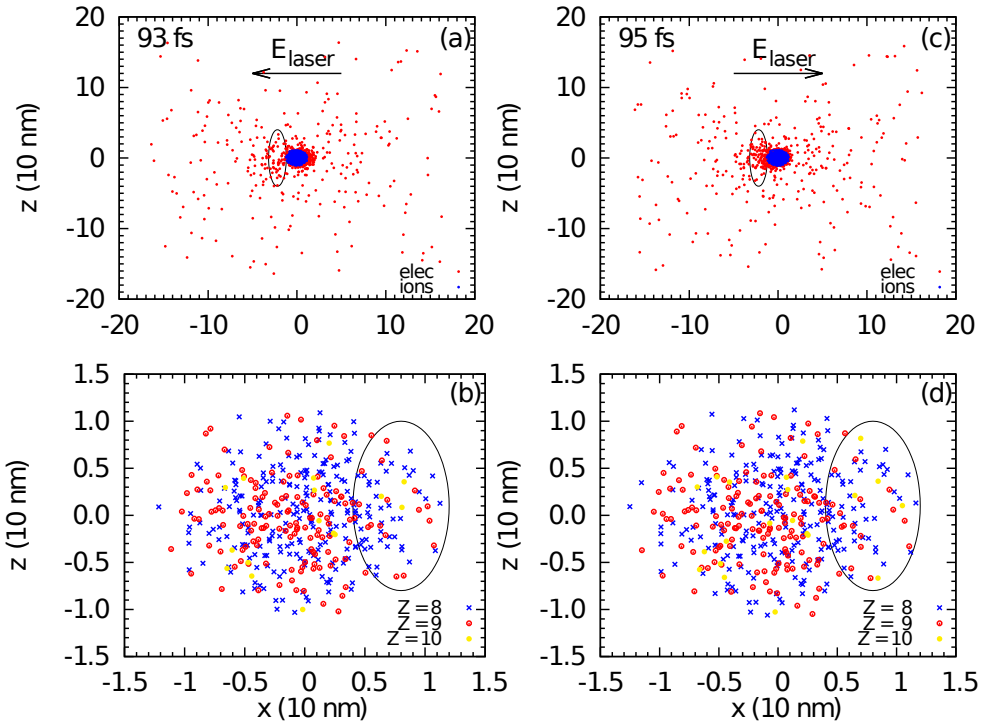

Figure 2.7: *Locations of the electrons and ions at 93 fs (a) with the distribution of different charge states at the same time (b). Similarly the positions of electrons and ions at 95 fs (c) with the distribution of different charge states at the same time (d). The ellipses are just to bring the focus to that particular area of the simulation domain.*

z axis denotes the directions along and perpendicular to laser polarization. It can be seen from the Figs. 2.7(a) and (c) that the laser electric field switches its direction from $93 fs$(a) to $95 fs$(c) during two consecutive time half cycles. Accordingly, electrons also change their position from one pole to the other pole with a change in electric field (encircled area). This flipping of the electrons population manifests the enhanced ionization of ions at poles. If we compare the different charge states at 93 fs (b) and 95 fs (d), it can be inferred that the ions at the pole are more ionized as compare to the ones which are at the equator (encircled area). The presence of higher charge states at the pole yields the asymmetric coulomb explosion along the laser polarization direction because of the charge imbalance introduced. Figure 2.7 confirms the presence of the charge flipping causes the asymmetric ion energy distribution along laser polarization

as predicted by *Kumarappan et al*[95].

2.2.3 Summary

In this chapter2, we have given a detailed description of our three dimensional time dependent relativistic molecular dynamic model. Starting from the initial conditions, various ionization mechanisms and further movement of charged particles, everything is explained quite extensively. Before using this code to study new problems in the field of laser-cluster interaction, we have to validate it. The existing code is verified by comparing its results with previous computational studies with the same input parameters. Various quantiles of interests like average charge per atom, average kinetic energy, cluster radius, energy distribution functions determined by using this code show a good level of agreement with previous computational results. We have also validated our code by directly comparing it with experimental results of asymmetric coulomb explosion of laser driven Ar clusters. The maximum ion energy in this case is found to be about 200 KeV which is quite close to the experiments. Further, we have calculated the distribution of ion energies along and perpendicular to laser polarization direction and observed an asymmetry along laser polarization direction. Thus we are able to match our results with the the asymmetry experiments where they also observed high ion yield along laser polarisation direction.

CHAPTER 3

Energetics of cluster nanoplasma : Effect of laser pulse duration and cluster density

The studies on laser driven clusters witnessed a great deal of interest from researchers all over across the world. Possibly the strongest reason of this great enthusiasm is the energetics of cluster nanoplasma, created after the irradiation due to short pulse intense lasers, that afterwards leads to the emission of highly energetic particles (both photons and ions). In this chapter3, we would like to address certain experimental parameters which strongly affect the energetics of cluster nanoplasma. Specifically, we intend to study how the FWHM pulse duration of the irradiating laser changes the absorption of laser energy by the cluster. Furthermore, we are also interested how the density of neighbouring cluster can affect the dynamics of the cluster under consideration. Specifically, we try to find out whether the final energies and charge states of ions after explosion depend upon the closeness of the clusters. All these issues will be raised in this chapter3 and we will try to find out the answer of these points by using our MD code.

3.1 Effect of laser pulse duration

3.1.1 Energy absorption : initial trends

As mentioned previously that the clusters are almost opaque to incident laser *i.e.* they absorb almost all the laser energy incident upon them[37]. Various theoretical models are put forward to explain this anomalous absorption of incident laser energy which is much higher compared to the gas and solid plane foil targets. In the introduction chapter1, we have described all these models in detail. It is noteworthy that, in spite

of a number of models proposed, the mechanism of energy absorption still remains debatable. We will briefly review all those mechanisms of energy absorption and find out the most suitable one which can adequately explain the results of enhanced energy by laser driven clusters.

Initial studies by *Ditmire et al* in the so called nanoplasma model, suggested linear resonance to be responsible for the enhanced energy absorption that occurs in the expansion stage of the cluster nanoplasma. Assuming the cluster as a dielectric sphere in the presence of spatially static yet time dependent electric, the electric field can be calculated as[56] $\mathcal{E} = 3\mathcal{E}_0/|\epsilon + 2|$, where $\mathcal{E}_0$ is the field outside the cluster and ϵ is the dielectric constant of the cluster plasma. It is important to note that electron density is assumed to be radially constant throughout the cluster expansion. Calculating the dielectric constant[1] of the plasma by Drude model of free electron gas[57], it can be shown that electric field approaches to maximum at time when $|\epsilon + 2|$ goes to minimum. Consequently, the heating of the plasma also enhances drastically at this point which is a clear-cut signature of the resonance. The condition $|\epsilon + 2|$ corresponds to plasma frequency $\omega_p = \sqrt{3}\omega$ or in terms of electron density $n_e = 3n_c$, where n_c is the critical density. Initially the cluster plasma is overcritical i.e. $n_e \gg 3n_c$ but as the plasma expands the electron density reduces and resonance occurs at $n_e = 3n_c$. It is also important to note that condition of resonance can also be obtained by microscopic modelling of the motion of inner electron cloud along the laser polarization direction as a driven and damped harmonic oscillator[69]. The eigenfrequency ($\omega_t = \sqrt{Q_{ion}}/R(t)^3 = \omega_p/\sqrt{3}$) of this oscillation is determined by charge and size of the cluster. The condition of resonance is achieved when this eigenfrequency (ω_t) matches with the laser frequency (ω) due to the electron emission and cluster expansion. The microscopic model suggested by Saalmann et al is equivalent to Ditmire's nanoplasma model as both of them yield the same resonance condition. This short interval of enhanced absorption was smeared out in the time with lesser peak value when non-uniformity of electron density is included in the cluster expansion [59] re-

[1] $\epsilon = 1 - \omega_p^2/\omega\,(\omega + i\nu_{ei})$, where ω_p, ω and ν_{ei} represent the plasma frequency, laser frequency and electron-ion collision frequency.

sulting in the long-time resonance at the critical density plasma layer.

Apart from linear resonance, literature also supports the idea of non-linear resonance i.e. lowering of the eigenfrequency or resonance frequency with increasing oscillation amplitude[81]. To explain NLR, a rigid sphere model of two inter-penetrating spheres (RSM) of positive charge (ions) and sphere of negative charge (electron) was considered. The potential between two spheres for small energy of excitation is harmonic with eigenfrequency $\omega_t \gg \omega$, where ω is laser frequency. As the amplitude of oscillation increases, the potential becomes anharmonic and the restoring force becomes weaker than that of the linear oscillator. Consequently, the eigenfrequency decreases and at some exciation energy it may become equal to laser frequency leading to the resonance, the so called "non-linear resonance. Apart from resonance absorption, various other energy absorption mechanism like vacuum heating [31], collision-less resonance absorption [97] and scattering at the cluster potential [98] have been also suggested. Although various energy mechanisms have been proposed, resonance absorption is still believed to be the main method for energy absorption.

However, certain simulation results in the literature completely contradict this perception of resonance occurring the cluster nanoplasma that is believed to be the cause of high absorption of laser energy. For example, Davis et *al.* found no such resonance in their MD simulations [99] and posed compelling arguments questioning the applicability of both the Drude model, used in linear resonance, and rigid sphere model, employed in non-linear resonance. The energy absorbed by the cluster is on the basis of capacitor model which treats the expanding cluster as two concentric spheres : an ion core of radius (R_i) surrounded by a large radius electron cloud (R_e). The energy absorbed per cluster is estimated by evaluating the electrostatic energy (E_c) of the spherical capacitor. In the limit $R_e \gg R_i \approx R_0$ and highly charged cluster $Z \gg$, the potential energy stored in the spherical capacitor can be written as $E_c \approx \eta^2 \left(N^2Z^2/2R_0\right) \sim \left(\eta^2 N^2 Z^2/2N^{1/3}\right) \sim N^{5/3}$, where N is the number of particles in the cluster and η is the fraction of outer ionization. It is important to note that energy absorbed by the cluster is highly non-linear as the exponent appearing in the superscript of N is greater than 1.

Other than the MD simulation methods which rejects the idea of resonance, were the results of Deiss et *al.*[100]. They suggested a new kind of heating mechanism of electrons in the large clusters by employing a generalized classical transport theory in the mean field. In this model, the electron dynamics is represented by the classical phase-space distribution whose evolution is determined by test-particle discretization. They did not observe any kind of plasma resonance. According to their studies, the high energy X-Ray emission from clusters was due to inner vacancies created by the highly energetic quasi free electrons arising due to their elastic large-angle back scattering at ionic cores in the presence of laser field [100].

The above discussion reflects that the reason responsible to the high energy absorption inside the cluster is still not clearly understood. We have tried to investigate the presence of resonance absorption in Ar cluster irradiated by the laser of various pulse durations, as the process of resonance is strongly correlated with the duration of the incident laser pulse.

3.1.2 Simulation parameters

We have considered the interaction of 806 nm laser pulse of intensity 8×10^{16} W/cm^2 with 30 Å argon (Ar) cluster. The time profile of the incident laser pulse is assumed to the Gaussian otherwise stated. The FWHM pulse duration of the pulse is varied in the range of 10-120 fs. The propagation of the laser pulse is along $y-$axis where as the polarization or the direction of the electric field is along the $x-$ axis. As also mentioned previously, the size of the simulation box is much smaller than the wavelength of the laser, only time variation of laser pulse is considered. Spatial variation of pulse is ignored across the dimensions of the cluster. The space and time evolution of the cluster is modelled with our fully relativistic time-dependent three-dimensional MD model. It is important to note that the relativistic effects are not important for the studies to be presented in this section as the laser intensity is not very high. The relativistic effect start affecting the dynamics of the cluster at high intensities ($\geq 10^{18}$ W/cm^2). For example, we may note the results of *Petrov at al*[70] at these ultra high

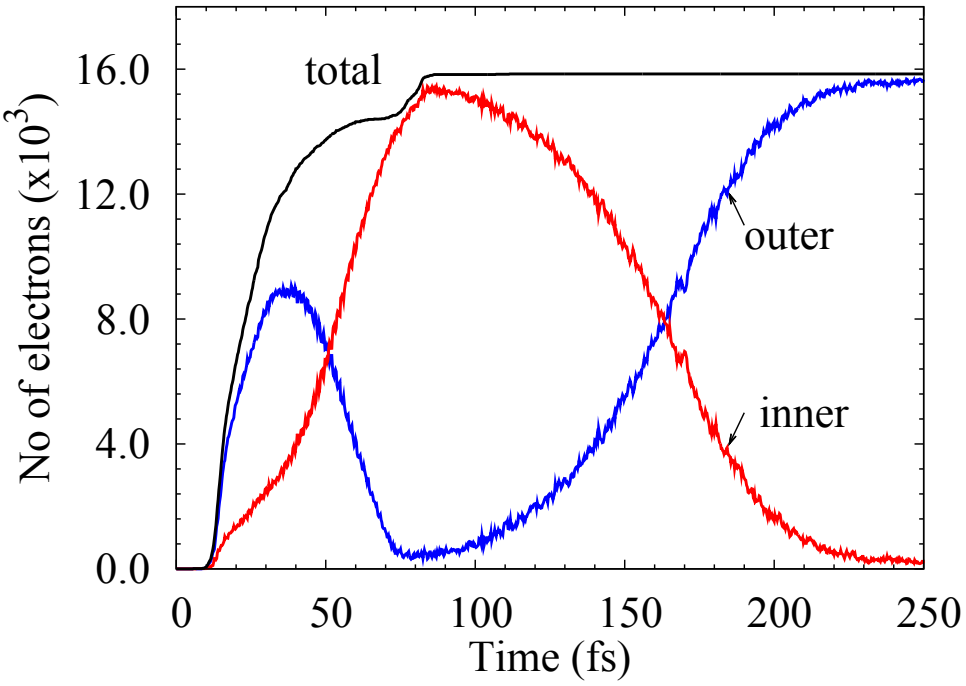

Figure 3.1: *Temporal variation of electron population for Ar cluster of radius* $R_0 = 30$ *Å irradiated by a representative gaussian laser pulse of duration* $\tau = 70$ *fs, wavelength* $\lambda = 806$ *nm and peak intensity* $I_p = 8 \times 10^{16}\ W/cm^2$.

intensities (10^{20} W/cm^2) where the magnetic field[1] starts affecting the shape and trajectory of electron cloud. The size of simulation box is considered to be $30R_0 = 900\mathring{A}$ wide, where R_0 is the intial radius of the cluster. The energy spectrum is calcu lated at 225 Å from the center of the simulation box for all the laser pulse durations. Laser pulse is linearly polarized along x- direction.

3.1.3 Results

The dynamics of cluster ionization and the subsequent coulomb explosion during the pulse irradiation is presented in Figs.3.1 and 3.2 for a representative laser pulse duration of 70 fs. The temporal evolutions of inner, outer and total no of electrons are

[1]At sufficiently high intensity, the magnetic field ($\mathcal{B} = \mathcal{E}/c$, where E is the electric field of the laser beam and c is the velocity of light.) becomes significant and can alter the dynamics of the particles.

shown in Fig. 3.1. As mentioned previously, inner electrons are those which are quasi free to move freely within the cluster but can not escape it whereas outer electrons

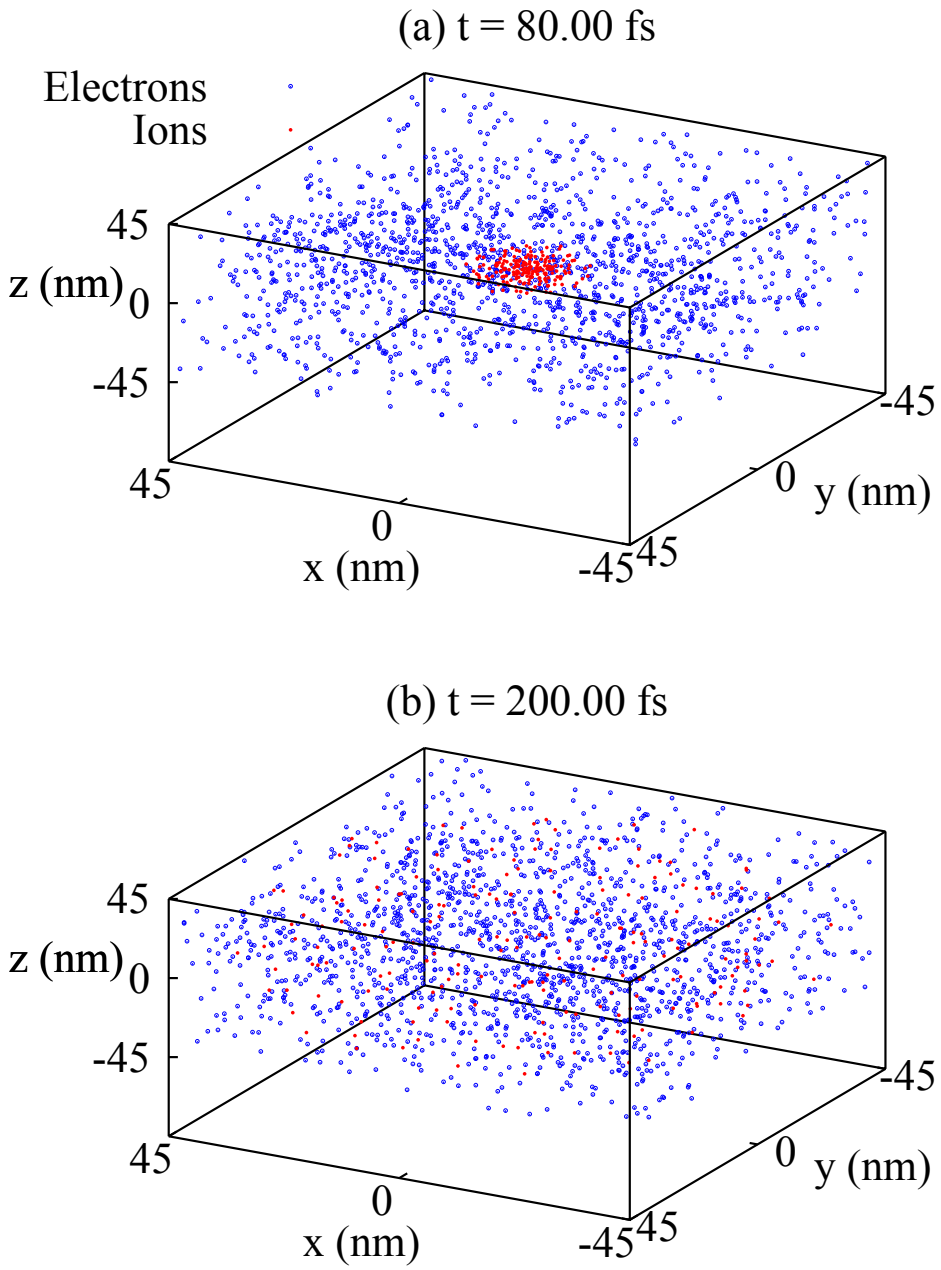

Figure 3.2: *Snapshots of particle positions at 80 fs (a) and 200 fs (b) for the same laser and cluster parameters as in Fig.3.1.*

leave the cluster boundary. The inner electrons cause ionization via collisions with atoms inside the cluster. On the other hand, outer electrons lead to further collisional ionization if they enter the neighbouring cluster. The time dependent variation in electron population is a result of constant interplay among the various processes *viz* ionization, removal of electrons from the cluster boundary and expansion of cluster. At time t=0, all particles are neutral and remain inside the cluster. As laser is switched on, various ionization processes lead to the rapid build-up of inner electrons along with slow increase in the number of outer electrons. As the time progresses, the number of outer electrons increases due to escape of electrons from cluster upto about 40 fs. Beyond this time, the decrement in the population of outer electrons and the increment in the population of inner electrons are caused by electron recapture due to cluster expansion. In Figs. 3.2(a) and 3.2(b), we show the snapshots of the electron and ion positions at two representative times before and after the coulomb explosion respectively of the cluster. At earlier times (Fig. 3.2(a)) ions remain almost immobile due to their heavy mass while electrons move out from the cluster. When sufficiently large number of electrons escape the cluster leaving behind it a positively charged sphere which explodes due to repulsion among ions. The time of occurrence of coulomb explosion depends upon the laser and cluster parameters. The position of ions and electrons after the coulomb explosion is shown in Fig. 3.2(b).

Fig.3.3 shows the temporal history of the average degree of ionization for different laser pulse durations. When the laser intensity approaches sufficient value to ionize the neutral Ar atoms through tunnel ionization, average charge per ion increases as shown in the Figure 3. The initial electrons produced by tunnel ionization gives rise to further ionization due to collisional ionization. The larger the pulse duration, later the ionization starts as the laser pulse reaches the ionization threshold intensity later for longer pulses. However, the average degree of ionization saturates to 8 for all the cases.

Below we discuss the issue of energy absorption by cluster in the context of linear resonance as predicted by the nanoplasma model[43]. More specifically, we want to see how the absorption of laser energy changes with the duration of incident laser

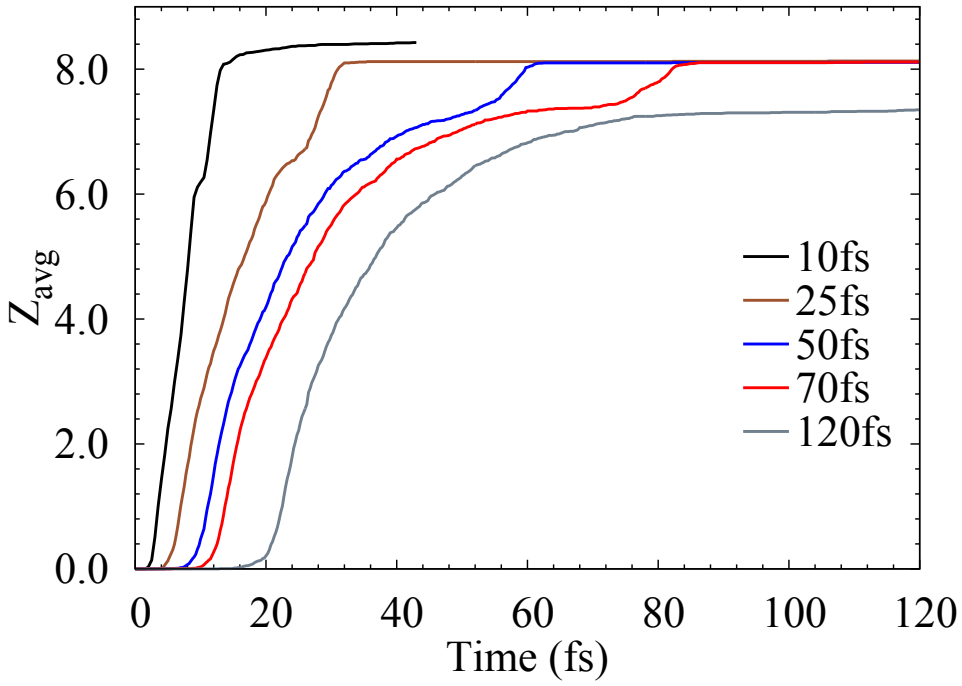

Figure 3.3: *Time history of average degree of ionization for Ar clusters for various laser pulse durations. The other laser parameters are same as in Fig. 3.1.*

pulse. In Fig.3.4, we present our results showing the effect of laser pulse duration on the energy absorption by cluster. In our MD code, we determine two quantities of interest in context of energetic of cluster nanopalsma : one is total energy absorbed by cluster and the second in the mean kinetic energy of ions. The former one is obtained by adding the total kinetic and potential energies of all particles (electrons and ions) which is further added to the energy spent in the optical field ionization *i.e* a sum over all ionization potentials upto the charge state under consideration for all ions. The latter is calculated by dividing the the total kinetic energy of ions by total number of ions at each time step. Figs. 3.4(a) and 3.4(b) respectively show the variation of total energy absorbed by the cluster and mean kinetic energy of ejected ions from the cluster with the laser pulse duration. As shown in the Fig. 3.4(a), the energy absorbed by the cluster is nearly $70MeV$ for the shortest pulse duration of $10fs$. As the pulse

duration is increased further, the absorbed energy increases further upto $\sim 110MeV$ for the case of $25fs$. The value of absorbed energy further decreases with the increase

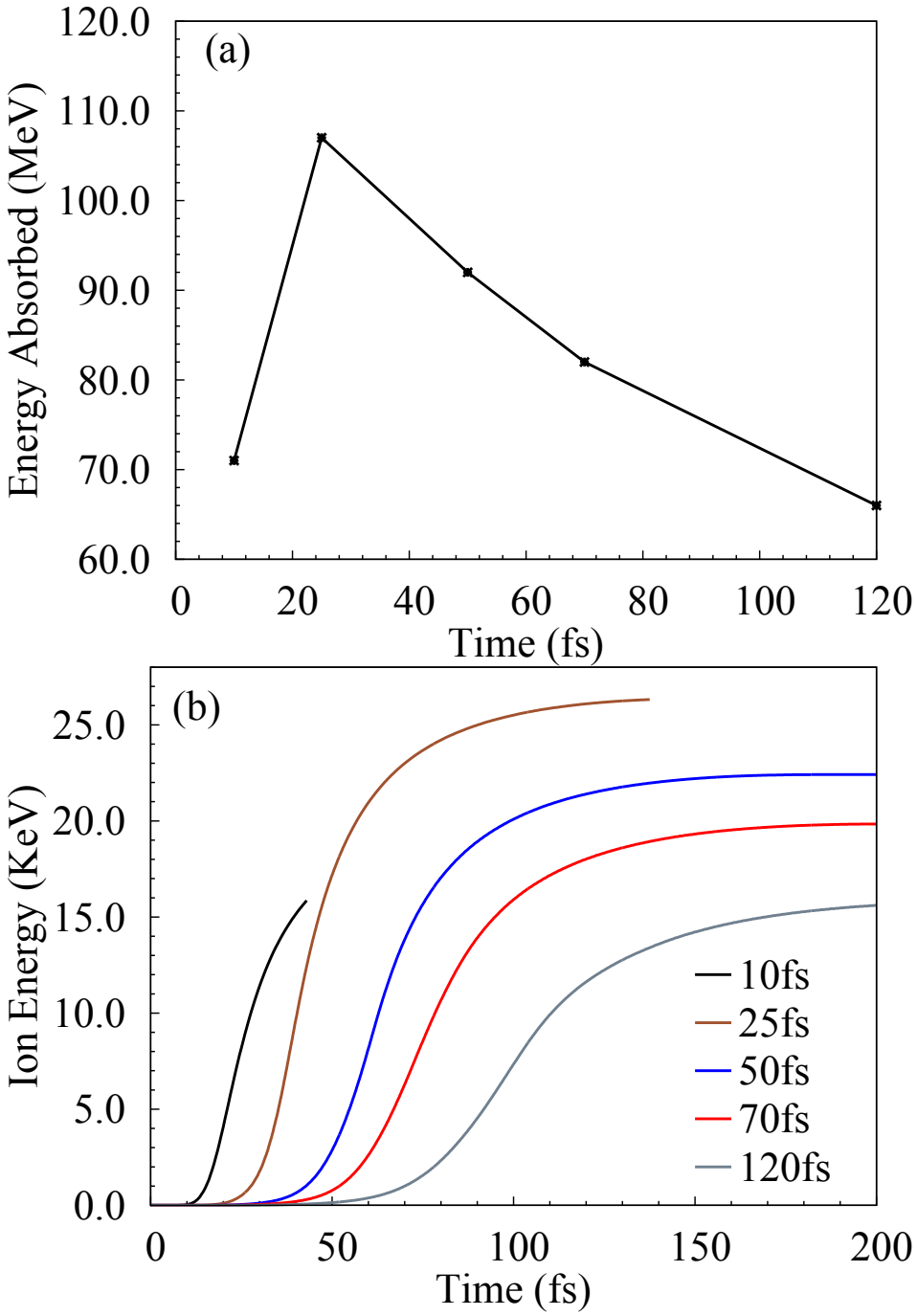

Figure 3.4: *Laser energy absorbed (a), and mean ion energy variation with laser pulse durations.*

in pulse duration and its value is $\sim 66MeV$ for the longest pulse duration of $120fs$. Clearly, we find that there exists an optimum value of pulse duration of about $25fs$ at which the energy absorption shows a much pronounced value compared to neighbouring values of pulse durations. Similar results are observed for the mean value of energy of ions (3.4(b)). A close inspection of Fig.3.4(b) for any particular pulse duration shows that average kinetic energy of ions first increases with the time and then saturates at some fixed value. The saturation of the average kinetic energy of ions with time corresponds to the fact that the charged particle is far away from the interaction region and its energy is not going to be further influenced by other charged particle interaction. For different values of the pulse durations, the saturating value of the mean energy is different as shown in the Fig. 3.4(b). Again, we observe that mean ion energy saturates to a value of 25 KeV for the optimum pulse duration of about 25 fs. This saturation value is lower for other pulse durations.

The presence of the optimum pulse duration for both the energy absorbed by the cluster and mean kinetic energy of ions can be explained in terms of linear resonance occurring in the cluster nanoplasma. Fig. 3.5 shows the temporal profile of laser intensity along with electron density (in units of n_c) inside the cluster for various pulse durations. As per the linear resonance theory, the resonance occurs when electron density (total number of inner electrons divided by the cluster volume) of expanding clusters equals the 3 times the critical density [43]. The dashed horizontal lines in these figures show the $n_e = 3n_c$ condition. The time at which this dashed line intersects the electron density curve represent the resonance condition ($n_e = 3n_c$). One can note that there are two such points of intersection. The 1^{st} crossover is because of electron population that is building up from zero to maximum value due to ionization. At this time of instant, number of electrons itself is very small which takes part in absorption process, though the density of electrons may be equal to $3n_c$ as the cluster is still frozen. Consequently, the absorption is very small at this time. The cluster expansion leads to 2^{nd} point of intersection ($T = T_R$) where the resonance absorption really occurs. For smallest laser pulse duration (10 fs), T_R appears after laser has passed its peak value (time of peak laser intensity is termed as T_P) as shown in Fig. 3.5(a). Similarly

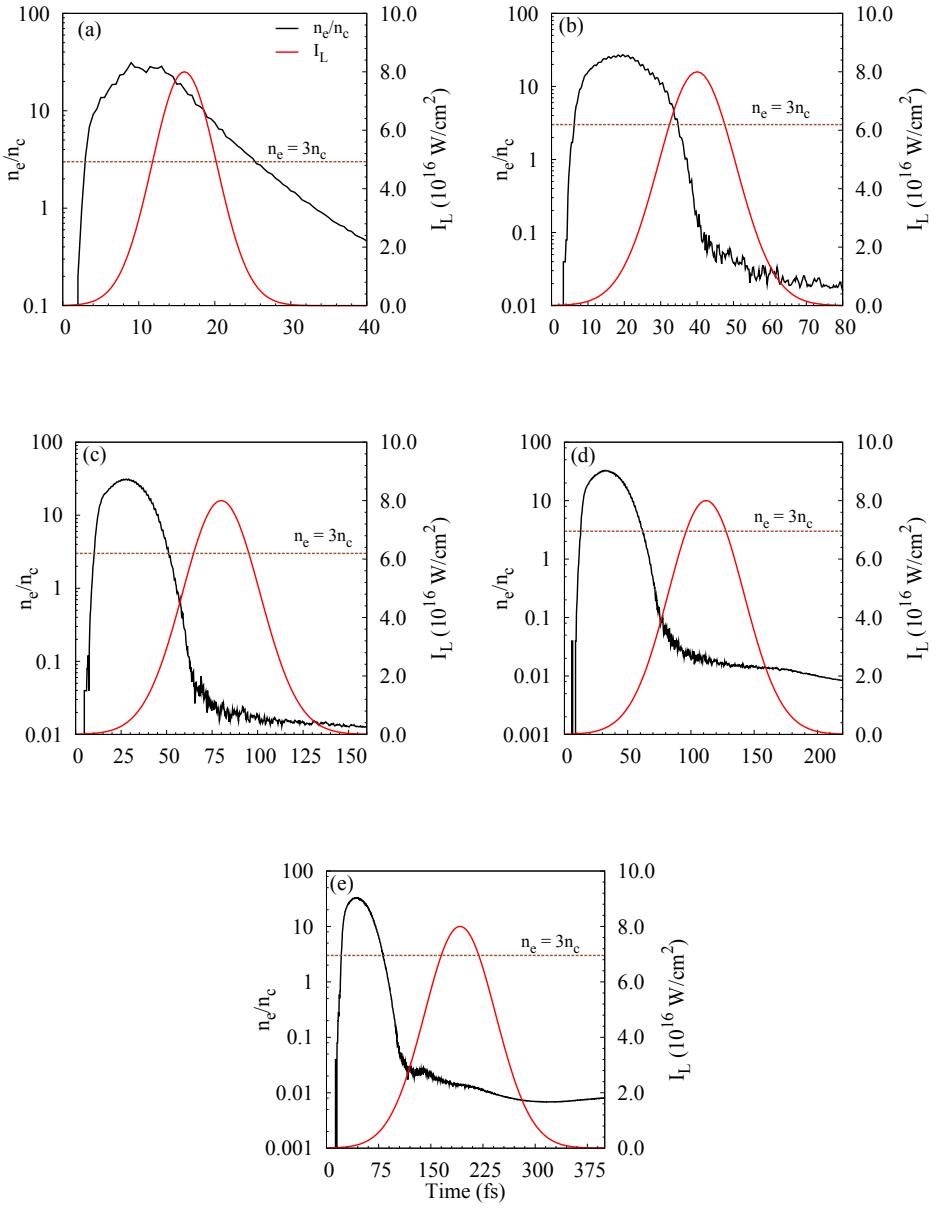

Figure 3.5: *Time Variation of normalised electron density (n_e/n_c) along with the laser intensity profile for laser pulse durations of 10 fs (a), 25 fs (b), 50 fs (c), 70 fs (d) and, 120 fs (e). The other laser parameters are same as in Fig. 3.1.*

for larger pulse durations (50 fs, 70 fs and 120 fs : Figs. 3.5(c), 3.5(d) and 3.5(e)), T_P happens to be much larger than T_R. For the case of 25 fs, $T = T_R$ and T_P are close by (Fig.3.5(b)). Consequently, the resonance occurs and the cluster absorbs maximum energy for this pulse duration.

Thus, the plasma resonance is strongly correlated with the temporal profile of laser

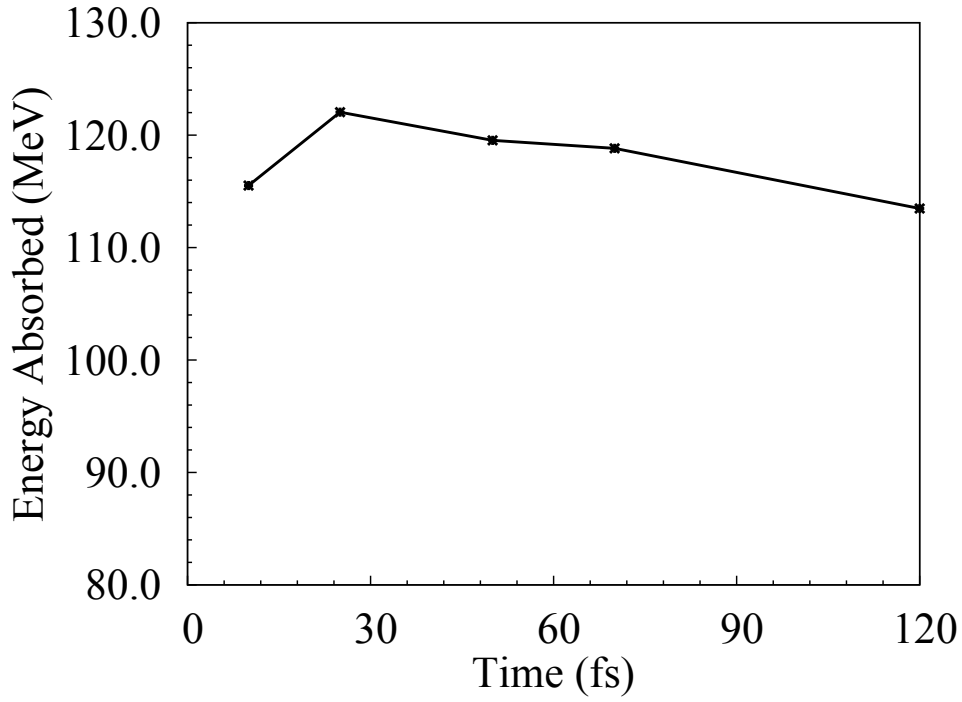

Figure 3.6: *Effect of pulse duration on total laser energy absorbed for super-Gaussian laser pulse.*

pulse as described in the previous paragraph. On these grounds, we should not expect such a optimum pulse duration for a temporally constant (ideally a rectangular pulse) laser pulse time profile. To confirm it, we repeated the above simulations for a pulse profile of 2^{nd} order super-Gaussian (nearly flat top). Results are presented in Fig.3.6. We do observe the energy absorbed to be almost constant (between 116 MeV to 124 MeV). This slight variation may be attributed to the fact that pulse shape is different ideal (rectangular). Thus we conclude that the presence of an optimum pulse duration is a clear indication of existence of linear resonance occurring during the cluster expansion. Zweiback *et al.* have studied experimentally the effect of pulse duration on laser energy absorption [60] at fixed laser energy. In their study, they measured the absorption for large Xe and Ar clusters with a laser of wavelength of 810 nm, capable of producing 50 mJ in 50 fs. They also found an optimum pulse duration for maxi-

mum absorption for relatively large cluster size (85 Å to 205 Å for Xenon and 110 Å to 165 Å for Argon). The cluster sizes employed in our simulations were rather smaller (30 Å). So we note that resonance is observed for a wide range of cluster sizes. One also expects an optimum cluster size for fixed laser pulse duration on the same argument given earlier. Indeed, an optimum cluster size was observed experimentally for a constant laser pulse duration [101].

3.2 Effect of cluster density : a computational study

The energetics of laser driven clusters is strongly influenced by the two important parameters namely size of the cluster (R_0) and number of clusters per unit volume in the interaction region or cluster density (N_{cls}). The effect of cluster size on the energetics of cluster nanaoplasma was investigated by *Springate et al*[101]. Using the Ditmire,s nanoplasma model, they showed that energy absorption by cluster also shows an optimum cluster size[101] similar to the optimum pulse duration for maximum absorption. It can be also explained on the same grounds as we described the optimum pulse duration for maximum energy absorption by clusters in the previous section. As suggested by the nanoplasam model, the maximum absorption of laser energy occurs for those cluster sizes for which the resonance condition $n_e = 3n_c$ is close by to the peak of the temporal profile of the laser pulse. Keeping the pulse duration same, smaller cluster expands quickly so the resonance condition appears much before the peak laser intensity. For much larger clusters, the resonance condition is achieved at later times when the laser has already passed it peak value. Thus a optimum cluster size is expected. It is important to note that gas expansion from the nozzle does not produce a clusters of identical sizes but a long-normal distribution of the form

$$f(N) \propto exp\left[-\log^2(N/N_0)/2w^2\right], \tag{3.1}$$

where N_0 is the most abundant cluster size and w is proportional to the full width half maximum (FWHM) of the distribution[102]. Once this distribution of size of the

clusters is considered, the optimum cluster size is flattened[102].

In our studies, we have tried to investigate how the cluster density changes the energetic of cluster nanopalasma. To simulate the effect of varying cluster density, one has to accordingly change the size of the simulation box *i.e.* R_{IC}. The size of the simulation box is equal to the distance between two clusters. If the clusters are densely packed in the interaction region, one has to take the smaller R_{IC} and vice-versa. We may note these studies on varying the density of the clusters are not arbitrary. They have a experimental backing too. As mentioned in the introduction chapter 1, these clusters are formed when the high pressure gas expands isentropically through a supersonic nozzle. The density of the clusters along with the size of the cluster are experimental parameters which are sensitive to the the backing pressure applied behind the super-sonic nozzle. Moreover, it was shown in the results of *Kim et al*[103] that both cluster size and cluster density increases with the backing pressure. The monotonous increase of cluster size with backing pressure is in accord with the results of *Hagena et al*[104]. After reaching an optimum value of backing pressure, the cluster density further reduces whereas cluster size go on increasing with increasing backing pressure[103].

3.2.1 Simulation parameters

In order to have some qualitative understanding on the effect of cluster density, we have investigated the dynamics of relatively small Ar clusters of sizes of $R_1 = 30\mathring{A}$ and $R_2 = 40\mathring{A}$ which corresponds to the total number of particles in the cluster as $N_1 = 1953$ and $N_2 = 4630$. These clusters are irradiated by a Gaussian laser of peak intensity $10^{16}W/cm^2$ with FWHM pulse duration of $30fs$. The wavelength of the laser lies in the NIR regime ($\lambda = 800nm$). Keeping the fact in the mind, as the size of the cluster increases with backing pressure, the cluster density also increases. Consequently, the inter-cluster distance reduces for the increase in the cluster size. Therefore, both the cases are studied using the inter-cluster distance of R_{ic} = $5R_0$ and $15R_0$ where R_0 being 30 Å and 40 Å. In this case, the electric field caused by neighbouring particles are included while calculating the ADK ionization. It might be a matter of debate

to simply add the field of the neighbouring particles to the laser field for the calculation of the tunnelling rate. As the field appearing in the ADK formula is the laser field which is harmonic in time whereas the local field are very fluctuating in time and they do not possess the harmonic character in time domain. But we have used this methodology as a first approximation. More correct determination of tunnelling rate while including the local field can be obtained by the treatment given by *Siedschlag et al*[86].

3.2.2 Results

The results on the cluster dynamics are shown in Fig. 3.7. In Fig.3.7(a), we present the

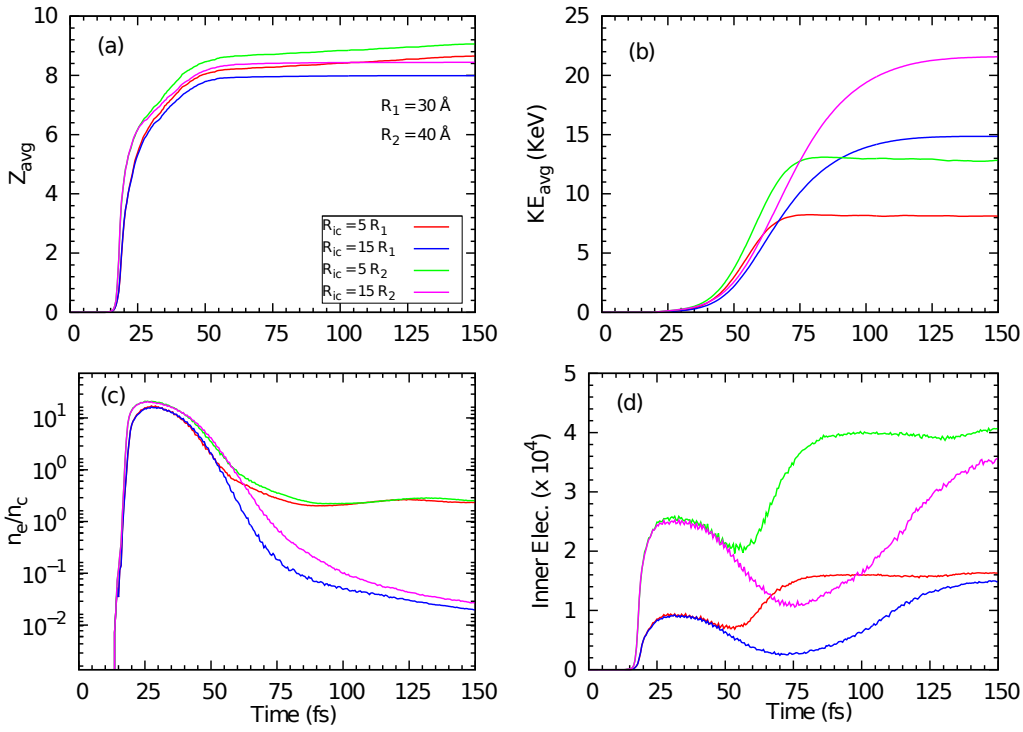

Figure 3.7: *Temporal evolution of Z_{avg} (a), average kinetic energy (b), cluster density (c) and number of inner electrons (d) for Ar cluster of radius 30 Å and 40 Å with R_{ic} = 5R_0 and 15R_0. The laser used is 30 fs, 800 nm with peak intensity of 10^{16} W/cm^2.*

temporal evolution of the average degree of ionization Z_{avg} for various clusters

radii and inter-cluster distances. It is important to note that both smaller ($R_1 = 30\mathring{A}$) and larger ($R_2 = 40\mathring{A}$) clusters yield to higher charge states in the case of higher cluster density (R_{ic} = 5 R_0) compared to their lower density (R_{ic} = 15 R_0) counterparts. However it should be also noted that the temporal profile of Z_{avg} for the case of 30Å with R_{ic} = 5 R_0 is significantly similar to the case of 40Å cluster with R_{ic} = 15 R_0. Furthermore, for the more consistent parameters of interest, (larger the cluster size, higher the cluster density or lower the inter-cluster distance) we observe that average charge state is higher for the case of 40Å cluster with R_{ic} = 5R_0 compared to the case of 30Å cluster with R_{ic} = 15 R_0. On the other hand, if we observe the plot of average

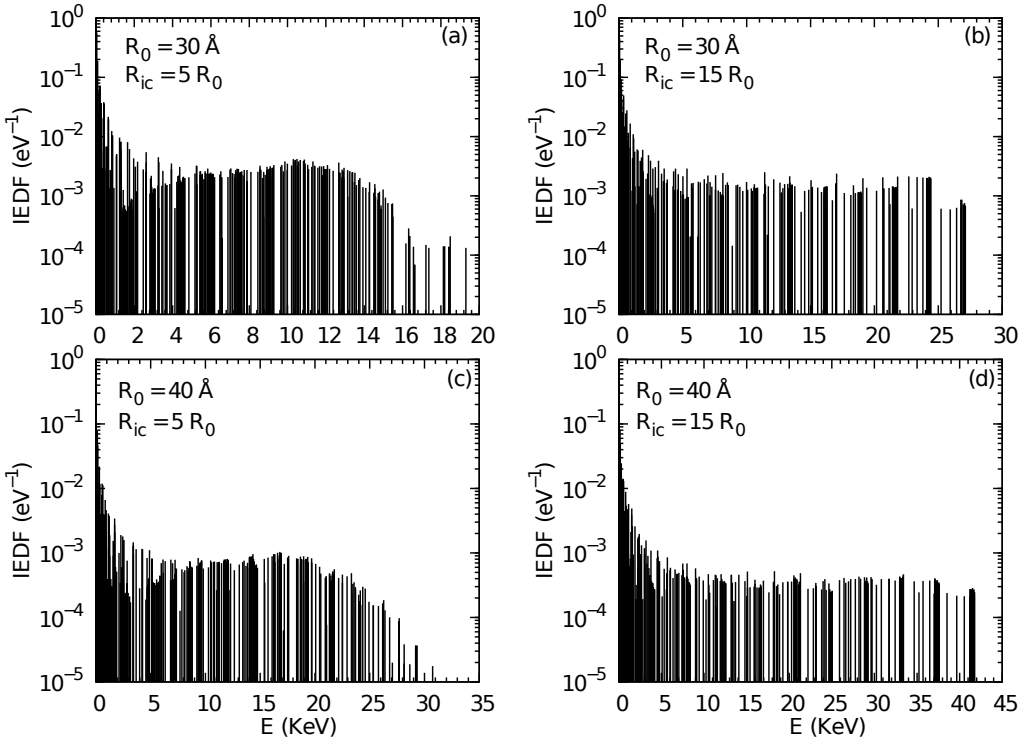

Figure 3.8: *Ion energy distribution function for 30 Å Ar cluster with R_{ic} = 5R_0 (a) and 15R_0 (b) and for 40 Å Ar cluster with R_{ic} = 5R_0 (c) and 15R_0 (d) is presented. The laser conditions are same as those in Fig. 3.7.*

kinetic energy of ions for these set of parameters (Fig. 3.7(b)), we observe the opposite trend. In fact, it is observed that the average kinetic energy for the case of 40Å cluster with R_{ic} = 5R_0 is less than that for the case of 30Å cluster with R_{ic} = 15 R_0.

This lowering of mean kinetic energy of ions for the larger cluster with smaller inter-cluster distance can be explained on the basis of shielding of the ions due to electrons. For the larger cluster with the higher cluster density, the number of electrons quickly increases in the smaller volume which efficiently shield the ions. In other words, the individual charge residing on the cluster ions reduces due to the shielding provided by the electrons which are near by. Consequently, the strength of the Coulomb explosion reduces which leads into the smaller average kinetic energy of ions for this case. This justification becomes more visible when we observe the temporal plots of electron density and number of inner electrons in both the relevant cases. In Figs. 3.7(c) and 3.7(d), both electron density and number of electrons inside the cluster are seen for the case of 40Å cluster with R_{ic} = 5 R_0, which results in lowering of the ion energies as compare to 30Å cluster with R_{ic} = 15 R_0.

This point is further strengthened when we plot the ion energy distribution function (IEDF) in the Fig. 3.8 for the concerned cases of cluster density and inter-cluster distance. Here we also observe that even though the number of atoms in 30 Å cluster are smaller by about a factor of 2.3 as compare to 40 Å cluster, the energies seen for 30Å cluster with R_{ic} = 15 R_0 (b) and 40Å cluster with R_{ic} = 5 R_0 (c) are of the same order. As explained earlier, the effect is due to the shielding of ions provided by the electrons in the vicinity.

3.3 Effect of cluster density : experimental verification

In this section, we want to briefly mention about the results of *Prigent et al*[90]. They investigated experimentally, as well as theoretically, the influence of laser intensity and pulse duration on the x-ray emission from argon clusters. In particular, they irradiated Ar clusters of mean size $< N >= 3.7 \times 10^4$ atoms/cluster with laser of peak intensity $I = 4.0 \times 10^{16} W/cm^2$ at FWHM pulse duration of $55 fs$ and measured the distribution of various charge states obtained in the experiment. To simulate these results, we need to know two more parameters other than the intensity and pulse duration of laser. They are cluster size in terms of radius(R_0) and inter-cluster distance

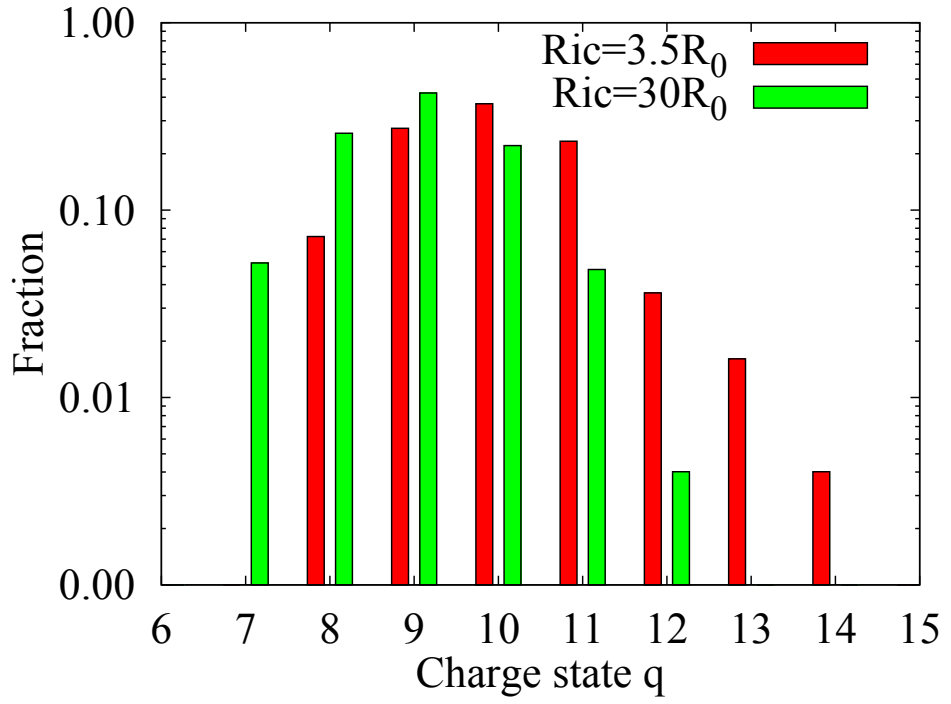

Figure 3.9: *Comparison between charge state distribution for different inter-cluster distances (R_{IC}) for I_p=4.0×10^{16} W/cm^2, τ=55.0 fs, λ=800 nm, and R_0=85 Å. Red bars for $R_{IC} = 3.5R_0$, green bars for $R_{IC} = 3.5R_0$.*

(R_{IC}) for application of periodic boundary condition so that effect of neighbouring clusters can be accounted for. R_0 for this case turns out to be $85\mathring{A}$ and two sets of values of R_{IC} are chosen : $3.5R_0$ and $30R_0$. As mentioned previously that inter cluster distance depends upon cluster density, larger the cluster density, lesser is R_{IC} and vice versa. In Fig.3.9, we show the results for fraction of various ionization states for the two values of R_{IC} : red bars for $R_{IC} = 3.5R_0$ and green bars for $R_{IC} = 30R_0$. We mention here that these results of fractional ionization are in good agreement with the findings of *Prigent et al* for the case of closely packed clusters *i.e.* for the smaller value of $R_{IC} = 3.5R_0$. It is important to note the emergence of additional charge states of 13 and 14 for the case of $R_{IC} = 3.5R_0$. These charge states were completely missing for $R_{IC} = 30R_0$. The appearance of new charge states for the smaller value of R_{IC} is due to the collisional ionization caused by the electrons with the neighbouring clusters.

The degree of collisional ionization with neighbouring clusters increases as we reduce the distance between two clusters.

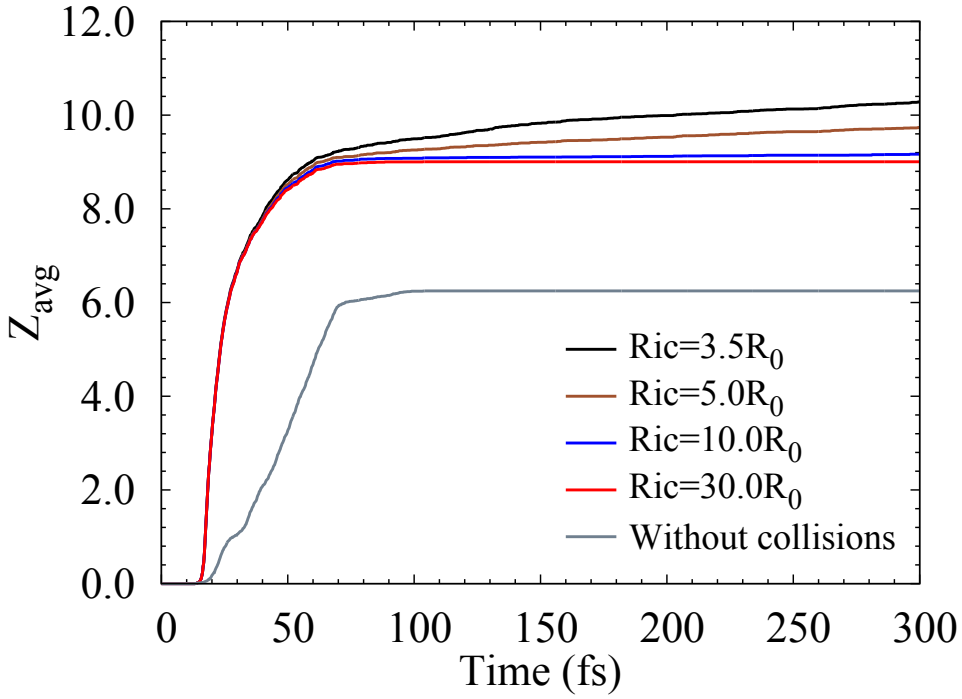

Figure 3.10: *Effect of collisional ionization and R_{IC} on average degree of ionization Z_{avg} for Ar clusters with the same simulation parameters as used in Fig. 3.9.*

To further strengthen this argument, we plot the temporal variation of average degree of ionization in Fig. 3.10. In this plot, the lower curve shows only the effect of tunnel ionization, collisional ionization is artificially switched off for this curve. The upper set of curves include the effect of collisional ionization along with the tunnel ionization. The various colours in the upper set of curves designate the different values of inter-cluster distance. It is important to note that once we ignore the collisional ionization, the value of average degree of ionization remains unaffected with the change in values of R_{IC} (lower most curve) and saturates at a value of ~ 6. The effect of inclusion of collisional ionization clearly increases the average degree of ionization. It is important to see that all plots in the upper set of curves for various values

of RIC are identical till time $t \sim 50fs$. After this time all of them starts diverging and finally saturated at different values for different values of R_{IC}. The saturating value of Z_{avg} is minimum for $R_{IC} = 30R_0$ and it increases continuously as R_{IC} is reduced further. Finally, Z_{avg} is maximum when the cluster are most closely placed to each other *i.e.* for the value of $R_{IC} = 3.5R_0$. At earlier time $t < 50fs$, the electrons collisionally ionize the atoms/ions of the parent cluster so Z_{avg} remains behave similarly before this time. After $t > 50fs$, the electrons cross the boundaries of parent cluster and start ionizing the atoms/ions of the neighbouring clusters. Thus, the saturating value of Z_{avg} is different for different values of R_{IC} *i.e.* the closer the clusters are, more effective the collisional ionization with neighbouring clusters. By appropriate selecting the value of inter-cluster distance, one can qualitatively match with the experimental results of fractional ionization as obtained by *Prignet et al*[90].

3.4 Summary

In this chapter, we have investigated the various parameters that affect the energetics of cluster the cluster nanoplasma. The first one is the pulse duration of the incident laser pulse. By using MD simulation results of absorbed energy by cluster and mean kinetic energy of ions for various pulse durations ranging from 10-120 fs, we have revalidated the the theory of linear resonance as given by Ditmire's nanoplasma model. Both of these parameters shown an optimum pulse duration for which they are maximum. We have shown that the optimum pulse duration is due to the fact that the condition of linear resonance ($n_e = 3n_c$) depicted by the time (t_R) is in closest vicinity to the peak of the laser pulse (t_P) for the optimum pulse duration of $25fs$ which leads to the maximum absorption of energy. For super-Gaussian pulse, we do not observe this kind of optimum pulse duration.

The second parameter that affects the energetics and charging dynamics of cluster nanoplasama is the cluster density. In computational domain, the effect of varying cluster density are studied by changing the value of inter-cluster distance. More the cluster density, less is the inter-cluster distance and vice-versa. Keeping in mind the

earlier results of *Kim et al*[103], the cluster size increases monotonously with backing pressure whereas the the cluster density first increases with backing pressure and then after a showing an optimum value, reduces further. We found that just by increasing the size of the cluster, one can not increase the the mean kinetic energy of ions after explosion. In fact, the smaller value of inter-cluster distance for larger sized cluster makes shielding of the ions due to electrons of neighbouring cluster more effective. Consequently, the energetics of the two cluster (sizes in increasing order but inter-cluster distance in decreasing order) remains comparable. Further, we were also able to match with the experimental results of *Prigent et al*[90] when smaller value of inter-cluster distance are used for the simulation. The emergence of additional charge states for smaller value of inter-cluster distance was explained on the basis of collisional ionization with neighbouring the clusters.

CHAPTER 4

Anisotropic ion emission from laser irradiated clusters : Breakdown of spherical isotropy in few-cycles pulse duration limit

As discussed in the introduction chapter, the expansion of the cluster after irradiation by the intense lasers is mainly categorised by two models : first one is hydrodynamic expansion and the second one is Coulomb explosion. The mode of expansion, selected by the cluster, depends upon the number of inner electrons[1] In the hydrodynamic expansion, the cluster possesses sufficient number of inner electrons and the whole cluster expands due to the electron gas pressure. Coulomb explosion occurs when most of the inner electrons have escaped from the cluster and the cluster explodes due to the repulsion among the residual positive charges. In both of these extreme situations, the cluster ions do not prefer certain particular directions in space to eject. In other words, the cluster explosion is completely isotropic. There are many instances when the situation is intermediate to above mentioned two modes of cluster expansion *i.e.* the number of inner electrons is less than that required for hydrodynamic expansion and more than that required for the Coulomb explosion. This is the situation when spherical symmetry of cluster expansion breaks down and the cluster ions show certain preferred direction for emission. This is known as anisotropic cluster explosion and depends strongly on the pulse duration of laser used for the irradiation. Moreover, the character of the anisotropy changes when the pulse duration is changed. In this chapter, we will study this anisotropy of cluster explosion for Ar and Xe clusters by using our MD code.

[1]Inner electrons are those which are ejected from the parent atoms but still confined inside the periphery of cluster due to the residual space charge. Outer electrons are one with sufficient energies to overcome the Coulomb barrier of the cluster and thus becomes free.

4.1 Earlier trends on anisotropic ion emission

Springate et al[101] first observed experimentally glimpses of anisotropic ion emission from Xe_{5300} clusters irradiated with $170fs$, $780nm$ laser pulse with peak intensity of $1.3 \times 10^{16} W/cm^2$. They measured the mean ion energy as a function of angle with respect to the laser polarization direction. The mean ion energy was found about 15% higher along the direction of laser polarization than perpendicular to it. They explained the observed anisotropy on the basis of angular dependence of electron emission from xenon clusters which earlier, was observed by Shao et al[40]. The electron energy component from the Xe clusters was found to consist of two parts : isotropic high energy "hot" component and anisotropic low energy "warm" component[]. The directional dependence of warm component of electron give rise to the anisotropy in the ion energies of exploding cluster.

In more detailed experiment performed by Kumarappan et al[95], the problem of anisotropy was studied for Ar clusters (2×10^3 to 4×10^4 Ar atoms) irradiated by laser of intensity $8 \times 10^{15} W/cm^2$ and pulse duration $100fs$. They measured experimentally the complete energy distribution of exploding ions. They observed that the ion energy distribution consisted of two components : a low energy isotropic component, and a high energy anisotropic one. The high energy part depends upon the laser polarization direction *i.e.* the ion yield is greater in the direction of laser electric field than perpendicular to it. It could not be explained by the argument given by the Springate et al[101] as the low energy warm electron component can not give rise to the observed anisotropy in the high energy part of ion energy distribution function. To explain the anisotropy results, Kumarappan et al used two earlier theoretical results of Ishikawa et al[68] and Kou et al[105]. First, the net field (laser field plus radial Coulomb field of charged particles) experienced by the ions is different in two consecutive laser half time cycles along the laser polarization direction. This is due to the extra contribution of radial field which remains in the same direction but the laser field changes its direction as the polarity of laser changes. This results in a net cycle averaged force on these ions along the laser polarization direction[68]. Second, the charge state distribu-

tion itself is asymmetric *i.e.* charge state are higher along the polarization direction. Consequently, the Coulomb explosion is asymmetric[105]. Taken together these two effects, Kumarappan et al were able to explain the anisotropy for the high energy ions that ejected from the surface of the cluster. For the ions interior to the cluster, the laser field is sufficiently shielded by the electrons and only the radial field remains into the picture. Consequently, the bulk of the cluster show less anisotropy. The anisotropic studies on hydrodynamic expansion of Xe clusters were also performed by Kumarappan et al[106]. They extended the hydrodynamic model[43] of cluster expansion and found the importance of the polarization induced surface charge distribution. The action of incident laser field on this induced surface charge distribution gives rise to a additional directional dependent cycles averaged pressure ($\propto \cos^2\theta$). This additional pressure has to be added to already present hydrodynamic pressure to account for the observed anisotropy. This kind of anisotropy was also observed in hydrogen clusters of initial size $20\mathring{A}$ irradiated with laser of peak intensity $\approx 10^{18} W/cm^2$[107]. Two values of laser pulse duration *viz.* 40 and 250 fs were selected. The degree of anisotropy, $\left[E_{av}(0\,\mathrm{deg}) - E_{av}(90\,\mathrm{deg})\right]/E_{av}(90\,\mathrm{deg})$, was observed to be $\approx 40\%$ with 40 fs and $\approx 25\%$ with 250 fs. The anisotropy was explained on the basis of model proposed by Breizman et al.[108] which models the cluster as two concentric spheres : outer one as ion sphere and inner one as cold electron core. It was demonstrated in Ref.[108] that ions at the surface of the cluster experience a nearly isotropic time averaged potential whereas ions from the deeper inside the cluster feel an accelerating potential that is more along the direction of laser polarization.

Recent experimental results [109, 110] on Ar_n clusters ($n = 400 - 900$) and Xe_n clusters ($n = 500 - 25000$) driven by $800nm$ laser at peak intensity of $\approx 5^{14} W/cm^2$ with pulse duration in few cycles limit ($\sim 3 - 4$ laser time cycles) demonstrate the complete reversal of the anisotropy of ion emission that was observed earlier with comparatively larger pulse duration ($\sim 100 fs$) of laser. They observed that ion yields were larger when the polarization of the laser is perpendicular to the detection axis than along it. This unexpected behaviour was explained qualitatively on the basis of spatially anisotropic shielding of ions due to the oscillating electron charge cloud

within the cluster. Similar studies were also performed by Skopalova et al[111] with Xe and Ar clusters. In these experiments, they observed that ion emission was more energetic in the direction perpendicular to the laser polarization than parallel to it. They also interpreted these result phenomenologically in terms of screening of the ionic field along laser polarization direction due to the collective oscillation of electron cloud.

Thus the anisotropy is categorised in two types.The first one ,in which the ion yield in more along the laser polarization direction than perpendicular to it, will be termed hereafter as "normal anisotropy". The second type of anisotropy deals with the higher ion yield along perpendicular to the laser polarization that will be termed here after as "atypical anisotropy". We have carried out detailed MD simulation studies on "atypical anisotropy" of ion emission from Ar and Xe clusters when irradiated with laser pulses of few time cycles. For the sake of completeness and comparasion, results of normal anisotropy are also presented in this chapter.

4.2 Anisotropy studies for Argon clusters

Our MD code is used to investigate this anisotropic ion emission from Ar clusters irradiated by NIR laser of wavelength 790 nm. Effect of various parameters of interest *viz.* laser pulse FWHM time duration, intensity and size of the cluster is investigated on the anisotropy. The variation of these laser and cluster parameters is performed as follows : pulse duration of the laser is varied from many time cycles ($100fs$) to few time cycles ($5fs$), intensity of the laser is changed from $5 \times 10^{14} W/cm^2$ to $3 \times 10^{16} W/cm^2$ and the cluster size is changed from $16\mathring{A}$ to $58\mathring{A}$. The incident laser pulse is assumed to be linearly polarized along x- direction. Our MD code calculates the phase-space data of all the particles (ion as well as electrons) and stores it after certain time steps. This selected phase space data is further post-processed to calculate the ion energy and electron energy distribution function (IEDF and EEDF). For the calculation of particle energy distribution function, the energy scale is divided into certain predefined equally spaced energy intervals (bin size) and particles are distributed into energy in-

tervals according to their energies. The location for the collection of particles (similar to detector locations as used in experiments) along the directions parallel and perpendicular to laser polarization is chosen to be far away from the cluster. This ensures that particles have achieved their maximum energies before they are detected. We also mention that the total simulation time is kept large enough so as even the lowest energy particle can reach the detector. The time for the particles to reach the detector can be roughly calculated with energies of the order of the saturated mean energy. Therefore we have kept the simulation time long enough (1 ps) for all the cases presented in this paper.

4.2.1 Effect of laser pulse duration

Below we discuss the results of "atypical anisotropy" of ion emission from cluster of radius 58 Å exposed to the laser pulse of intensity $4.5\times10^{15}W/cm^2$. The laser pulse duration is varied over a range of 5 to 100fs. For all the simulation results, we have used open boundary conditions(OBC). The choice of OBC is guided by the fact that most of the anisotropy measurement experiments employ low density clusters[107, 111]. Therefore, a preference is made to choose OBC over periodic boundary conditions(PBC) in our simulations to replicate the experimental scenario as well as to look at the nature of anisotropy in the absence of other clusters. Moreover, we have found that changing the value of R_{IC} does not alter the degree of anisotropy although it may change the other parameters (average degree of ionization, mean ion energy etc.). The ion energy distribution functions (IEDF) for four pulse durations (5,10,20 and 100 fs) are shown in Figs.4.1(a)-(d). It is important to note that the intensity of the laser pulse is kept constant for all the pulse durations. Consequently, the integrated radiation energy flux $F \equiv I \cdot \tau$ increases continuously as the pulse duration of the laser is changed from 5fs to 100fs ($F \equiv 22.5, 45, 90, 450 J/cm^2$ for $\tau = 5, 10, 20, 100 fs$). The continuous enhancement in the in the energy content of the pulse with the increase in the pulse duration leads to the increased maximum energy (E_{max}=5,7.5,18 and 100 KeV) of the ions as longer pulse duration is employed for cluster irradiation (Figs.4.1(a)-(d)). We also observe that the value of the maximum yield of ions reduces as the pulse dura-

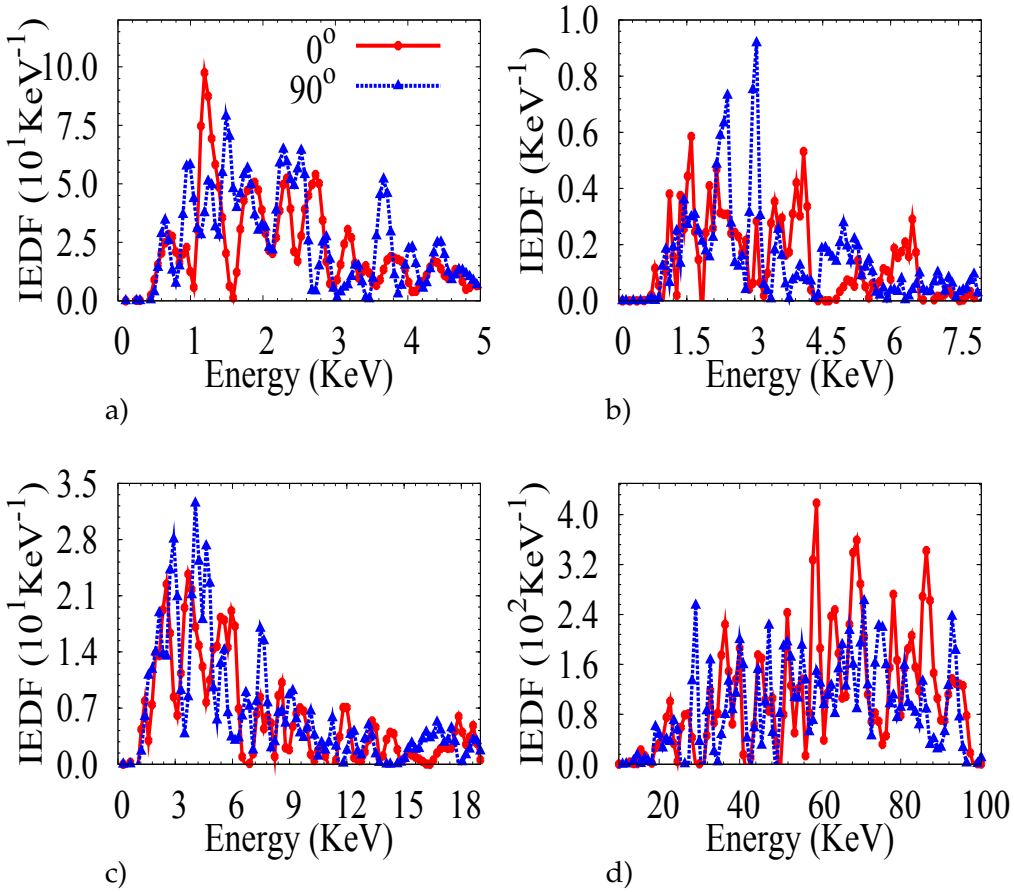

Figure 4.1: *Ion energy distribution function (IEDF) along laser polarization (red:*$0°$*) and perpendicular direction (blue:*$90°$*) for laser pulse duration of 5 fs a), 10 fs b), 20 fs c), and 100 fs d). The cluster radius is taken as* $58\mathring{A}$ *whereas the intensity of the laser is chosen as* $4.5\times10^{15}W/cm^2$.

tion is increased . This can be explained as follows : as the the longer pulse durations are used, the range of energy spectrum broadens *i.e.* higher energy ions start ejecting from the cluster. As we are using the same cluster size or same number of particles for irradiation with various values of the laser pulse duration. Consequently, the lowering of the maximum fraction of particles occurs along the y-axis as the range of energy values along the x-axis increases for longer pulse durations of the laser.

Further, we observe t hat the ion yield along laser polarization direction ($0°$) happens to be more compared to perpendicular direction ($90°$) for the case of the longest pulse duration used in the simulation (Fig.4.1(d)). This is the "normal anisotropy" , as mentioned earlier in the previous section, which has been observed for many laser

cycle pulse duration and explained phenomenologically on the basis of "charge flipping" model[95, 112]. MD results also confirmed [113] that the electrons change their position from one pole to other as a response of changing laser electric field. This flipping of the electron population leads to augmented ionization states of ions at the poles that further causes the asymmetric cluster explosion due to the charge imbalance introduced. When the pulse duration of the laser is further reduced to few time cycles (10 and 20 fs), we observe that the nature of the anisotropy starts changing : more ions start emitting along 90° rather than 0° (Figs. 4.1(b)-(c)) for lower energy part of IEDF spectrum. Moreover, we find that there exists an optimum pulse duration ranging between 10-20 fs for which this "atypical anisotropy" is seen prominently. As mentioned in the previous section that same kind of anisotropy was also observed experimentally for Ar clusters irradiated by low intensity laser pulse of few cycles duration[109]. The collective dynamics of inner electron cloud can explain observed anisotropy. For intermediate pulse durations (10 to 20 fs), the well developed electron cloud oscillates with the laser frequency and it strictly follows the laser electric field. We have also confirmed this collective oscillations of inner electrons under the presence of external laser electric field by looking at the snap-shots of particle positions at two consecutive laser half cycles (19 and 20 fs) as shown in Fig 4.2. In Fig 4.2, we see the oscillations of aggregated electron cloud strictly follows the external laser electric field or laser polarization direction. It is important to note that the direction of this oscillation always remains opposite to the external laser field in the two consecutive laser half cycles(Figs. 4.2(a) and (b)) as the electrons are negatively charged particles. Consequently, it appears that inner electron charge gets smeared more along the the direction of the laser electric field rather than the perpendicular direction. This elongation of electron cloud effectively shields the ions more along 0° compared to 90°. This initial shielding effect finally results in ion anisotropy of coulomb explosion. At the time of explosion, more ions will emerge along perpendicular direction of laser polarization rather the parallel direction due to shielding as explained earlier. It is also noteworthy that this "atypical anisotropy" is observed for low energy ions in the IEDF plots as shown in Fig.4.1. The reason is that these ions emerge from the deep

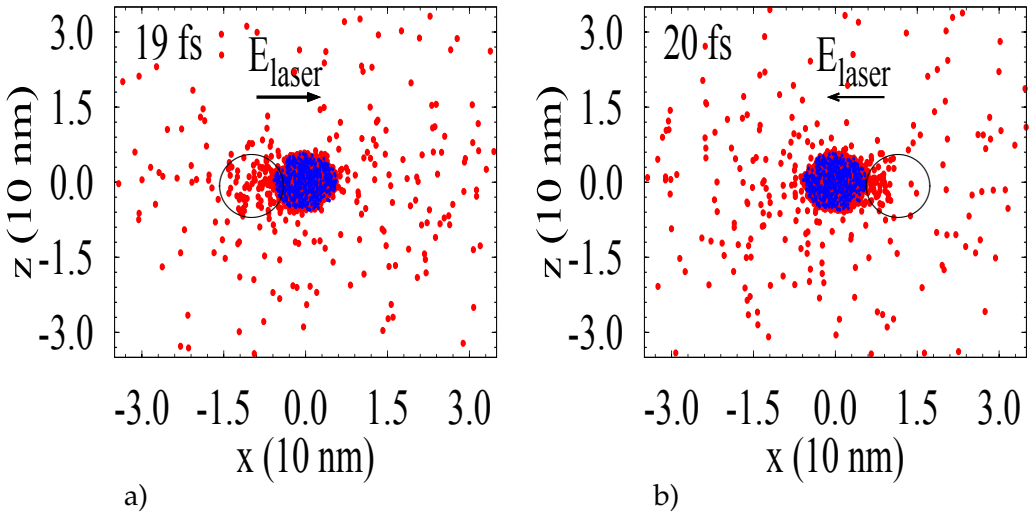

Figure 4.2: *Snapshots of particle (red dots: electrons and blue dots: ions) positions at 19 fs a), and 20 fs b). The encircled area represents the aggregation of electron opposite to the laser electric field.*

inside the cluster where they were being quite effectively shielded by the oscillating electrons cloud, compared to the ions at the periphery of cluster.

For the case of many pulse duration (100fs) of the laser(Fig.4.1(d)), more energy is deposited inside the cluster as the integrated radiation flux is maximum for this case. It leads to the emergence of higher charge states as described earlier. Further, the increased collisional heating of electrons distorts the ordered motion of electron cloud along the laser electric field causing the reduced shielding of the ions. The simultaneous presence of higher charge states and reduced directed motion of electron cloud diminishes the observed "atypical anisotropy" for the longest pulse duration. Rather the "charge flipping" dynamics happens to be more important when longer pulse durations are employed that leads to the normal anisotropy of cluster explosion. For the case of the shortest pulse duration of 5 fs, the "atypical anisotropy" again disappears (Fig.4.1(a)). For this case, the integrated radiation flux of the laser pulse is minimum which leads to minimum absorbed energy by the cluster. Consequently, the formation of sufficiently sized electron cloud is not achieved. The absence of well developed electron sphere may lead to disappearance of "atypical anisotropic" emission of cluster explosions for the case of shortest laser pulse duration used in the simulation.

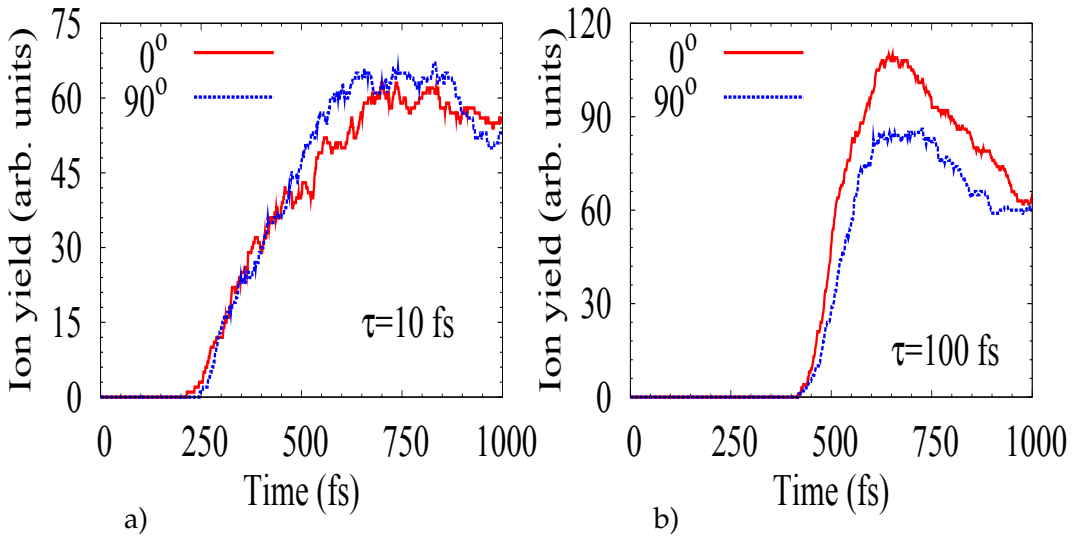

Figure 4.3: *Ion yield along laser polarization (red:*0°*) and perpendicular direction (blue:*90°*) for pulse duration of 10 fs a) 100 fs b). The other parameters are kept same as 4.1.*

To get a quantitative picture, we show in Fig. 5.3 instantaneous ion yields for the cases of pulse duration of few cycles *i.e.* 10 fs (Fig. 4.1(b)) and many cycles *i.e* 100 fs (Fig. 4.1(d)). For the case of 100 fs (Fig. 5.3(b)), the ion yield along 0° always remains well above than that along 90° at all time steps (equivalently for all energies). As the pulse duration is reduced (10 fs), the high energy ions (which reach detector earlier) emit almost isotropically(Fig. 5.3(a)). After about 500 fs, we start observing more ions along 90° . Although the difference between the two curves is small, it leads to significant number when integrated over time.

4.2.2 Effect of laser pulse intensity

In this section, we intend to study the effect of laser pulse intensity on the "atypical anisotropy". As found in the previous section, the laser pulse duration of $10fs$ is obtained as an optimum pulse duration that exhibited most prominent signatures of "atypical anisotropy" for Ar cluster of size $58\mathring{A}$ at laser pulse intensity of $4.5 \times 10^{15}W/cm^2$. For these studies, the size of the cluster and the pulse duration of the laser are fixed at $58\mathring{A}$ and $10fs$ whereas the intensity of the laser is varied from $5.0\times10^{14}W/cm^2$ to $3.0\times10^{16}W/cm^2$. The results for corresponding IEDF's are presented in Fig. 4.4. It

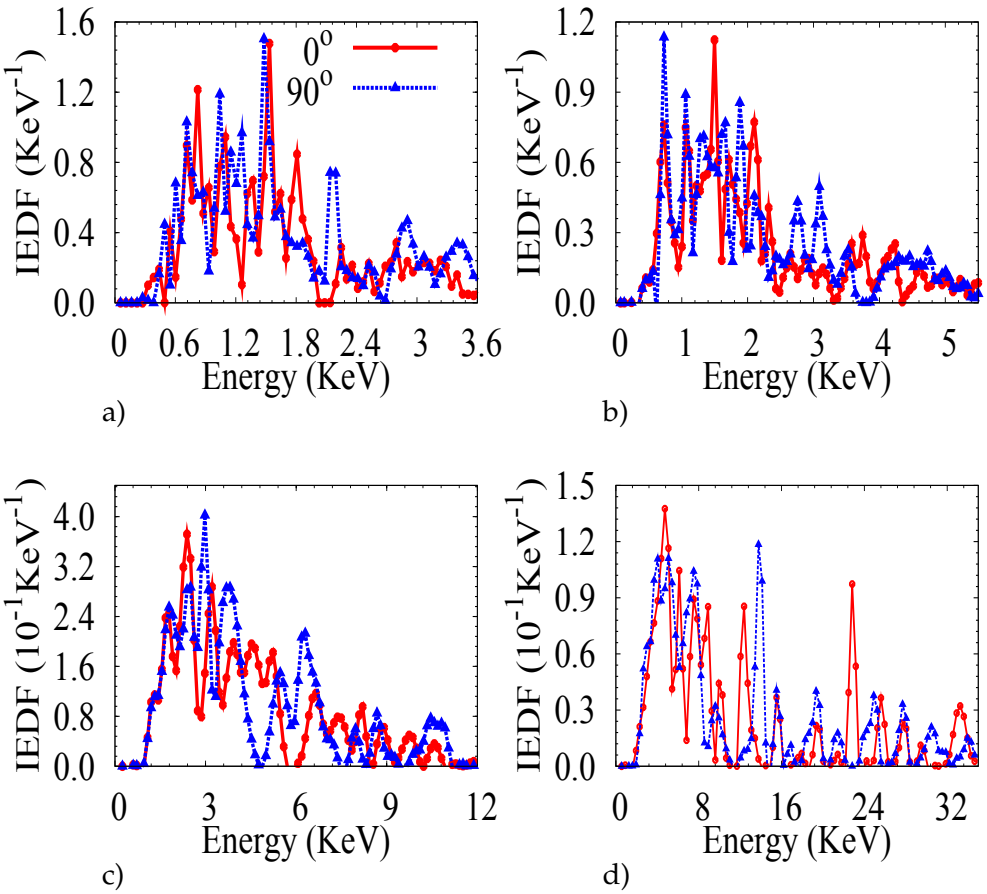

Figure 4.4: *Ion energy distribution function (IEDF) along laser polarization (red:*0°*) and perpendicular direction (blue:*90°*) for 58 Å radius Ar cluster irradiated by laser pulse of FWHM duration of 10 fs and intensities* 5.0×10^{14} *a),* 1.0×10^{15} *b),* 8.0×10^{15} *c), and* $3.0\times10^{16} W/cm^2$ *d).*

is noteworthy that as the intensity of the incident laser pulse increases for fixed pulse duration, the range of the energy spectrum shifts towards higher energy side with a corresponding reduction in the absolute yield for ion energies at lower side of the spectrum. It can be explained on the basis of enhanced energy content for the incident laser beam (F$\equiv 5, 10, 80, 300 J/cm^2$ for I=$5.0\times10^{14}, 1.0\times10^{15}, 8.0\times10^{15}, 3.0\times10^{16} W/cm^2$) as intensity is increased. For lower intensities (Fig. 4.4(a)), ions almost seem to emit isotropically and the same trend is also followed for higher intensities (Fig. 4.4(d)), whereas there exist (Fig. 4.1(b)) an optimum intensity around $4.5\times10^{15} W/cm^2$ for which ion yield is more along perpendicular direction of laser polarization than parallel direction. The absence of "atypical anisotropy" in the lower side of the intensity

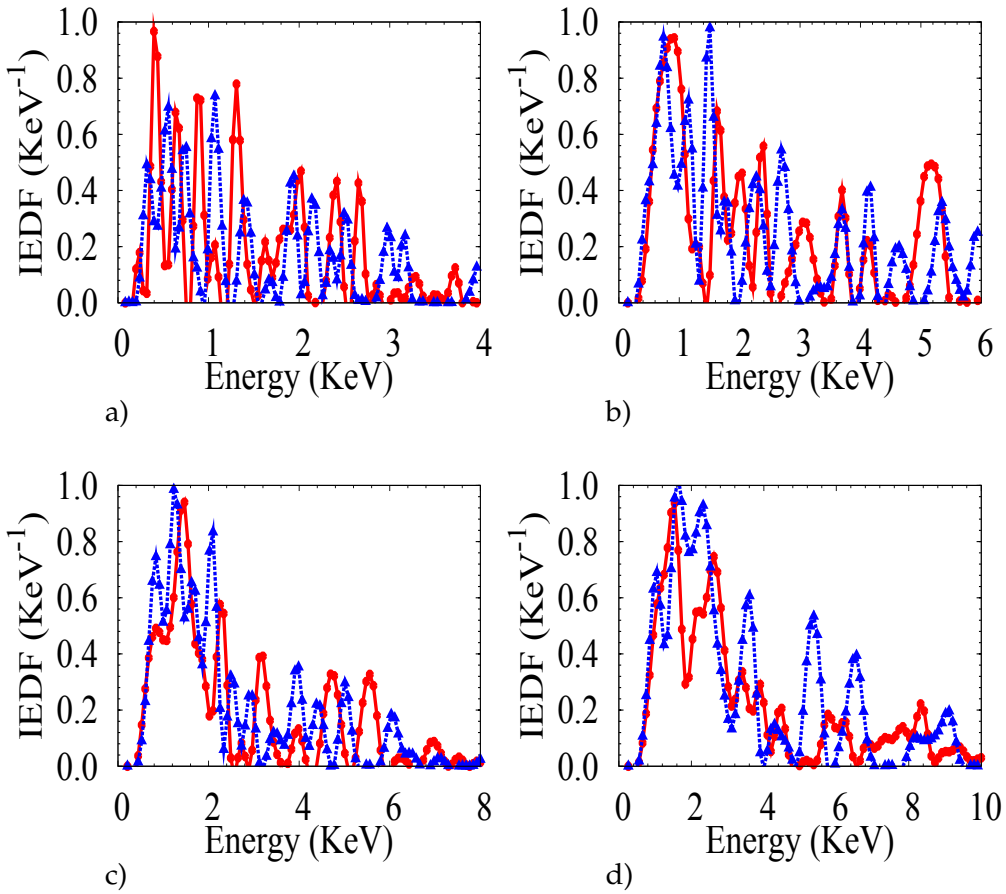

Figure 4.5: *Ion energy distribution function (IEDF) along laser polarization (red:0°) and perpendicular direction (blue:90°) for cluster size 16 Å a), 24 Å b), 33 Å c), and 45 Å d) irradiated by laser pulse of intensity* $4.5\times10^{15} W/cm^2$ *and FWHM pulse duration of 10 fs.*

range considered can be explained due to unavailability of inner electron cloud that is responsible for shielding of ions. When the intensity becomes quite high, the increased value of electron density inside the electron cloud facilitates the collisional ionization that further hampers the directed motion of electron cloud along the laser polarization direction. The damping of amplitude of electron cloud motion reduces the effect of shielding of ions by these electrons that lead to the normal isotropic emission. It may be noted that "charge flipping" dynamics of the ions is not able to overtake here as the pulse duration are really short that causes almost isotropic emission of ions from the cluster.

4.2.3 Effect of cluster size

Here, we have tried to see the effect of cluster size on the nature of anisotropy. For these studies the size of the cluster is varied from $16\mathring{A}$ to $45\mathring{A}$ with intermediated values as $24\mathring{A}$ and $33\mathring{A}$ whereas the laser intensity and pulse duration are chosen as $\sim 4.5 \times 10^{15} W/cm^2$ and $\sim 10fs$, respectively. The selection of these values of intensity and pulse duration are inspired from the studies performed in previous paragraphs where these parameters exhibited most pronounced signatures of "atypical anisotropy". The Normalised IEDF plots are shown in Figs. 4.5(a)-(d) for various values of cluster sizes. As the size of the cluster is increased (Figs. 4.5(a)-(d) and Fig. 4.1(b)), "atypical anisotropy" increases. For sufficiently small clusters, this kind of anisotropy is absent because the cluster explodes before accumulation of enough number of inner electrons. As the size of the cluster increases, the explosion of cluster gets delayed as well the inner electrons population also increases. These effects result into observed anisotropy of cluster explosion. Similar trend were observed for the variation of optimum pulse duration with number of particles inside the cluster[111].

4.3 Anisotropy studies for Xenon clusters

As mentioned in the section 4.1, both types of anisotropy (Normal and atypical) was observed experimentally in Xe clusters in the domain of large pulse duration and extremely short (few cycles pulse) pulse duration, respectively[101, 106, 110, 111]. In this section, we intend to present the results of both kind of anisotropies in the Xe cluster explosion using our MD code.

4.3.0.1 Comparasion with the earlier experimentally observed anisotropy

For this comparative study, we have used our MD code with the open boundary conditions. The use of OBC is to mimic the experimental environment where the low density clusters are used for laser irradiation. First, we present our results of normal anisotropy with long pulse duration. The choice of the simulation parameters is taken as of 50 Å Xe cluster irradiated with laser beam of peak intensity of 1.3×10^{16} W/cm^2

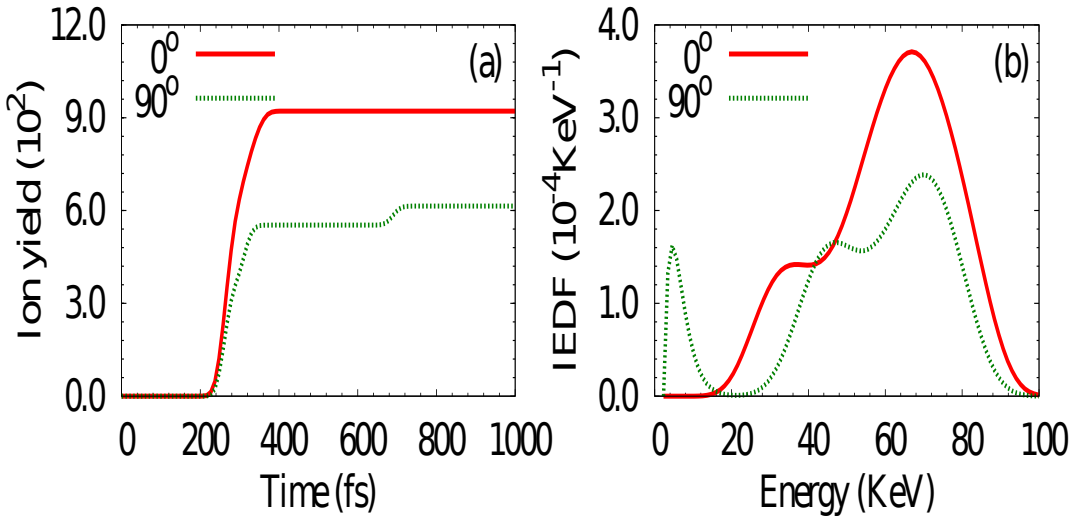

Figure 4.6: *Time variation of ion yields (a) and ion energy distribution functions (b) along and perpendicular direction of laser polarization from 50 Å Xe cluster. The laser intensity is $1.3\times10^{16} W/cm^2$ at pulse duration of 170 fs.*

at pulse duration of 170 fs. These are the typical values used in the experiments with relatively long pulse durations. The outcome of this investigation is shown in Fig.4.6. The temporal evolution of time integrated (integration from time $t = 0$ to $t = t$) yield of ions is plotted in Fig. 4.6(a). As it is evident from this plot that collection of ions starts at nearly 200 fs and it continues to increase till 400 fs. The integrated ion yield becomes nearly constant after this time. The ion yield along laser polarization direction (0°) is more than that along perpendicular direction (90°). The distribution of ions according to their energies (IEDF) is shown in Fig.4.6(b). We observe that ions show a preferential direction of emission (parallel to laser polarization) for a wide range of energy spectrum ranging almost from 20 KeV to 100 KeV. These results clearly show the signatures of normal anisotropy that exhibits itself into the pronounced emission along the laser polarization direction. These results are explained by considering the polarization of surface charge distribution along with that of the dielectric medium inside the cluster due to external laser field. The laser field exerts a direction dependent pressure ($P_{pol} \sim \cos^2\theta$, where θ is the angle between laser polarization axis and sight of observation) on the induced surface charge distribution. This pressure maximizes itself along 0° which results into enhanced ion yield and more energetic ions along the

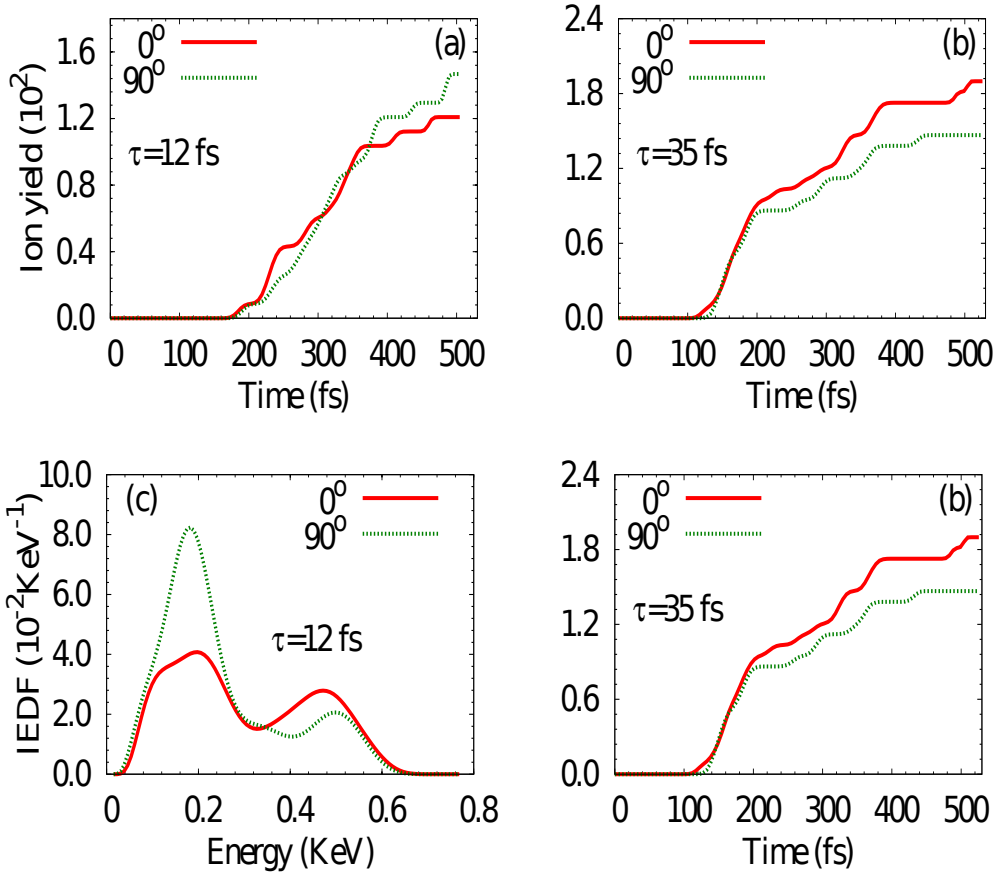

Figure 4.7: *Time variation of integrated ion yields (a,b), and distribution of various ionic species according to their energies (c,d) from 25 Å Xe cluster irradiated by laser pulse durations of 12 fs and 35 fs. The laser intensity of 5×10^{14} W/cm^2 is used.*

laser polarization direction[106].

To observe the "atypical anisotropy", we have to consider the case of extremely short pulse duration (few cycles pulse). For these results, we have considered the case of a small Xe cluster with radius $25\mathring{A}$. This cluster is driven by the laser of intensity 5×10^{14} W/cm^2 at pulse durations of 12 and 35 fs, respectively. The laser and cluster parameters used in the simulation are nearly same as used in experiment of Mathur *et. al.* [110]. Time variation of integrated ion yields along direction parallel (0°) and perpendicular (90°) to laser polarization are plotted for laser pulse durations of 12 and 35 fs in Figs. 4.7(a) and 4.7(b), respectively. For the case of 12 fs, ions start appearing at around 200 fs whereas they appear at about 120 fs for 35 fs laser pulse duration. It indicates that higher energy ions are generated for longer pulse duration.

Presence of higher energy ions for longer pulse duration is a consequence of increased energy content for the pulse as the peak intensity is kept constant for both the pulse durations. For the case 12 fs, the ion yield along 90° is more than that along 0° ("Atypical anisotropy") whereas opposite trend is observed for the case of 35 fs("Normal anisotropy"). The reversal of anisotropy from normal to atypical in few cycle laser pulses can be explained on the basis of initial spatial shielding of ions by electrons and it will be discussed in the next paragraph. To further strengthen our observation about directional preference of ion emission, we have shown (Figs. 4.7(c) and 4.7(d)) ion energy distribution function (IEDF) plots for both pulse durations of 12 and 35 fs. Again we observe the reversal of anisotropy as laser pulse duration is changed from $\tau = 35$ fs to $\tau = 12$ fs. Maximum ion energy and ion yield for the case of $\tau = 12$ fs are observed to be 0.8 KeV and $\sim 8 \times 10^{-2}$ KeV^{-1} respectively. On the other hand, maximum particle energy increases up to 3 KeV and maximum yield reduces to a value of $\sim 2.4 \times 10^{-2}$ KeV^{-1} for $\tau = 35$ fs. The broadening of energy spectrum along with the decrease in maximum yield of ions is a result of increased energy content for the longer pulse.

4.3.0.2 Computational results for anisotropy

In this section, we present our detailed results of anisotropic ion emission from 56 Å Xe cluster exposed to laser pulse of intensity 4.5×10^{15} W/cm^2. The pulse duration of the incident laser beam is varied from 10 to 100 fs. These simulation parameters are nearly same as used for anisotropy studies for Ar cluster as discussed in section 4.2. Results for various time integrated IEDF plots are shown in Figs. 4.8(a-d) for laser pulse durations of 10, 20, 30 and 100 fs respectively. We also show the temporal evolution of integrated yield of ions for the above mentioned pulse durations in Figs.4.9(a-d). We note that as the pulse duration of laser is increased, the maximum cut off energy appearing in IEDF spectrum increases. This happens because more integrated radiation energy flux ($F \equiv I \cdot \tau$; $F = 45,\ 90,\ 135,\ 450$ J/cm^2 for $\tau = 10,\ 20,\ 30,\ 100$ fs) interacts with the cluster at constant peak intensity as the pulse duration is increased for various cases. It may be noted that ion yield for shortest pulse duration ($\tau = 10$ fs)

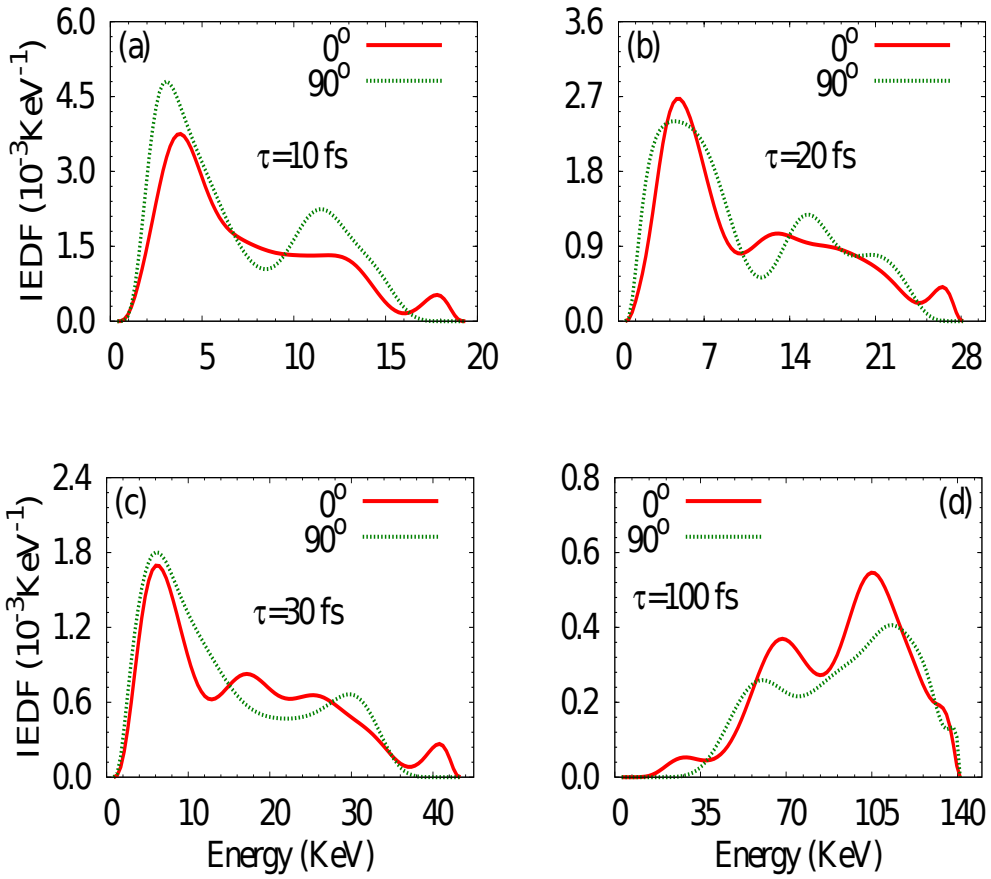

Figure 4.8: *Distribution of various ionic species according to their energies (IEDF) for 56 Å Xe cluster exposed to laser of intensity 4.5×10^{15} W/cm^2 for FWHM pulse duration of 10 fs (a), 20 fs (b), 30 fs(c) and 100 fs (d).*

remains higher along the direction perpendicular direction to laser polarization than parallel to it. Same kind of anisotropy was also observed in our numerical simulation for Ar cluster with few cycles laser pulses, as discussed in the section 4.2. These results can be explained on the basis of spatial shielding of ions by collective oscillations of inner electrons in the presence of external laser electric field. For few cycle laser pulses, incident laser field terminates before any significant outer ionization leading to build up of inner electrons. This inner electron cloud oscillates in harmony with the external laser electric field. This collective oscillation of inner electrons under the presence of external laser electric field can also be observed (Fig.4.10) in snap-shots of particle positions at two consecutive laser half cycles (14 and 15 fs). In Fig. 4.10, the aggregated inner electron cloud is shown under area bounded by the ellipses. It may

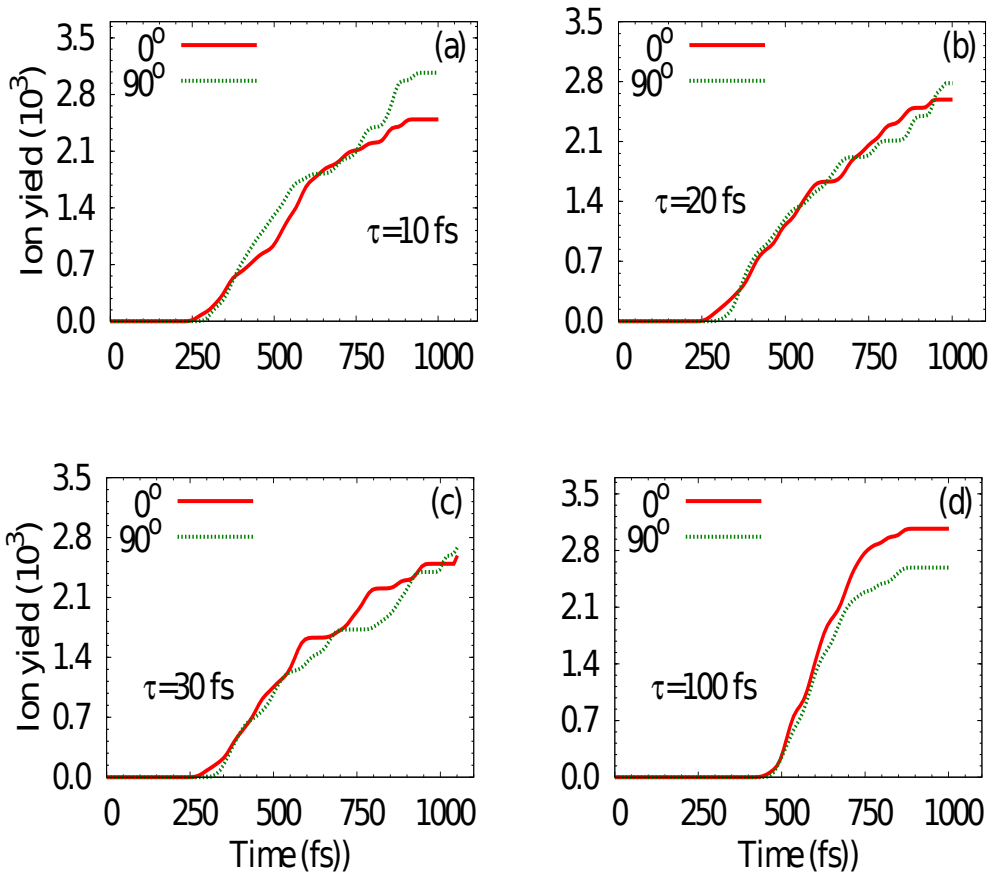

Figure 4.9: *Temporal evolution of integrated ion yields for FWHM pulse duration of 10 fs (a), 20 fs (b), 30 fs(c) and 100 fs (d). The other laser and cluster parameters are same as used in Fig.4.8*

be noted that each dot depicting the particle is a macroparticle (collection of identical real particles) rather than a real particle. This means that a sufficient number of real particles (inner electrons) undergo oscillation along the direction of laser electric field. It is also noteworthy from Figs. 4.10 (a) and (b) that the direction of oscillation of electrons always remains opposite to external laser electric field. On the other hand, no aggregation of inner electrons is observed along the direction perpendicular to laser polarization. Collision effects of electrons with other particles is also not significant for the few cycle laser pulse duration that can otherwise hampers the directed motion of electron cloud. Consequently, the inner electron charge elongates itself along the direction of laser electric field due to their continuous rapid oscillation in harmony with the laser field. The smearing of the electronic charges shields the ions effectively

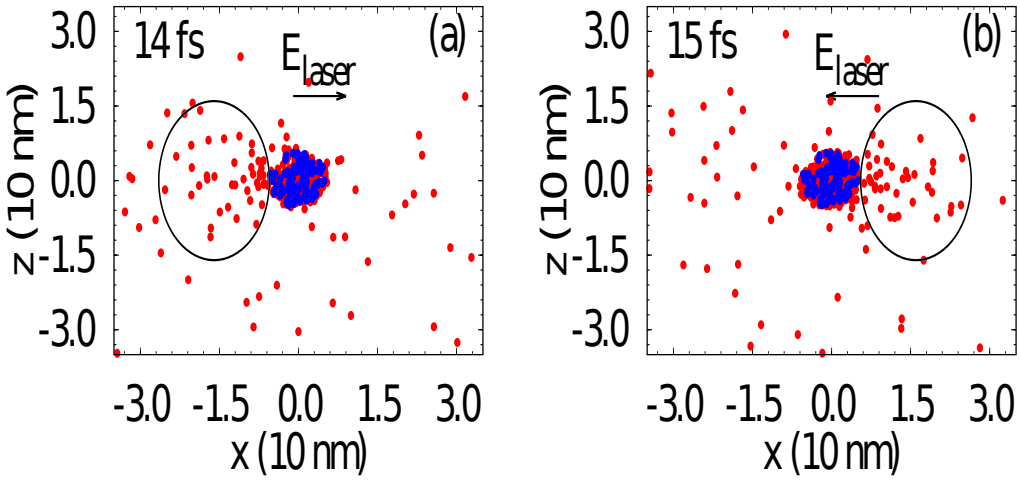

Figure 4.10: *Locations of macroparticles (red dots: electrons and blue dots: ions) at 14 fs (a), and 15 fs (b) for laser pulse duration of 10 fs. The other laser and cluster parameters are kept same as used in Fig. 4.8. The area bounded by ellipses represents the aggregated electron cloud which oscillates opposite to the laser electric field.*

along laser polarization than perpendicular direction. This initial shielding of ions results into the observed anisotropy of ions for the few cycle laser pulse. As the pulse duration is increased, collision effects start affecting the directional motion of electron cloud that results into the reduced shielding of ions due to the oscillating electron cloud. This effect reduces the observed preferential direction of cluster explosion. For still longer pulse durations, surface effects start dominating the ion anisotropy. The effect of anisotropic pressure due to the laser field on the induced surface charge of Xe cluster governs the emission of more ions along laser polarization direction than perpendicular direction.

Till now we have explained the "atypical anisotropy" by looking at the oscillation of inner electron cloud along the laser polarization direction that shields the ion explosion along the direction of electric field of the laser. To understand this shielding phenomenon in more detail, the knowledge of electric field at the periphery of expanding cluster will be more useful. Therefore, we calculate the the time variation of electric fields along the direction parallel to laser polarization (E_0) and perpendicular to it (E_{90}) for laser pulse durations of 10 and 100 fs (Fig.4.11). The spatial locations

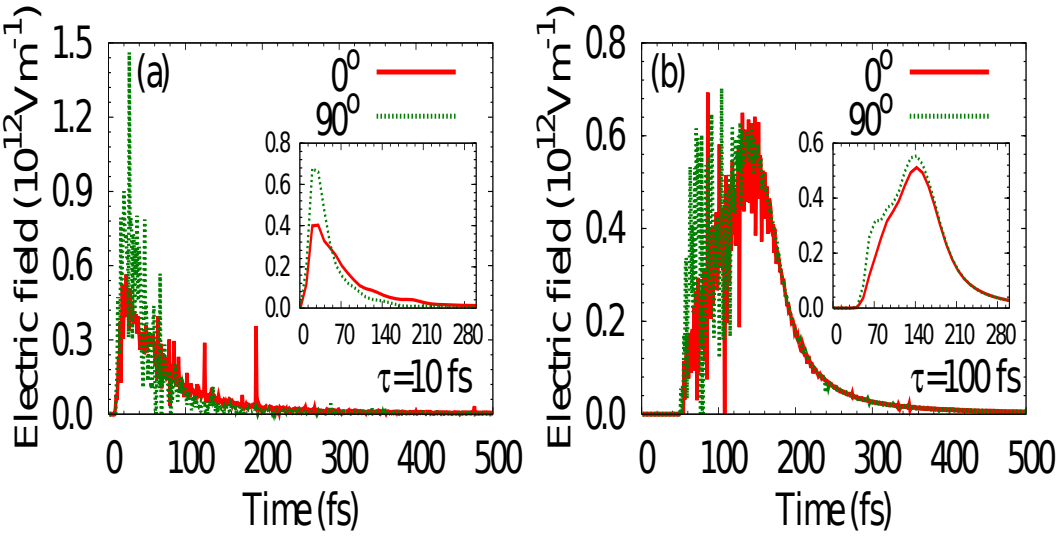

Figure 4.11: *Temporal variation of electric field at the surface of the cluster for laser pulse durations of 10 fs (a), and 100 fs (b). The other laser and cluster parameters are same as used in Fig.4.8. In the inset of each plot, we have shown the smoothed electric field till 280 fs.*

(x,y,z) for electric field calculations are selected as (R(t),0,0) and (0,0,R(t)) where R(t) is the instantaneous radius of the expanding cluster. The electric field due to both electrons and ions are vectorially added at the desired locations and the x-component of the resulting field at (R(t),0,0) is defined as E_0. Similarly, the z-component of resulting field at (0,0,R(t)) is defined as E_{90}. We observe that E_{90} is more than E_0 for pulse duration of 10 fs (Fig.4.11(a)) whereas these two fields do not differ significantly for pulse duration of 100 fs (Fig. 4.11(b)). We may note that the situation remains unchanged for 10 fs case even after addition of laser field to radial field calculated above whereas E_0 becomes more than E_{90} for 100 fs. These variations of electric fields explain the anisotropy in the ion emission for pulse durations of 10 and 100 fs. It may be worth mentioning about the normal anisotropic ion emission (ion yield is more along 0° than 90°) from Ar clusters ($\sim$ 40 nm) that has also been studied using a different theoretical approach *viz.* particle-in-cell method [89] in many pulse cycle regimes ($\sim$ 60 fs) for various laser intensities and cluster sizes. Our study deals with anisotropy (ion yield is more along 90° than 0°) for Xe clusters ($\sim$ 50 Å) in few cycle pulse duration regime ($\sim$ 10 fs). We have also carried out MD simulations for other laser intensities and cluster radii. The nature of anisotropy does not change due to variations in laser

and cluster parameters.

4.4 Summary

To sum up, we have used a three dimensional molecular dynamic model to study the interaction dynamics of Argon and Xenon clusters irradiated with laser pulses of moderate intensities and pulse durations ranging from many cycles to few cycles. For the case of many cycles pulse duration, we observe normal anisotropy in which more ions are ejected along the direction of laser polarization (0°) than perpendicular to it (90°). The situation changes completely when few cycles laser pulse are used for irradiation *i.e.* more ions are emitted along 90° than 0°. The reversal of anisotropy is explained on the basis of initial spatial shielding of ions due to oscillation of inner electrons along the direction of laser polarization. Moreover, the calculation of electric field on the periphery of expanding cluster gives higher electric field along 90° than that along 0°. This direct calculation of electric field supports the shielding argument made earlier to explain the "atypical anisotropy" for the case of few cycle laser pulse duration.

CHAPTER 5

Carrier envelope phase effects in the regime of few cycles laser pulses

Nowadays, it has been possible to routinely generate the laser pulses with time duration upto few laser time cycles due to the revolution made in femtosecond laser technology during the last decade[11]. As mentioned in the chapter 1, the generation of few cycles laser pulses depends upon the combination of two techniques namely self phase modulation (SPM) and negative group velocity (GVD) dispersion. The pulse spectrum is artificially broadened through SPM and then re-compressed spectrally with the use of $-ive$ GVD. There are mainly two methods of generation of few cycles laser pulses. The First one relies on the use of gas-filled hollow wave-guides as SPM reagent and prism dispersive delay line as a pulse compression technique [12]. In the second method, self-guiding of laser pulses through filamentation is used instead of external guiding which provides a medium to occur SPM. Finally, the ultra-short pulse is achieved by re-compressing the output[13]. In such short laser pulse where the duration of the the laser pulse approaches towards the time period of the laser oscillation, the initial phase of the carrier wave with respect to the envelope becomes an important parameter[11]. The correct knowledge of this quantity, commonly known as CE phase (ϕ), is required to completely describe the laser electric field ($\mathcal{E}(t) = \mathcal{E}_0(t)\cos(\omega t + \phi)$). Thus the strong field interactions originating from few cycles laser pulses become sensitive to the correct value of the CE phase. In this chapter, we intend to study the effect of this CE phase (ϕ) on the ionization dynamics of small Xenon clusters in limit of few cycles laser pulse duration.

5.1 CE phase : Importance and signature on atoms coupled with few cycle laser pulses

As discussed in the previous paragraph, the complete description of electric field of the few cycles laser light needs all three quantities : field amplitude ($\mathcal{E}_0$), frequency (ω) and CE phase (ϕ), simultaneously. Generally, it is not possible to generate the laser pulses in succession with fixed initial CE phase from the oscillator due to the difference between the phase velocity and group velocity of the pulse. Due to this process, the carrier wave slides under the envelope as the pulse circulates in the mode-locked laser[114] and pulse to pulse CE phase changes accordingly. Now, it has been possible to to control this parameter by appropriate feed back techniques[115, 116] and also, direct measurement of ϕ has been demonstrated[117, 118].

When these CE phase stabilised lase pulses are coupled with the individual atoms, it lead to the very interesting phenomenons. For such ultra-short laser pulses with stabilised laser pulses, the probability of tunnelling of the electron from the parent atoms depends strongly on the value of the instantaneous electric field. Thus the release time of the electron from the parent atoms is dependent on the instantaneous electric field that inherently contains the information of ϕ. Now this released electron from tunnel ionization follows the laser field. It is important to note that this electron may return to the parent atom depending on which instant of time in the laser cycle, the electron was ejected from the atom. When the electron approaches to the atom, it can lead to high harmonic generation(HHG) by recombination, above-threshold ionization(ATI) by elastic scattering or non-sequential double ionization(NSDI) by inelastic scattering with it. It is possible to control these various re-scattering processes via a control over CE phase. Indeed, it is experimentally observed that HHG[117] and ATI[118] are strongly dependent on ϕ. NSDI [119–122] is of particular interest as it can affect the ionization dynamics of an isolated atom. Similar to HHG and ATI, NSDI also showed dependence on CE phase as demonstrated by measuring electron-electron momentum correlation[123] or measuring the asymmetric parallel momentum distribution of residual ion[124]. The asymmetry was explained by considering the phase dependent

tunnel ionization rate, kinetic energy of returning electron and time duration in which re-collision occurs[125].

Recent experiments on Xe and CS_2 atoms in strong laser fields clearly demonstrated the strong dependence of ionization dynamics of various atoms on CE phase[126] of the laser pulse. They observed that the fractional charge states of various ionic species normalized against singly ionized charged state shows a major variation when ϕ is changed from 0 to $\pi/2$[126]. Literature mentions about the previous analytical studies showing the significance of CE phase on ionization of atoms. Rastunkov *et al*[127] have studied the CE phase dependence of ionization of hydrogen atoms by a high power single-cycle pulse in the Landau-Dykhne approximation. Here, the initiating mechanism of ionization due to high power laser is tunnel ionization. It has been found With exponential accuracy that the ionization by laser pulse with CE phase $\phi = 0$ is much more effective than that with CE phase $\phi = 90$. The Effect of ϕ is not only limited to the tunnelling ionization of atoms but also can be extended to other ionizing mechanisms such as photo-ionization. Photo-ionization of Xe and H atoms exposed to attosecond pulses (Mean photon energy $\sim$ 100eV, pulse duration $\sim$ 100 as) has been analytically studied by using first-order time-dependent perturbation theory[128, 129]. The laser wavelength used in these studies varies from vacuum ultra violet (VUV) to soft X-ray (SXR) region that means the initial ionizing mechanism to be photo-ionization in place of tunnel ionization. The results obtained in this investigation also indicated the presence of strong CE phase dependence of photo-ionization probability. It may be noted that these theoretical predictions can be useful for various VUV intense laser cluster experiments performed by using light sources such as DESY free electron laser (FLASH)[130, 131].

5.2 CE phase : Effect on small clusters driven by phase stabilised few cycles laser pulses

Most of the experimental and analytical studies, as mentioned in previous paragraphs, concentrate only on individual atoms which are exposed to few cycle laser pulse with

controlled CE phase. All these results clearly indicate a strong dependence of ionization on phi. In stead of isolated atoms, we have chosen small clusters of Xenon atoms and tried to see how the, initial phase of the carrier wave with envelope, affect the ionization dynamics of these small clusters.

5.3 Simulation methodology

We have used our code MD-ILAC to study this problem. The code has already been discussed in detail in chapter 2. This code is modified to accommodate the effects occurring in few cycles laser pulses. In stead of Gaussian laser pulse, we have used a conventional model of an n-cycle laser pulse, the $\sin^2$ pulse. The temporal variation of the electric field of the n-cycle laser pulse is given as

$$E(t) = E_0 sin^2(\omega t/2n) cos(\omega t + \phi); \;\; 0 < t < nT \tag{5.1}$$

, where ω and T denotes frequency and time period of the laser pulse, respectively. The spatial variation of laser intensity is ignored as it was done previously, due to much smaller size of the cluster in comparasion of the wavelength of the laser pulse. The wave-vector of the electromagnetic wave is assumed to be along y axis whereas its electric and magnetic field are aligned along x and z direction respectively.

The initial ionizing mechanism used originally in the code was tunnel ionization and the corresponding ionization rates are calculated by using Ammosov, Dellone and Krainov (ADK) formula [26] as,

$$\begin{aligned} \nu_{ofi} = & \left(\frac{3En^{*3}}{\pi \bar{Z}^3}\right)^{1/2} \frac{(2\ell+1)(\ell+|m|)!}{2^{|m|}(|m|)!(\ell-|m|)!} \\ & \times \left(\frac{2e}{n^*}\right)^{2n^*} \frac{1}{2\pi n^*} \left(\frac{2\bar{Z}^3}{En^{*3}}\right)^{2n^*-|m|-1} \\ & \times \left(\frac{\bar{Z}^2}{2n^{*2}}\right) exp\left(-\frac{2\bar{Z}^3}{3n^{*3}E}\right) \frac{1}{2.4 \times 10^{-17}} \quad s^{-1} \end{aligned} \tag{5.2}$$

. In this equation, $E = \sqrt{2 \times 10^4 \, I/(c\,\varepsilon_o)}/5.14 \times 10^{11}$ is the electric field in atomic units, $I(W/cm^2)$ is the intensity of laser light and c is the speed of light in SI units,

ε_o is the permittivity of free space, $\bar{Z}$ is the degree of ionization, $n^* = \bar{Z}/\sqrt{2I_p}$ is the effective quantum number, I_p is the ionization potential in atomic units, e is the charge of electron, ℓ and m are the orbital and magnetic quantum numbers of outer electron respectively. Ionization rate is calculated for each value of m and averaged over it.

We want to mention that the tunnel ionization rates are obtained as a quasi-classical solution of the ionization of atom in the presence of alternating electromagnetic field under certain simplifying assumptions [24]. One of the assumptions is that these formulas are derived for non-relativistic case where the speed of electron is much less than the speed of light. Consequently the effect of magnetic field is not considered in this solution. It is also important to note that ADK rate given in (5.2) is obtained after a time averaging over one complete laser cycle. Consequently, the electric field appearing in equation (5.2) is only the amplitude part of the laser electric field. This formula does not consider the instantaneous electric field of the laser which has explicit information about the CE phase part of the pulse. This ADK rate formula has to be modified to accommodate the effects of CE phase which become extremely important for the laser pulse approaching towards the limit of few laser time cycles. As a first approximation, we have followed the idea given by Bauer *et al*[132] to account for the effects of CE phase in tunnel ionization rate. In stead of using amplitude of electric field in ADK rate (5.2), we use absolute value of time dependent electric field ($|E(t)|$)[132]. All the calculations made in this chapter use this modified ADK formula in our studies on the ionization dynamics of Xe clusters.

Once a sufficient number of electrons get accumulated inside the cluster, they further undergo inelastic collisions with other atoms and produce more electrons. A fitting formula [88] is used to calculate the collisional ionization rate for clusters with $Z < 28$ whereas Lotz's formulation [79] is used for atomic species with Z ≥ 28 as,

$$\nu_{ci} = 6.7 \times 10^{-7} \, \frac{n_e \, a \, q}{I_p \sqrt{kT_e}} \int_{I_p/kT_e}^{\infty} \frac{e^{-x}}{x} dx \qquad s^{-1} \tag{5.3}$$

where, n_e (cm^{-3}) is electron density, $a = 4.5$ is constant, q are number of electrons in outer orbital of particular ion, I_p (eV) is the ionization potential for a particular ion,

kT_e (eV) is the electron kinetic energy. It is important to note that the energy of electron depends upon the time of its removal from atoms by tunnel ionization which in turn depends upon the CE phase (ϕ) of incident laser field. If the electron is born such that it sees the accelerating laser field, it will gain more energy than if it would have seen the decelerating laser electric field. Consequently, the resultant kinetic energy of electrons will also affect the collisional ionization rate. Thus, the ionization of ions due to the inelastic collisions with electrons also becomes an indirect function of CE phase. We also want to mention that the collisional ionization rate (5.3) also accounts automatically for collisions with parent as well as with other atoms due to fact that particle trajectories are strictly followed with oscillating electric field of laser.

All other details of the code like particle motion as calculated by equation motion, calculation of distribution functions (IEDF and EEDF) are kept same as in the original code. The changes made in the code to study this particular problem are already mentioned in this section.

5.4 Results

The detailed MD simulation studies have been carried out on the ionization dynamics of high-Z clusters (Xe_{400}). These clusters are driven by strong laser pulse with wavelength lying in near infra-red wavelength region ($\lambda \sim 800$ nm). Open boundary conditions are used unless otherwise stated for the simulation box *i.e.* once the particle leaves the simulation box, it never reappears in the simulation box. The main objective of this investigation is to find out the dependence of ionization of cluster atoms on the pulse duration of the incident laser pulse. For that, the pulse duration of the laser pulse is varied from few cycles τ_1 ($\tau_1 = 2T_0$, where T_0=2.67 fs is one laser time cycle for $\lambda = 800$ nm) to many cycles τ_2 ($\tau_2 = 8T_0$). The peak intensity of incident laser pulse is kept at 1.0×10^{16} W/cm^2 that gives the peak strength of electric field (E_0) for this intensity to be equal to 2.74×10^{11} V/m. The temporal variations of instantaneous electric fields along with their envelopes are shown in figures 5.1(a) and 5.1(b) for $\tau = 2T_0$ and $\tau = 8T_0$, respectively. For each pulse duration, these plots also

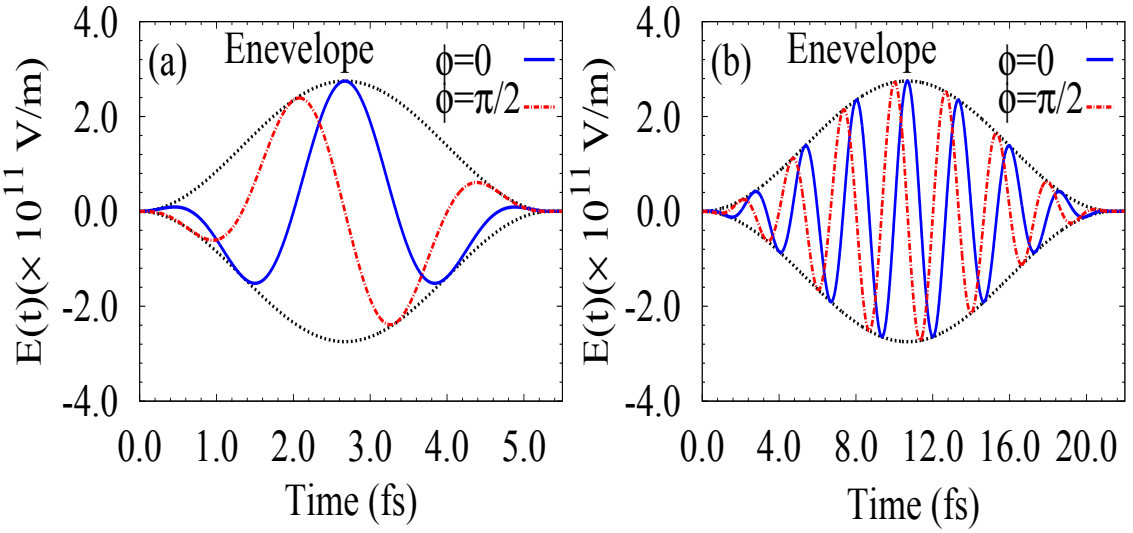

Figure 5.1: *Time envelope and instantaneous electric field for laser of pulse durations $2T_0$ (a) and $8T_0$ (b). The peak intensity of the laser pulse is kept same at $1\times10^{16}W/cm^2$ for both the cases. Solid blue and red dot dashed lines represent the electric field variations for CE phases of $\phi = 0$ and $\phi = \pi/2$, respectively. The electric field envelope is shown by the dotted line.*

consist of field variations for CE phases of $\phi = 0$ and $\phi = \pi/2$ separately. The laser pulse profile with CE phase $\phi = 0$ corresponds to the situation in which the peak of the electric field and center of the field envelope coincide. For the laser pulse with CE phase $\phi = \pi/2$, the electric field peaks before the center of field envelope.

5.4.1 Optical field ionization : Cycle averaged tunnelling rate

In this section, we present the ionization results of various cluster atoms when cycle averaged ADK tunnelling rates, given by equation5.2, are used for optical field ionization of cluster atoms. As mentioned earlier that these rates do not consider the phase part of the electric field of incident laser pulse. The fraction of various charge states produced due to irradiation of Xe_{400} cluster by pulse durations of $\tau = 2T_0$ and $\tau = 8T_0$ are plotted in Figures 5.2(a) and 5.2(b), respectively.

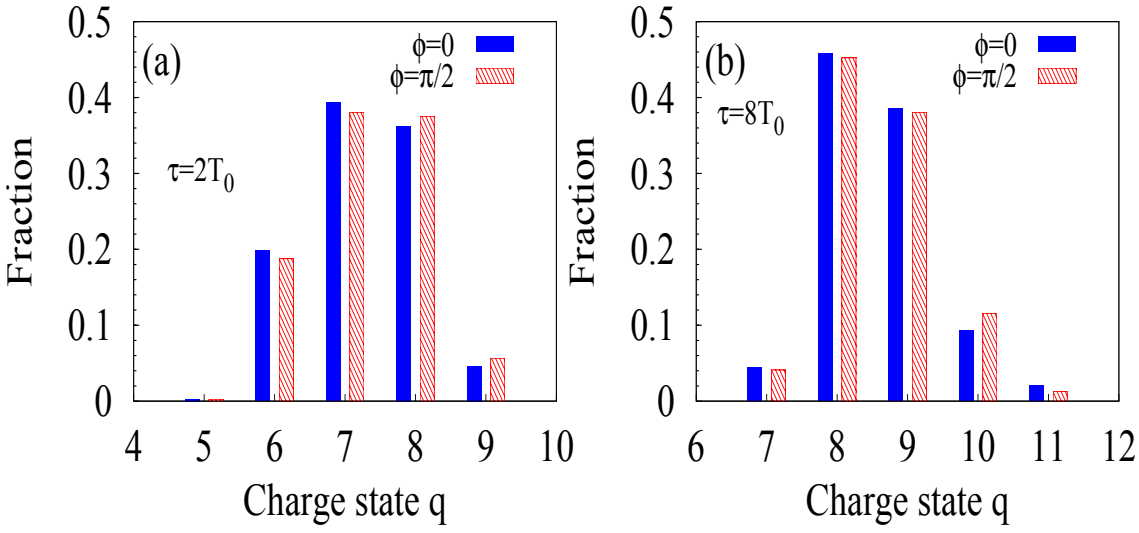

Figure 5.2: *Fraction of various charge states for Xe_{400} cluster irradiated by laser of pulse durations $2T_0$ (a) and $8T_0$ (b). Solid blue and hatched red bar correspond to CE phases of $\phi = 0$ and $\phi = \pi/2$, respectively. The intensity of the laser is same as used in figure 5.1. For optical field ionization, cycle averaged ADK tunnel ionization rates are used.*

For the longer pulse duration of$\tau = 8T_0$, we note the presence of new charge species like Ar^{+10} and Ar^{+11} while these higher charge states are completely missing for the shorter pulse duration of $\tau = 2T_0$. The reason for this mismatch is that the incident laser intensity is kept constant for the two pulse durations. Consequently, the corresponding integrated radiation energy flux $F \equiv I \cdot \tau$ increases accordingly from 53.4 J/cm^2 to 213.6 J/cm^2 as the pulse duration is increased from $2T_0$ to $8T_0$ at constant laser intensity. More incident integrated radiation energy flux (F) gets coupled to the Xe_{400} for longer pulse duration. Apart from this fact, ionization due to collisions is also more effective for longer laser pulse duration. The reason is that the colliding electrons feel the presence of incident laser field for much longer time for many cycles pulse duration that leads to more collisions with other ions. These two effects are responsible for the new charged species for $\tau = 8T_0$. From these plots (Figures 5.2(a) and 5.2(b)), we also do not observe any significant difference in the yield of ionized species for $\phi = 0$ and $\phi = 90$ for the case of few cycles laser pulse duration of $\tau = 2T_0$.

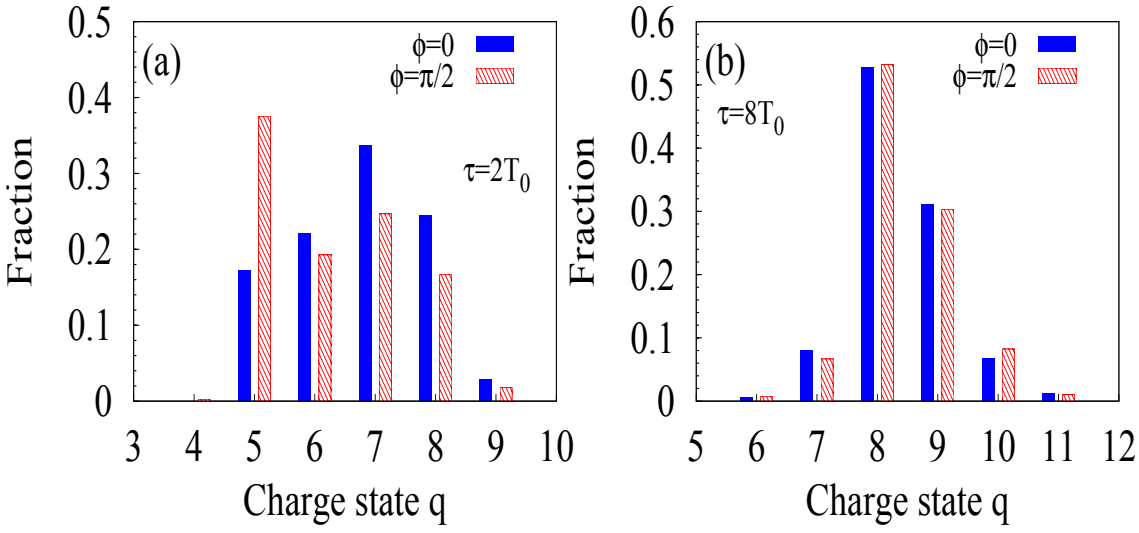

Figure 5.3: *Fraction of various charge states for Xe_{400} cluster irradiated by laser of pulse durations $2T_0$ (a) and $8T_0$ (b). Solid blue and hatched red bar correspond to CE phases of $\phi = 0$ and $\phi = \pi/2$, respectively. The intensity of the laser is same as used in figure 5.1. Absolute value of time dependent electric field ($|E(t)|$) is used in ADK tunnel ionization rate to account for the effect of the CE phase (ϕ) on ionization dynamics of Xe_{400} cluster.*

Same is also observed for longer pulse duration of $\tau = 8T_0$. It is worth mentioning that initial ionization of the cluster by laser electromagnetic radiation is due to tunnel ionization. As we have used cycle averaged ADK tunnel ionization rates for these results, we do not observe any noticeable difference in yield of ionic species for the two values of CE phase (ϕ).

5.4.2 Optical field ionization : Modified tunnelling rate

In section, we present the results of ionization dynamics of same Xe cluster as used in previous studies. The only difference is that we use modified ADK tunnelling formula for these results as our studies involve the laser pulse durations of few cycles. As mentioned earlier, modified tunnelling formula used the absolute value of time dependent electric field in stead of amplitude of the electric field that was earlier used in the conventional ADK rates (equation 5.2). The results for fraction of various charge states for these two pulse durations with modified ADK rate are presented in figures 5.3(a) and

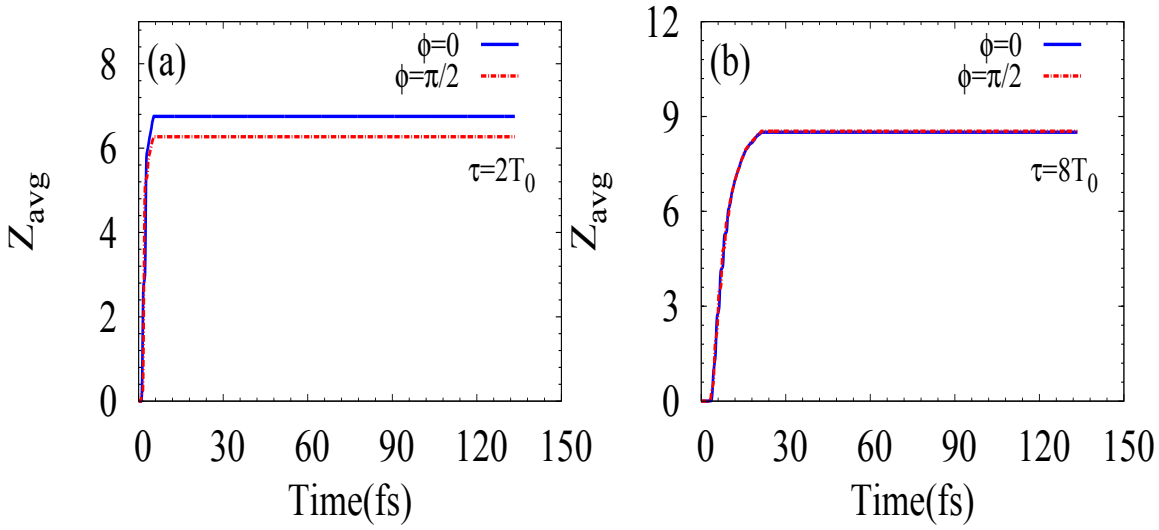

Figure 5.4: *Average degree of ionization for Xe cluster irradiated by laser of pulse durations $2T_0$ (a) and $8T_0$ (b). Solid blue and red dot dashed lines correspond to CE phases of $\phi = 0$ and $\phi = \pi/2$, respectively. The laser intensity is same as used in figure 5.1.*

5.3(b), respectively. If we compare the fractional ionization shown in this plot (Fig. 5.3) with the results (Fig. 5.2) presented in previous section with cycle averaged ionization rates, we find that the picture has completely changed. The ion yields of different ionic species show significant difference for CE phases of $\phi = 0$ and $\phi = \pi/2$ (figure 5.3(a)) when laser pulse of $\tau = 2T_0$ is used for irradiation. The difference in yield of various ionic species for two different phases ϕ is due to the different instantaneous electric field variations. The electron emitted after tunnel ionization will produce more ionization if it sees the rising edge of the electric field as compared to the case when it sees the falling edge of electric field. It is important to see that this difference in yield for the two phases diminishes (figure 5.3(b)) when many cycles pulse duration of $\tau = 8T_0$ is used to irradiate the Xe cluster. It is also important that this result is similar to the one shown in figure 5.2(b) where cycle average ionization rates are used for ionization. It means that effect of CE phase on ionization dynamics is only important for few cycles laser pulse duration. For many cycles pulse duration, these effects average out so that we do not observe any noticeable difference in the yield of ionic species for

the two phases. To further confirm these findings, we have also shown in figure 5.4(a) the time evolution of average degree of ionization (Z_{avg}) for $\phi = 0$ and $\phi = \pi/2$ for the case of $\tau = 2T_0$. We observe that Z_{avg} is higher for the case of $\phi = 0$ than that for the case of $\phi = \pi/2$. As expected, no difference in Z_{avg} (figure 5.4(b)) is seen for $\phi = 0$ and $\phi = \pi/2$ when many cycles pulse duration ($\tau = 8T_0$) is used.

Here, we want to mention that the previous results were obtained with the open boundary conditions. It is also required to see the effect of neighbouring clusters on the ionization dynamics of the Xe clusters in the case of ultra-short pulse duration limit. To account for the effect of neighbouring clusters, we have used periodic boundary conditions with the size of the simulation box of $3R_0$. It is worth mentioning that size of the simulation box is equivalent to the distance between two clusters. With this condition in mind, we have repeated the calculations for the pulse duration of $\tau = 2T_0$ in the presence of neighbouring clusters. We do not observe any significant difference in the average degree of ionization as well as the fractional ionization yield for CE phase of $\phi = 0$ and $\phi = \pi/2$. This may be due to the small cluster size and ultra short nature of irradiating laser pulse duration.

5.4.3 Effect of electron scattering

The results on ionization dynamics of Xe_{400} clusters, presented in the previous section, show the effect of both the phase dependent tunnelling part as well as collisional ionization of ions/neutral due to the electrons. Now we are solely interested in how the electron re-scattering affects the CE phase dependent ionization dynamics in extended atomic systems like atomic clusters for the case of few cycles laser pulse duration. It has been reported that electron re scattering in atomic clusters plays an important role[133] in long pulse duration limit. It is also important to note that the back scattering of electrons in atomic systems is found to be CE phase dependent[125]. As far as our MD model is concerned, it has the capability to deal with inelastic scattering of electrons with ions via Lotz' type collisional ionization. It is also important to note that our calculations automatically incorporates the back scattering of electrons with parent ions as well as forward scattering with other ions. Our MD model tracks indi-

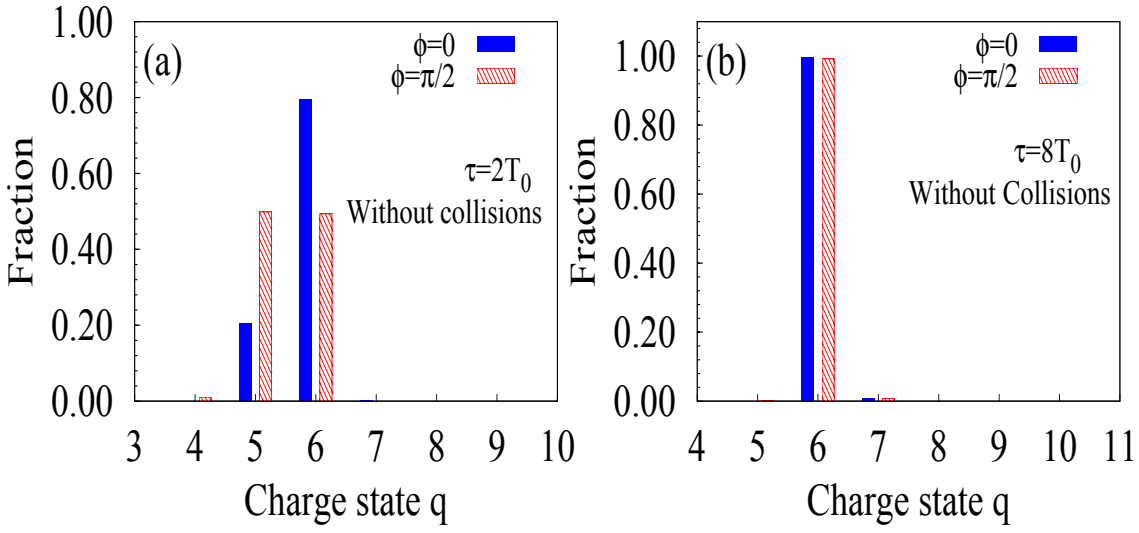

Figure 5.5: *Fraction of various charge states for Xe_{400} cluster irradiated by laser of pulse durations $2T_0$ (a) and $8T_0$ (b). Solid blue and hatched red bar correspond to CE phases of $\phi = 0$ and $\phi = \pi/2$, respectively. The intensity of the laser is same as used in figure 5.1. For these calculations, collisional ionization is artificially switched off.*

vidual particle, be it electron or ion, under the influence of external electromagnetic as well as internal electrostatic field. We can also artificially switch-off the collisional ionization part in our code and then compare these results with the ones when both tunnelling and collisions are present in the model. The difference between the two results indicates the importance of electron scattering in cluster ionization dynamics.

In Figures 5.5(a) and 5.5(b), we show the yield of various ionized species in the absence of collisional ionization for the two cases of laser pulse durations. The time evolution of average degree of ionization for the two cases is shown in figures 5.6(a) and 5.6(b). For the case of shorter pulse duration of $\tau = 2T_0$ (figure 5.6(a)), the absolute value of average degree of ionization(Z_{avg}) reduces for both the cases of CE phases($\phi = 0$ and $\phi = \pi/2$) as compared to their counterparts where the collisional ionization was included (figure 5.4(a)). It is further noted that the difference between the values of Z_{avg} reduces for CE phases of $\phi = 0$ and $\phi = \pi/2$. It shows that the collisions of electrons with ions are also dependent on the phase of incident electric

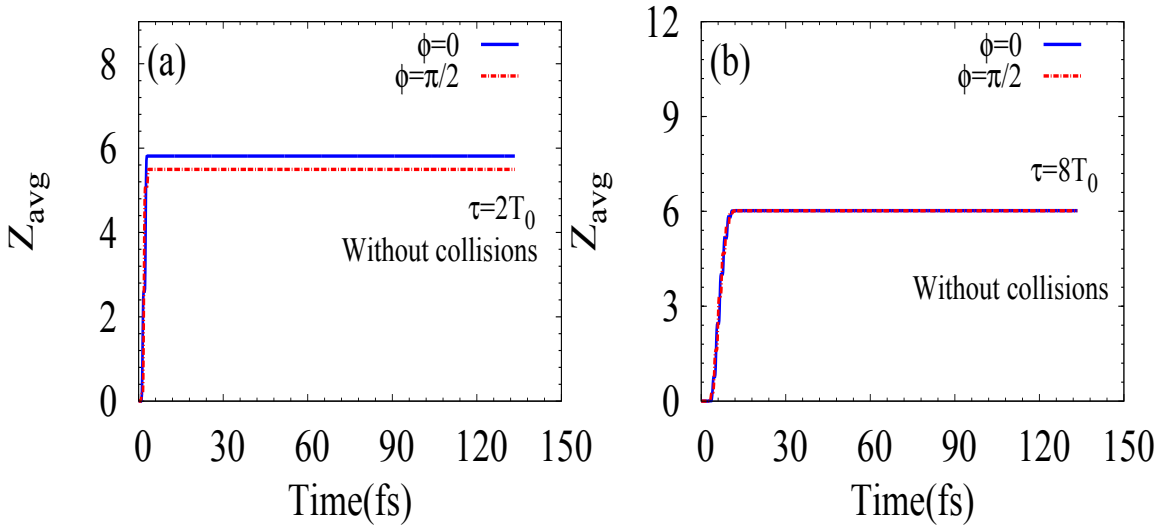

Figure 5.6: *Average degree of ionization for Xe cluster irradiated by laser of pulse durations $2T_0$ (a) and $8T_0$ (b). Solid blue and red dot dashed lines correspond to CE phases of $\phi = 0$ and $\phi = \pi/2$, respectively. The laser intensity is same as used in figure 5.1. For these calculations, collisional ionization is artificially switched off.*

field. This in turn affects the collisional ionization dynamics of Xe cluster. To further confirm this observation, we consider the results shown in figure 5.5(a) which shows the fraction of various ionized species for two CE phases. In the absence of collisional ionization, higher charge states ($Xe^{+n}, n = 7 - 9$) disappear which were present when collisional ionization was included in the calculations (figure 5.3(a)). It is also concluded from the comparison of two figures (figures 5.3(a) and 5.5(a)) that the difference in fractional yield of these higher charged states in the presence of collisions(figure 5.3(a)) is a consequence of phase dependent collisional ionization. Average degree of ionization ($Zavg$) reduces significantly for both CE phases of $\phi = 0$ and $\phi = \pi/2$ in case of longer pulse duration of $\tau = 8T_0$ (Fig.5.6(b)) when collisional ionization is neglected. As expected, Z_{avg} remain same for both the cases of CE phases ($\phi = 0$ and $\phi = \pi/2$).

5.5 Summary

To sum up, we have used our MD model to investigate the ionization dynamics of small Xe_{400} clusters irradiated by an intense laser ($I = 10^{16}W/cm^2$) pulses in the near infra-red wavelength region ($\lambda = 800nm$). The laser pulse duration is varied from few cycles ($\tau = 2T_0$ with T_0 as one laser time cycle) to many cycles ($\tau = 8T_0$). The present code is modified to accommodate the effects in few cycles pulse duration limit. The laser pulse profile is modified to conventional sin^2 type pulse. The optical field ionization mechanism namely ADK type rates are also modified such that the the amplitude of the electric field is replaced by the absolute value of time dependent electric field. For the case of few cycles pulse duration ($\tau = 2T_0$), we observe that the yield of various ionic species changes when the carrier-envelope phase ϕ of the incident laser field is varied from 0 to $pi/2$. This difference in yields for various ionic species is observed only when the ADK tunnel ionization rates use the instantaneous electric field rather than the peak strength of electric field (used in cycle average ADK rate). The difference in the temporal evolution of electric field decides the birth of electron and its further collisions with other and parent ions. When the many cycles laser pulse duration ($\tau = 8T_0$) is used, these effects average out and we do not observe any difference in yield of various ionic species.

CHAPTER 6

Neutron production from laser driven clusters

As mentioned in the introduction chapter1 that laser driven clusters exhibit nearly 100% energy of the incident laser pulse even though the average density of the gas jet is modest ($10^{19}cm^{-3}$)[37]. This pronounced enhancement in the energy absorption was related to the local solid like density of the atoms inside the cluster, plasma resonance and absence of any thermal dissipation of incident energy[43]. The consequence of this enhanced energy absorption of laser energy translated into the emission of energetic ions in the range of 10 keV-1MeV for large Xe clusters[39]. Explosion of deuterium and tritium clusters is of prime importance due to the emission of high-energy (keV) deuterons and tritons that can lead to generation of neutrons via the various nuclear fusion reactions. The different dd and dt fusion reactions read as

1. D + D $\xrightarrow{50\%}$ He^3 + n
2. D + D $\xrightarrow{50\%}$ T + p
3. D + T $\rightarrow$ He^4 + n

In this chapter, we have investigated the explosion dynamics of deuterium clusters under the influence of the laser pulse with intensity range $10^{15} - 10^{19}W/cm^2$. The effect of cluster size and inter-cluster distance is also explored in the context of neutron yield from laser driven deuterium clusters. These computational studies are performed with the coupled molecular dynamic code (MD-ILAC) with the one-dimensional beam energy deposition model.

6.1 Earlier trends and motivation

The use of laser driven deuterium clusters as a neutron source is motivated by various factors like table-top dimensions of the whole set-up, nearly point like emission of neutrons from deuterium clusters, monochromaticity in the energy distribution, high-repetition rate and temporal durations as short as a few hundred picoseconds[134]. Such a short, nearly point like neutron source offers to use them as a source of neutron pulse, either pump or probe, to carry-out ultra-fast studies with neutrons. Other source for neutron generation like sources involving accelerators exist but these devices give rise to neutron pulses with duration longer than a few nanosecond[135, 136]. A large number of neutrons are also generated by the irradiation of solid, deuterated plastic targets by a 500-J, 5-ps laser (Petawatt laser with power $10^{15}W$) but they exhibit a broad energy spectrum[137]. Fast fusion neutron ($100ps$) are also regularly produced in large scale inertial confinement fusion experiments where the fusion burn time is limited by the inertially confined compresses plasma core[138]. However, these experiments are carried out at big national laser facilities with low repetition rate (one shot per hour).

In view of the limitations posed by these alternate sources to produce neutrons, high-intensity femtosecond laser driven deuterium clusters offer energetic deuterium or tritium ions which fuse together to give rise a short, nearly monochromatic pulse of neutrons that can be used to carry out ultra-fast studies. The first direct demonstration of using laser irradiated clusters as neutron sources (Fig. 6.1) was shown by pioneering experiments performed by Ditmire and his group[46]. They used a table-top laser producing 120 mJ of laser energy in pulses with 35-fs pulse duration at NIR (820 nm) wavelength region. The repletion rate of the laser was 10 Hz. The average size of the deuterium clusters used in this was experiment was nearly $50\mathring{A}$. The laser spot size within the gas jet was about 200 μ that gives rise to the peak intensity of the laser to be about $2 \times 10^{16}W/cm^2$. Due to the laser heating of the deuterium clusters, clusters explode and form a plasma cylindrical filament of diameter 200 μ and length 2 mm. The accelerating deuterium ions from neighbouring clusters in this plasma fil-

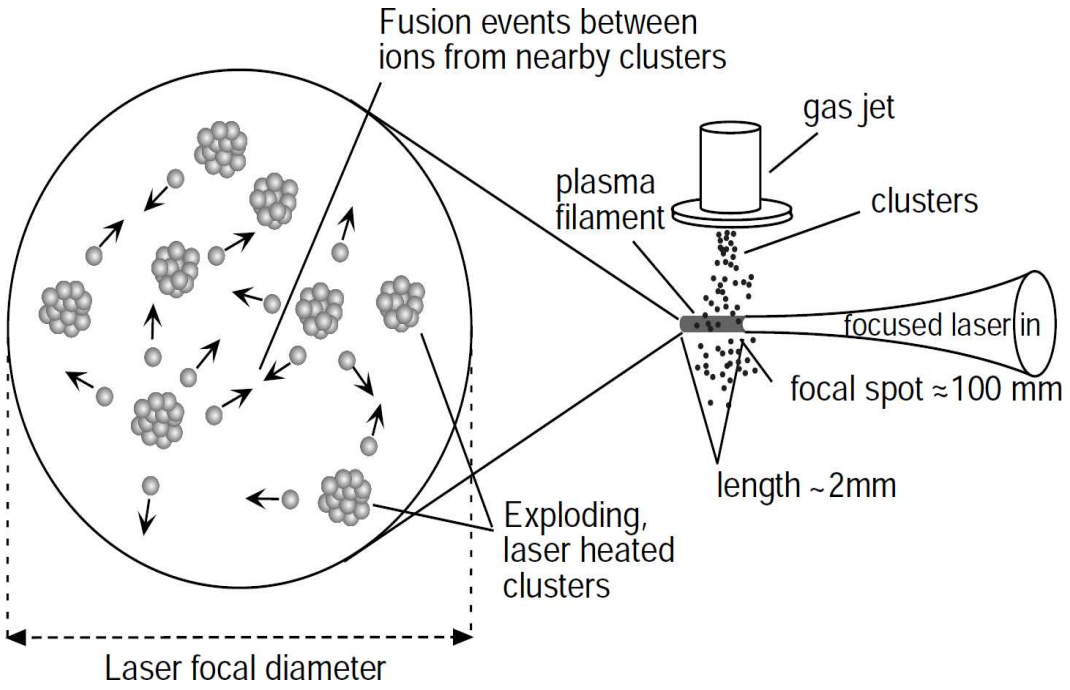

Figure 6.1: *Layout of the deuterium cluster fusion experiment conducted by Ditmire et al[46].*

ament possess energies in multi KeV range. These fast deuterium ions with sufficient energies fuse together to give neutrons of the characteristic energy of 2.45 MeV. In this experiment, the efficiency of the neutron production was about 10^5 fusion neutrons per joule of incident laser energy. In the experiments of Zweiback at al[139, 140], it was established that neutron yield was strongly dependent on the cluster size, laser focal geometry, and deuterium gas jet parameters. In order to explain the dependence of neutron yield on the size of the cluster, they used an analytical model of Coulomb explosion of deuterium cluster which gives rise to greater kinetic energy of ejected ions after the explosion of the large clusters. Further, the d-d fusion cross section is also rapidly varying of function of the kinetic energy of ions. Consequently, the neutron yield increased with the cluster size. Neutron yield was also shown to be limited by the laser propagation effect as the pulse traversed through the gas plume. The role of laser pulse duration in the neutron yield was investigated by Madison *et al*[141]. They found the cluster explosion energy and resultant fusion yield to be dependent on the laser pulse rise time, a parameter related to the pulse duration of the laser. Their experimental observations were backed by the results of particle simulation that

showed that the explosion energies of the clusters were determined by the a single parameter : the ratio of the cluster ionization time (t_{ion}) to its intrinsic expansion time (t_{exp})[141]. The cluster explosion energies were maximised in the limit of ionization time (t_{ion} related with the rise time of the laser pulse) approaching towards zero. In any real situation with finite t_{ion} (t_{ion} would increase with increase in pulse duration), the final energies of the ions after Coulomb explosion would always be smaller than the maximum achievable ion energies leading to reduced neutron yield for longer pulse duration.

The problem of nuclear fusion in laser-cluster interaction was also studied by Kishimoto *et al* by using particle-in-cell methods[75]. It was observed that the expansion of the irradiated cluster was dependent on the two parameters : cluster size (a) and the electron excursion length ξ (dependent of the laser field). The two regimes of interest *viz.* Coulomb explosion ($a \ll \xi$) and hydrodynamic ambipolar expansion ($a \gg \xi$) were identified. They found the high fusion neutron yield in Coulomb explosion regime with greater cluster size. Molecular dynamic studies performed by Last and Jortner [142, 143] found enhanced neutron yield from the Coulomb explosion of heteronuclear clusters $(D_2O)_n$, as compared with homonuclear clusters $(D)_n$. The increased neutron yield for $(D_2O)_n$ clusters was the result of higher kinetic energies of D^+ ions triggered by the highly charged O^{+q} ions. This theoretical finding was further supported by experiments conducted by Madison *et al*[144]. By using a 100 fs, 100 TW laser pulse, they studied the ion emission characteristics and fusion neutorn yield from D_2 and CD_4 cluster plasmas in the similar regimes of cluster size and average gas density. They found higher kinetic energies of the D^+ ions in the case of CD_4 clusters compared with D_2 clusters. It was also observed that fusion neutron yield from the CD_4 cluster plasma at low pulse energy was higher that that from D_2 clusters.

By using molecular dynamic model, Petrov and Davis [145, 146] studied the neutron production from high intensity laser-cluster interaction in an alternate beam-target geometry (Fig. 6.2). They used the laser driven clusters as a source of high energy deuterium ions which reacted with the walls of a surrounding fusion reaction chamber with walls coated with DT fuel or other deuterated material such CD_2 of and

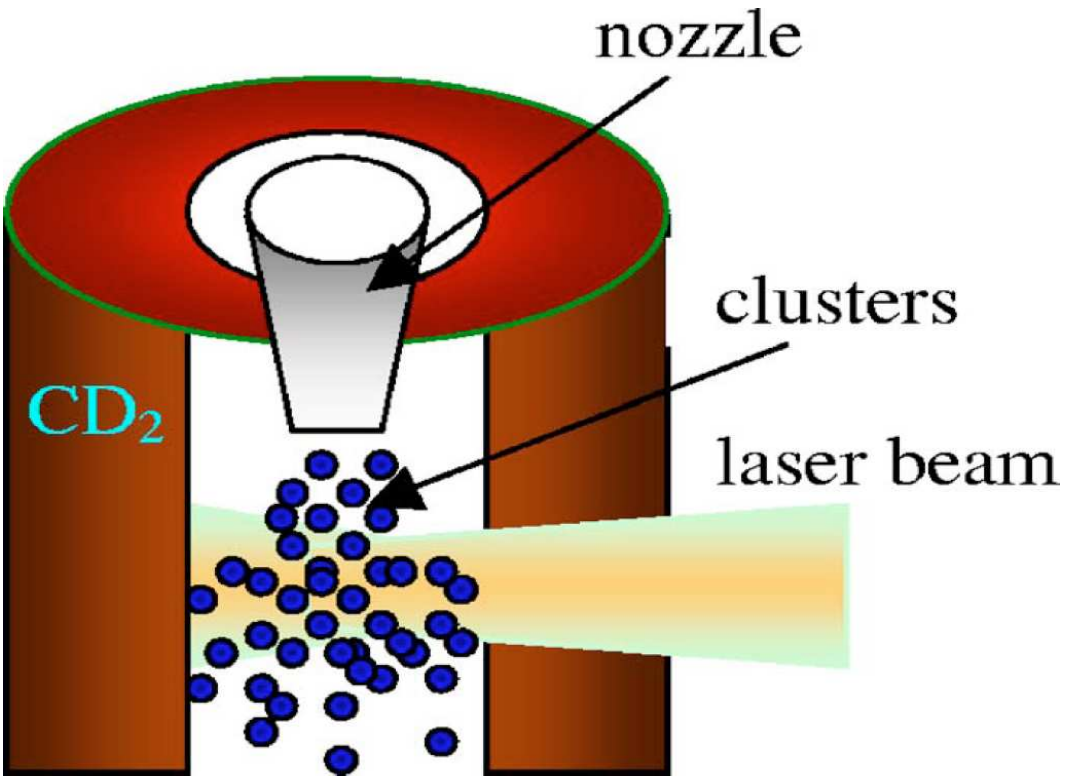

Figure 6.2: *Schematic of the proposed geometry by Davis* et al*[145] for neutrons generated from laser driven cluster.*

generated a large amount of neutrons. They estimated a high neutron yield of $10^6 10^7$ neutrons/Joule with the laser intensity of $10^{16} - 10^{18} W/cm^2$ and clusters with initial radius of $20nm$.

We have also studied interaction dynamics of high intensity laser pulses with deuterium clusters by using our MD code. The yield of fusion neutrons is calculated in the beam-target design as mentioned in the previous paragraph. Consequently, the code is modified to include the beam-target geometry. In particular, we have investigated the dependence of neutron yield on various laser and cluster parameters like laser intensity, cluster radius and cluster density. The former two parameters are straight forward while the effect of latter parameter *i.e.* cluster density is studied by varying the inter-cluster distance that is equivalent to size of the simulation box used in the MD model. The details of the simulation methodology is given in next section.

6.2 Simulation methodology

For the calculation of neutron yield from laser driven deuterium clusters, the present code is modified in two ways. First, the earlier version of MD-ILAC as described in the chapter2 is a serial code and the present problem of neutron generation involves large deuterium clusters. So, serial version of MD-ILAC is made parallel using OpenMP framework by Holkundkar[147] to save the computation time in length simulations. This parallel version of MD-ILAC gives the cluster properties after laser irradiation. These properties are the laser energy absorption, conversion efficiency into ion kinetic energy, mean ion energy and ion energy distribution function (IEDF). These values of deuterium clusters serve as an input to the other one dimensional beam energy deposition model coupled to the parallel version of MD-ILAC.

In the beam energy deposition model,the high energy ions ejected from the Coulomb explosion of deuterium clusters interact with target[145, 146]. As mentioned previously, the target surrounding the exploding cluster is in the form of a cylindrical vessel with internal walls coated with deuterium or tritium containing compound. In particular, one can use CD_2 for d-d and LiT for D-T reaction. Once Deuterium ions enter the target, they slow down because of various processes involved like ionization, excitation etc. As a result the kinetic energy of the ions is transferred to the target. This phenomenon of slowing down of the high energetic ions is characterized by the term *Stopping Power*. The stopping power of the deuterium ions into the target material is calculated with a widely used software SRIM (Stopping Range of Ions in Matter) [148]. The stopping power is a function of the type of source ion, its initial energy and the properties of the target material. It is important to note that this calculation of stopping power from SRIM is more accurate than other analytical formulations based on Bethe-Bloch fromula as mentioned by Krainov et al[149]. The reason is that SRIM calculation of stopping power depends upon the experimental data[150].Once, the stopping power in target material is calculated with the SRIM code for desired energy range then, we perform a non-linear fit for the same. This is made to get an analytical function describing the stopping power as a function of ion energy.

The total number of neutrons produced per pulse in a fusion reaction is given by[151],

$$Y = N_d \langle y \rangle, \tag{6.1}$$

where N_d is the number of the deuterons produced from the exploding cluster and $\langle y \rangle$ is the average reaction probability. The average reaction probability ($\langle y \rangle$) can also be thought as the neutron yield per ion and it is defined as [151],

$$\langle y \rangle = \int_0^{E_{max}} P(E) y(E) d\epsilon. \tag{6.2}$$

In this equation, $P(E)$ denotes the energy distribution of the cluster ions with maximum energy defined as E_{max}. $y(E)$ appearing in this equation represents the reaction probability for an ion with the initial energy E penetrating into target[151],

$$y(E) = \int_0^{E} \frac{\sigma(E') N_0}{S(E')} dE'. \tag{6.3}$$

Here, N_0 is the target density, $\sigma(E)$ is the fusion cross section of the deuterium ions with target material and $S(E)$ is the stopping power of the target material. The fusion cross-section σ is calculated by the fitted expression by J. D. Huba [152]. The fusion cross section for the DD and DT reaction is presented in Fig. 6.3. As mentioned earlier, the calculation of stopping power is performed with the help of SRIM [148] for a certain energy range of the deuterium ions which is determined by the MD simulations. The stopping power of Deuterium ions in Deuterium and Tritium target of density 5×10^{22} cm^{-3} is also presented in Fig. 6.3. It is noteworthy that the stopping power is almost same both the target material, tritium as well as deuterium . However, reaction probability seems to be slightly larger for d-t reaction as compare to d-d reaction because the fusion cross section for d-t reaction is more that that for d-d.

As mentioned in the equation 6.1, the fusion neutron yield calculation also requires the knowledge of total number of deuterium ions (N_d) produced per unit joule of laser energy absorbed other than the average reaction probability ($\langle y \rangle$). As it has been experimentally verified that clusters absorb nearly (>95%) all laser energy incident

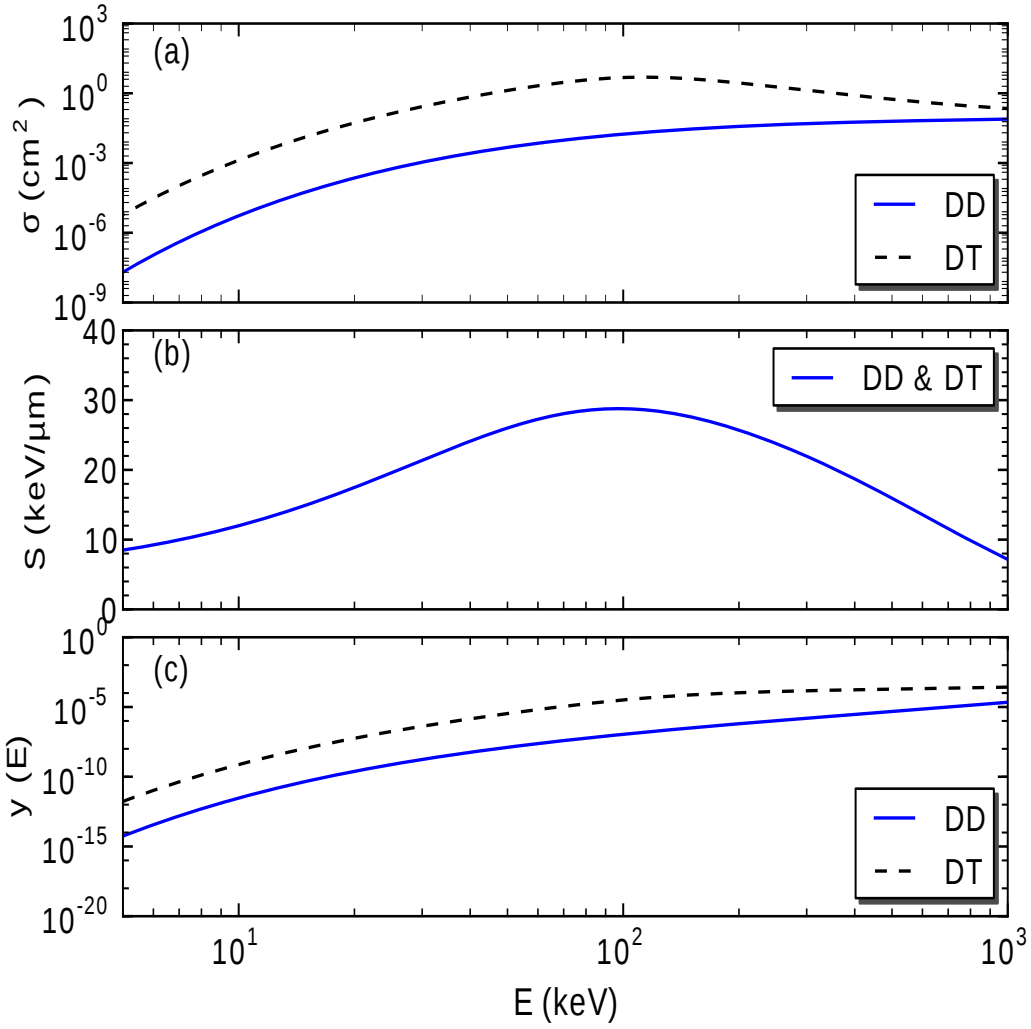

Figure 6.3: *Fusion cross section for D-D and D-T reaction (a), stopping power of D in D and D in T (b) and reaction probability for D-D and D-T reactions (c) as a function of Deuterium ion energy for target density of* 5×10^{22} *cm*$^{-3}$.

upon them[37]. In view of this, we assume the complete absorption of incident laser energy in the cluster plasma for the calculation presented in this chapter. Further, the fraction of the absorbed energy that is transferred to ions is denoted by η (conversion efficiency of laser energy to ions energy). Now, the total number of Deuterium ions are estimated by the ratio of the total energy absorbed by ions to the average kinetic energy of an ion.

$$N_d = \eta E_{Laser}/E_{ave} \tag{6.4}$$

In above mentioned equation, E_{Laser} and E_{ave} denote the energy of the laser pulse

and average kinetic energy of the ions respectively. This approach for calculating the neutron production is required because effectively we are simulating only single cluster, however in actual practice there will be many clusters in the focal volume of the laser. We may note that the average energy of ions from all the clusters present in the focal volume is assumed to be same while writing Eq. 6.4. This in turn implies that the strength of electric field does not vary significantly over the focal spot of the laser.

Thus the number of neutrons produced per unit joule of energy absorbed is given by Eq. 6.1 provided that the total number of deuterons are calculated by Eq. 6.4 and the average reaction probability is estimated by Eq. 6.2.

6.3 Results

We have used our MD code coupled with the beam energy deposition model, to calculate the neutron yield from the deuterium clusters driven by high intensity femtosecond laser pulse of FWHM pulse duration of 50 fs in NIR wavelength regime ($\lambda = 800nm$). In particular, we have studied the effect of various laser and cluster parameters like cluster size, laser intensity and inter-cluster distance on the neutron yield. As mentioned earlier, the inter-cluster distance in our MD simulation is actually the size of the simulation box with the periodic boundary conditions for particles on all the surfaces. If particle(s) hit the surface, they reappear in simulation domain from opposite surface with same velocity. In view of this one can effectively simulate the presence of the neighbouring cluster which are also undergoing the same interaction dynamics.

6.3.1 Effect of cluster size

In this section, we intend to present the effect of the cluster radius on the neutron yield. For these studies, the intensity of the laser is kept at $10^{18}W/cm^2$ while the size of the cluster is varied over the range $80 - 200\mathring{A}$. The results are presented in Fig. 6.4. It is observed that the amount of energy absorbed from the cluster increases as $\sim$ R^5. We may note that the number of particles in a cluster varies as $\sim R^3$. Hence the

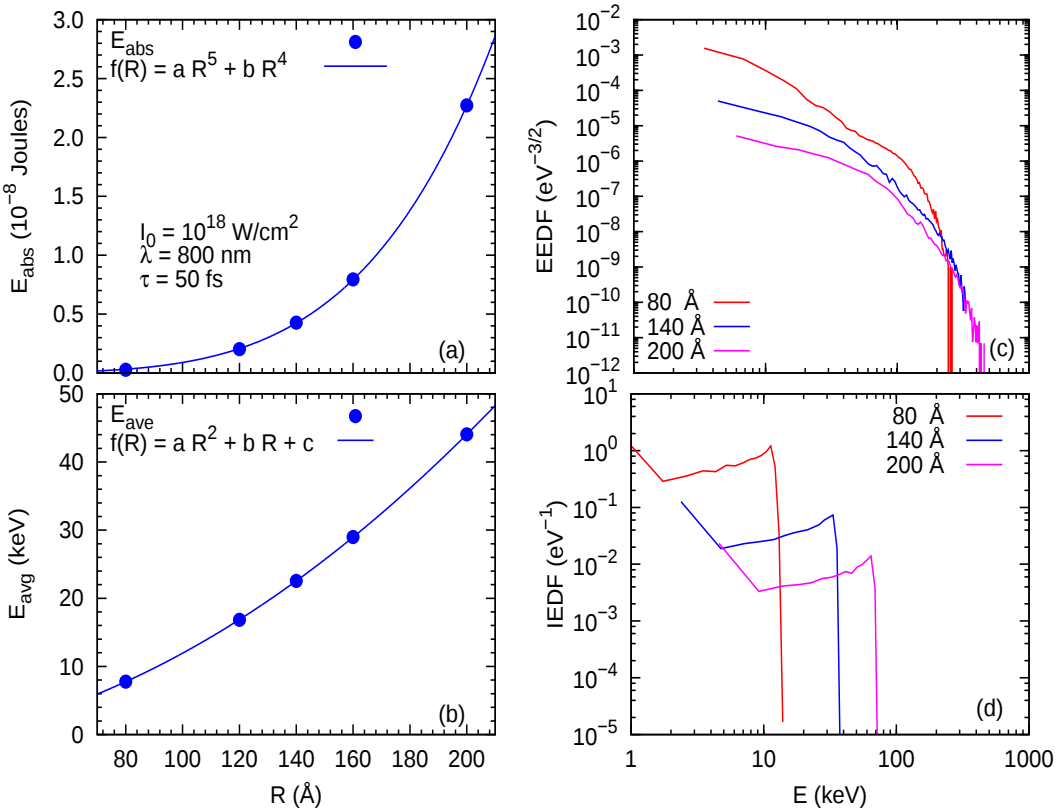

Figure 6.4: *Variation of absorbed laser energy (a) and average ion energy (b) with cluster radius. The corresponding EEDF (c) and IEDF (d) are also shown. The NIR (λ=800nm) laser intensity is considered to be 10^{18} W/cm^2 with FWHM pulse duration of 50 fs.*

average kinetic energy of the ions varies as $\sim R^2$ as also reported by previous studies [92, 139, 153, 154]. It has been also found that the maximum kinetic energy of the ions is 5/3 times the average kinetic energy of the ions, which is also in excellent agreement with the earlier studies on laser driven deuterium clusters[92, 139, 153, 154]. The results for electron energy distribution function (EEDF) and ion energy distribution function (IEDF) are also shown in Figs. 6.4(c) and 6.4(d). The EEDF follows Maxwell-Boltzmann distribution till a particular energy and then it suddenly drops with a cut off energy of about 400 keV. The corresponding IEDF is also in good agreement with the theory [153].

A quick recap of the pure coulomb explosion model is required to appreciate the

simulation results presented in the above paragraph[154]. It is important to note that pure Coulomb explosion of the cluster is related with the condition when the ionization (inner/outer) time scales are shorter than the time scales involved in the motion of ions. In other words, the all the electrons leave the cluster completely before the significant movement of cluster ions occurs. In the uniform cluster explosion model[154], movement of deuterium ions on the surface of the cluster with a radius R_0 can be expressed by the Newton equation of motion

$$m_d \frac{d^2R(t)}{dt^2} = \frac{N_e(t)e^2}{4\pi\epsilon_0 R^2(t)}. \tag{6.5}$$

In this equation, m_d is the rest mass of the deuterium ions, e is the electron charge, $R(t)$ is the outer radius of the expanding cluster, and $N_e(t)$ is the amount of electrons removed from the cluster at the time instant t by the laser field. If we define $N_e(t) = q(t)N_c$, where $N_c = 4\pi R_0^3\rho/3$ is the total number of deuterium atoms inside the cluster with ρ as the atomic density of the cluster and $q(t)$ is the average charge per atoms, eq. 6.5 can be written as

$$m_d \frac{d^2R(t)}{dt^2} = \frac{q(t)N_c e^2}{4\pi\epsilon_0 R^2(t)}. \tag{6.6}$$

When the cluster explosion end at infinity, the total potential energy of of the deuterium ion at initial position $R(t)$ will appear as kinetic energy of deuterons due to energy balance requirement that can be written as

$$E_i = \frac{1}{4\pi\epsilon_0}\frac{4\pi}{3}e^2\rho r^2. \tag{6.7}$$

The maximum energy will be achieved by the deuterons residing on the surface of the cluster which is given by

$$E_{max} = (E_i)_{r=R_0} = \frac{1}{4\pi\epsilon_0}\frac{4\pi}{3}e^2\rho R_0^2 \tag{6.8}$$

, where R_0 is the initial radius of the cluster. Thus the maximum kinetic energy of the deuterium goes as square of the initial cluster radius. As mentioned earlier that

deuterium cluster is in the form of uniformly charged sphere, so one can write the number of deuterium ions in spherical shell of width dr as $dN = \rho 4\pi r^2 dr$. Now, the kinetic energy distribution function of deuterium ions can be written as

$$\begin{aligned}
\frac{dN}{dE_i} &= \frac{dN}{dr}\frac{dr}{dE_i} \\
&= \frac{4\pi\rho r^2}{\frac{1}{4\pi\epsilon_0}\frac{4\pi}{3}e^2\rho 2r} \\
&= 4\pi\epsilon_0\frac{3}{2e^2}r \\
&= 4\pi\epsilon_0\frac{3}{2e^2}\sqrt{\frac{4\pi\epsilon_0 3E_i}{4\pi e^2\rho}} \\
&= 4\pi\epsilon_0\frac{3}{2e^3}\sqrt{\frac{3\epsilon_0 E_i}{\rho}} \propto \sqrt{E_i}
\end{aligned} \tag{6.9}$$

Thus the energy distribution function of deuterium ions after pure Coulomb explosion is proportional to the square root of the energy. We can also calculate the average energy of cluster ions after cluster explosion, which is given as

$$E_{avg} = \frac{\int E_i dN}{\int dN} = \frac{3}{5}E_{max} \tag{6.10}$$

Now let us re-examine our simulation results on average kinetic energy and maximum kinetic energy of cluster ions after Coulomb explosion, as shown in Fig. 6.4. As mentioned earlier that the average kinetic energy of the ions varies as $\sim$ R^2 and maximum kinetic energy of the ions is 5/3 times the average kinetic energy of the ions. Now it is clear from the eqns. 6.10 and 6.8 that these simulation results are well justified by invoking a uniform spherical explosion of cluster under intense laser irradiation[92, 139, 153, 154].

Now we will discuss our results of neutron yield for various cluster sizes. The result for number of neutrons produced per joule of laser energy is shown in Fig. 6.5 for both the cases of Deuterium and Tritium containing target. It is observed from this plot that the neutron yield is more for Tritium target than that for Deuterium target. The main reason for this difference is primarily the increased cross section for d-t fusion reaction than that for d-d fusion reaction which is also shown in Fig. 6.3. It is

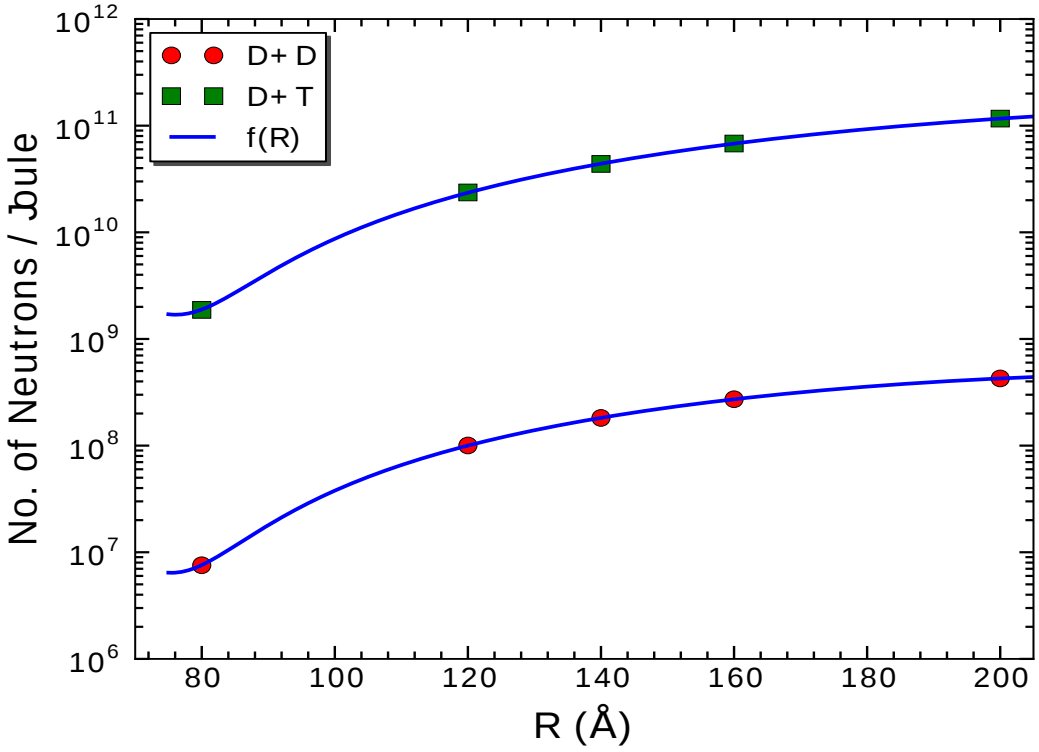

Figure 6.5: *Total number of neutrons per joule for both Deuterium and Tritium targets. The solid line show the fitted third degree polynomial. The laser parameters are same as used in Fig. 6.4*

also seen from Fig. 6.5 that neutron yield per unit joule of absorbed energy increases monotonously with the cluster size for both Deuterium and Tritium target. Moreover, these results of increasing neutron yield with size of the cluster are well fitted by third degree polynomial. To understand this variation, let us reconsider the Eq. 6.1 for neutron production which depends upon the three parameters *viz.* conversion efficiency (η), number of deuterons (N_d) produced from the exploding cluster and average reaction probability or neutron yield per ion ($\langle y \rangle$). It is found that the conversion efficiency η varies from 0.47 to about 0.5 when the size of the cluster is varied from 80 Åto 200 Å. As it is observed from Fig. 6.4 that the amount of energy absorbed by the cluster varies as $\sim$ R^5 and average kinetic energy as $\sim$ R^2. The conversion efficiency of the absorbed energy to the kinetic energy of the ions is calculated as $\eta = N_0 E_{ave}/E_{abs}$, where $N_0 = (R/R_w)^3$ is the number of Deuterium ions present in a cluster of radius

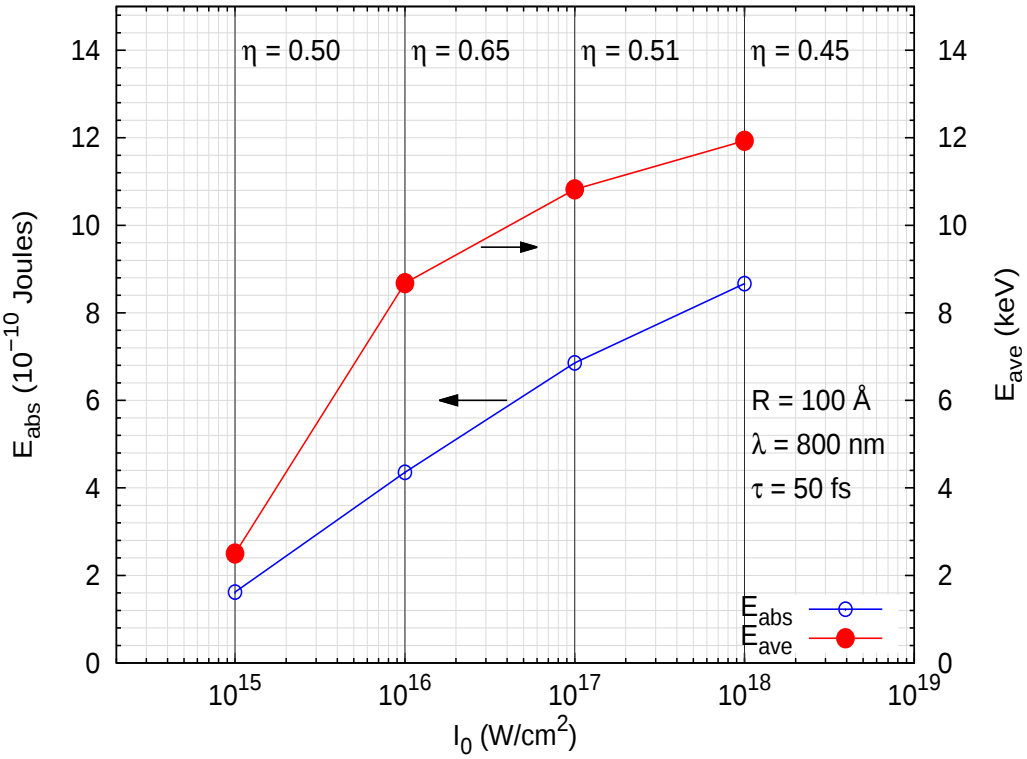

Figure 6.6: *Variation of absorbed laser energy and average ion energy with laser intensity. The conversion efficiency is also shown for each laser intensity. The cluster size is considered to be 100Å whereas other parameters are same as used in Fig. 2.*

R. It can be inferred from the scaling of E_{ave} and E_{abs} with R that the conversion efficiency η is more or less independent on the cluster radius, which is also observed in the simulation. Here we want to mention that MD simulations of Xe clusters of various radii have also reported the similar observation about η where it becomes nearly independent of radius for large clusters[71]. From Eq. 6.4 it can be inferred that N_d will vary as $\sim$ R^{-2}, as η is independent of the cluster radius. As can be seen from Fig. 6.5 that the number of neutrons/joule vary as $\sim$ R^3 which is only possible if average reaction probability or the number of neutrons per ion (Eq. 6.2) vary as $\sim$ R^5, which in our case is justified as the amount of laser energy absorption also varies as $\sim$ R^5, which can lead to the more number of neutrons per ion.

6.3.2 Effect of laser intensity

In this section, we present our results of ionization dynamics and neutron yield for the

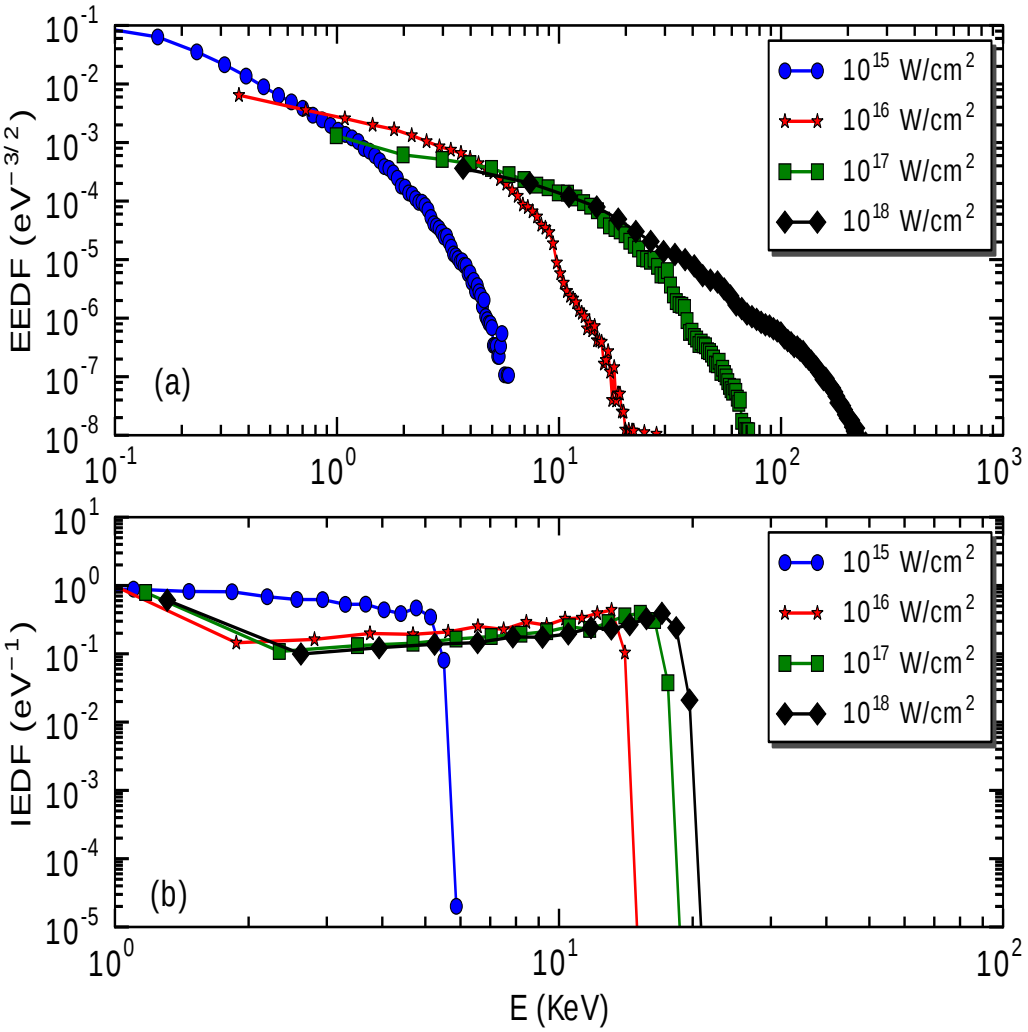

Figure 6.7: *The electron energy distribution function (a) and ion energy distribution function (b) for different laser intensities. The other laser and cluster parameters are same as used in Fig. 6.6.*

deuterium clusters driven with various values of laser intensity. For this, the size of the cluster is kept at 100Åand intensity of the laser is varied from 10^{15}-10^{18} W/cm^2 at FWHM pulse duration of 50 fs. In Fig. 6.6, we show the amount of energy absorbed and average kinetic energy for various laser intensities. The average kinetic energy for the intensity 10^{18} W/cm^2 is about 12 keV which along with the intensity dependence is consistent with the results presented by Petrov et al. [146]. We may note that the

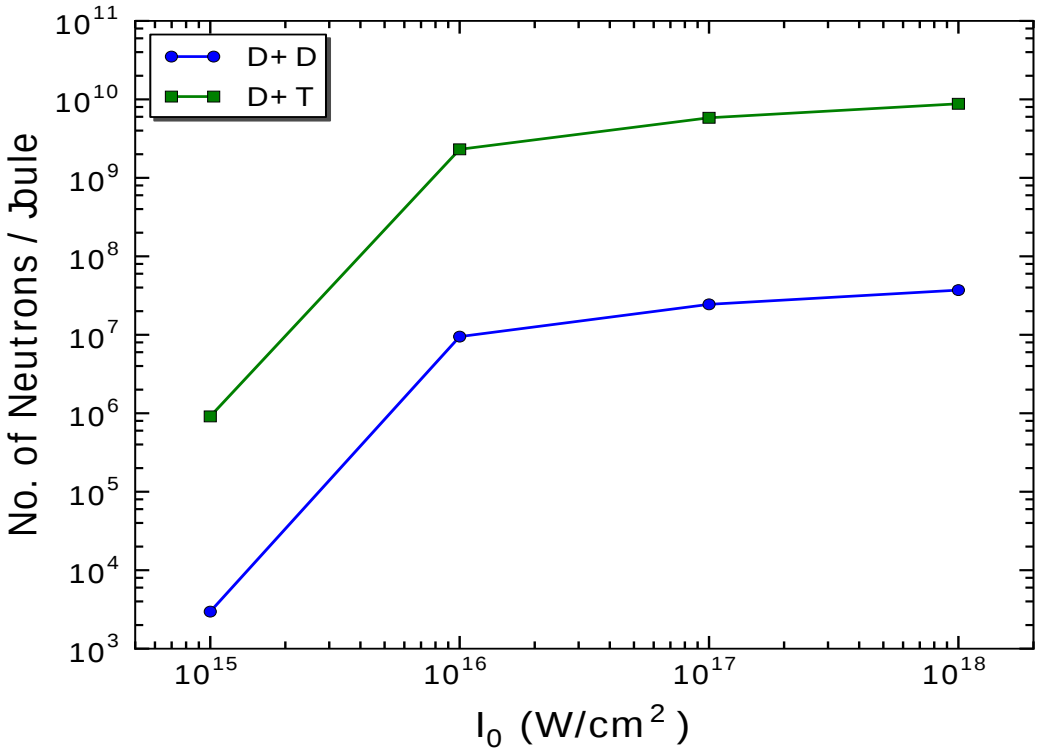

Figure 6.8: *The variation of neutron yield with laser intensity for laser and clusters parameters as used in Fig. 6.6.*

conversion efficiency exhibits some optimum value at laser intensity of 10^{16} W/cm^2, but it will not help in the production of the neutrons. The reason is that the neutron yield calculation depends more strongly on the average kinetic energy of ions than the conversion efficiency.

The electron and ion energy distribution (EEDF and IEDF) for different laser intensities are presented in Fig. 6.7 (a) and (b), respectively. The energy distribution is similar to one we already discussed in Fig. 6.4. The maximum ion energy is again 5/3 of the average kinetic energy of the ions for particular laser intensities and the electron energy distribution follows the Maxwellian distribution as we have discussed earlier. The calculated neutron yield for various values of laser intensity is also presented in Fig. 6.8. For these calculations, all other laser and cluster parameters are kept same as used in Fig. 6.6. We observe from this plot that neutron yield does not change significantly after a threshold value of 10^{16} W/cm^2. As the neutron yield calculations are strongly correlated with the kinetic energies of deuterium ions after explosion from

the cluster. It is clear from Fig. 6.6 and 6.7 that the change in average and maximum kinetic energy of the ions is not as prominent as the variation made in the laser intensity. For example, the average kinetic energy of the ions for 100 Å radius cluster just changed from 9 to 12 keV, when the laser intensity changed by 2 order of magnitude. This is mainly because of the ionization mechanism involved with Deuterium ions in the cluster. For very moderate intensities also the cluster is fully ionized and afterwards the dynamics is more or less independent on the laser intensity. This is the reason why neutron yield changes slightly after an intensity threshold of 10^{16} W/cm^2.

6.3.3 Effect of cluster density

This section deals with the studies performed on neutron yield calculation for deuterium clusters over a range of values of cluster density. This parameter, cluster density, is an experimental parameter which defines the number of cluster in a focal volume of the laser. The experimental results of Kim *et al* [103] reveal that both average cluster radius and average cluster density are functions of the gas backing pressure in the supersonic nozzle. The variation of average cluster size with the gas backing pressure presented in these results is consistent with the well established Hagena's empirical law [104] but the average cluster density shows an optimum value for a particular value of backing pressure. Moreover, Dorchies *et al* [51] have reported that both the cluster size and cluster density show a spatial distribution in focal volume of the laser where clusters are formed after passing through the nozzle. It is important to note that the energetics of the cluster explosion is strongly dependent on the number of clusters per unit volume of laser focal volume which may ultimately influence the neutron production. To study the effect of average cluster density (N_{cls}) on neutron yield by using our MD simulation, we have to vary the corresponding simulation parameter, namely, inter-cluster distance (R_{IC}) in our computational studies. Higher is the N_{cls} in the laser-cluster interaction region lower is the R_{IC} and *vice-versa*.

To shed some light on the effect of the N_{cls} on the neutron production, we have simulated the interaction of 50 fs, 800 nm laser of peak intensity 10^{18} W/cm^2 with 100 Å radius cluster by varying R_{IC} in multiples of the cluster radius. The correspond-

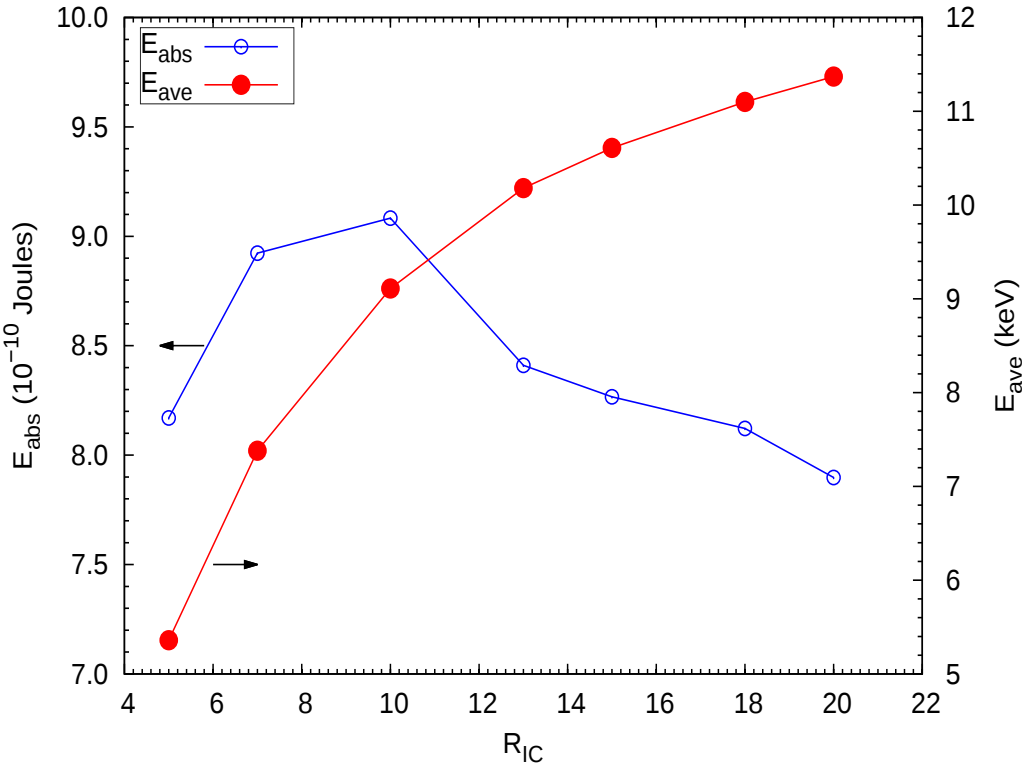

Figure 6.9: *Variation of absorbed laser energy and average kinetic energy with inter-cluster distance ($R_{IC} = n \times R_0$, n is an integer.). The laser and cluster parameters are same as used in Fig. 6.4.*

ing results of average kinetic energy of ions and total laser energy by the cluster are presented in Fig.6.9. We note that the value of average kinetic energy of ions is about 12 keV for $R_{IC} = 20R_0$ which is the same as presented in Fig. 6.4(b) for 100 Å cluster radius. We observe that the average kinetic energy varies as $\sim R_{IC}^3$ that can be explained on the basis of the shielding effect. The smaller is the inter-cluster distance, the larger is the number of clusters per unit volume with same interaction dynamics. Keeping this in mind, it is possible that the coulomb field required for the cluster explosion will be shielded by the electrons of the neighbouring clusters that results in the poor average kinetic energy of the cluster ions. As R_{IC} increases, the clusters become more sparse in the interaction region that reduces the shielding of ions by electrons

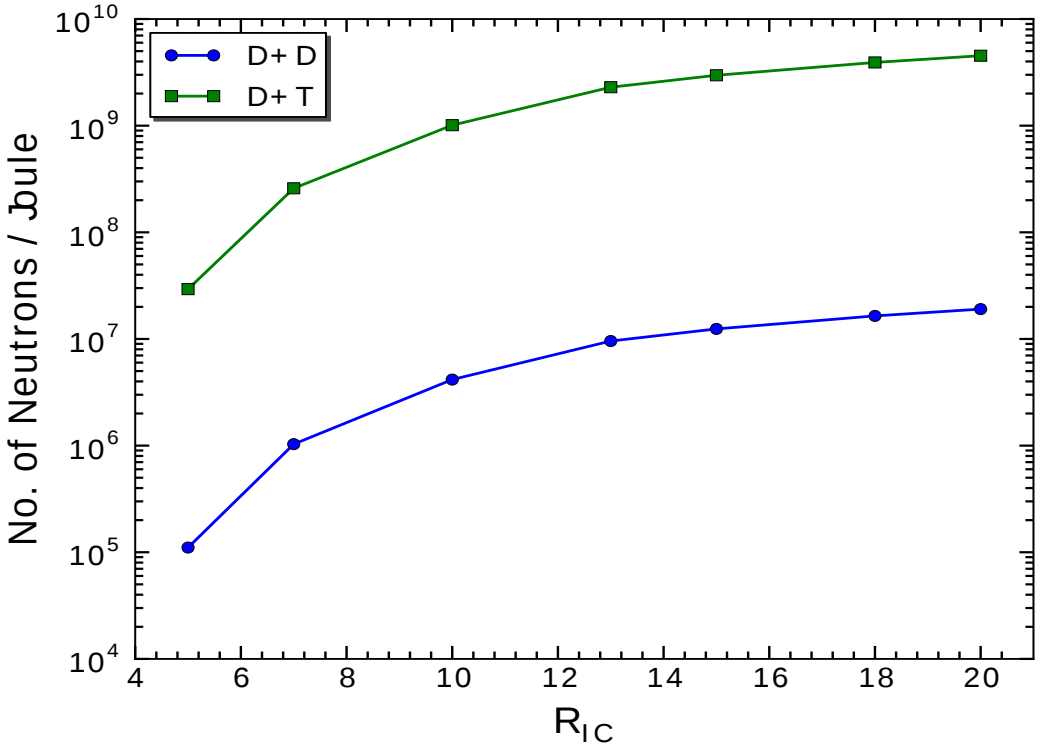

Figure 6.10: *Variation of neutron yield with inter-cluster distance for laser and clusters parameters as used in Fig. 6.9.*

of neighbours. Consequently, the average kinetic energy of the ions increases. This fact is also reflected in the energy absorbed by the cluster as a whole. The amount of laser energy absorbed is calculated by taking the contribution of total kinetic energy of the particles (electrons + ions), corresponding potential energy and energy required to ionize the cluster atoms. However as can be seen in Fig. 6.9, the absorption is not very prominently changing as we vary the inter-cluster distance but there is an optimum inter-cluster distance at which we see a relatively larger absorption. This optimum inter-cluster distance can be understood in terms of the interplay between kinetic and potential energy of the system. For lower R_{IC} the main contribution in absorbed energy is because of the kinetic energy of the particles, however for larger R_{IC} the drop in potential energy will effectively lower the amount of energy absorbed. The neutron yield for various values of the inter-cluster distance is presented in Fig. 6.10. It is observed that for higher number of clusters per unit volume (lower R_{IC}) the neutron yield is small as compared to the low cluster densities. It is mainly because of

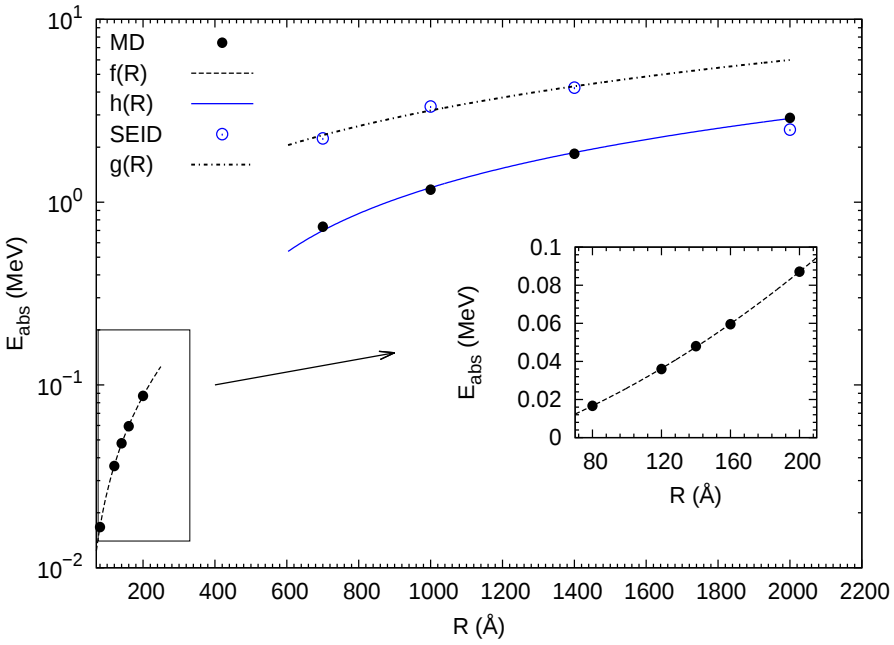

Figure 6.11: *Variation of absorbed laser energy per particle with cluster radius. Filled circles denotes the result of our MD simulation while open circles values are taken from results of Ron* et al*[151]. The laser conditions for the clusters having radius upto 200 Å are same as in Fig. 6.4. For larger clusters ($\geq$ 700 Å) a 30 fs, 800 nm with peak intensity of 10^{19} W/cm^2 laser is used. The function $f(R)$ is a quadratic fit to the amount of laser energy absorbed per particle for smaller clusters. On the other hand functions $h(R)$ and $g(R)$ are linear fit for larger clusters. The inset shows the magnified version of the results for smaller clusters.*

the average kinetic energy is low for the case of low R_{IC} as we mentioned in Fig. 6.9.

6.3.4 Role of large clusters : clusters vs nanodroplets

As mentioned in the section6.3.1, the Coulomb explosion of larger deuterium clusters give rise to the higher deuterium ion energy and thus higher neutron yield. We want to further investigate this result by using much larger cluster of size few thousands angstroms known as nanodroplets. Our main interest lies in the fact whether the same trend follows for neutron yield for nanodroplets as it was for clusters of moderate size. However, these studies with present version of MD code poses some limitations that we will address in this section.

In this regard, we want to mention about the results of neutron generation driven

by Coulomb explosion of nanodroplets by Ron *et al*[151]. For these studies, they have used SEID (Scaled electron and ion dynamics) molecular dynamic simulation[155] and also considered the attenuation of incident laser intensity as it propagated through the nano-droplet assembly. The simulation parameters for these studies were 800 nm, 30 fs laser pulse with peak intensity ranging from 2×10^{18} - 5×10^{19} W/cm^2 and nanodroplets of various sizes (70 - 300 nm). The results of Ron *et al* established the fact that the effect of laser intensity attenuation can be ignored for the highest intensity of 5×10^{19} W/cm^2 but it has a significant effect in the lower intensity regime (2×10^{18} - 1×10^{19} W/cm^2). Due to effect of laser intensity attenuation, both the absorbed laser energy and average kinetic energy of the deuterons from nanodroplet show a drop after the radius greater than 140 nm in this intensity regime. It is not possible to compare these results of Ron et. al. [151] with our MD code for all cluster sizes mentioned in that article. The reason is that our MD code is not capable to handle much bigger clusters due to the absence of intensity attenuation module. But we can still probe the validity of these results till the cluster size 140 nm (70 nm, 100 nm and 140 nm) as the intensity attenuation effects arise only after this cluster size. In Fig. 6.11, we compare our simulation results of absorbed laser energy per particle with those reported for nanodroplets[151]. The absorption per particle for smaller clusters ($\leq$ 200Å) are also presented in Fig. 6.11, where the laser conditions are same as used in Fig. 6.4. It should be also noted that in Fig. 6.4(a) we have plotted the total absorbed energy which varies as $\sim R^5$. However in Fig. 6.11, we have plotted the absorbed energy per particle which varies as $\sim R^2$ (function $f(R)$ in Fig.6.11 inset). This is due to the fact that the number of particles in a cluster varies as $\sim R^3$. It can be observed from this figure that the absorbed energy per particle varies linearly with cluster radius (70$\leq$R$\leq$ 140 nm) for both our and results of Ron *et al*[**?**]. This is due to the fact that the effect of attenuation of laser intensity in nanodroplet assembly is weak in this size regime. Further increase of nanodroplet size results into a transition from weak intensity attenuation region to strong intensity attenuation region . This leads to the breakdown of linear scaling of absorbed energy on cluster size[151]. Our results do not agree with the results of Ron et al[151] after this transition radius due to the absence of laser intensity attenuation

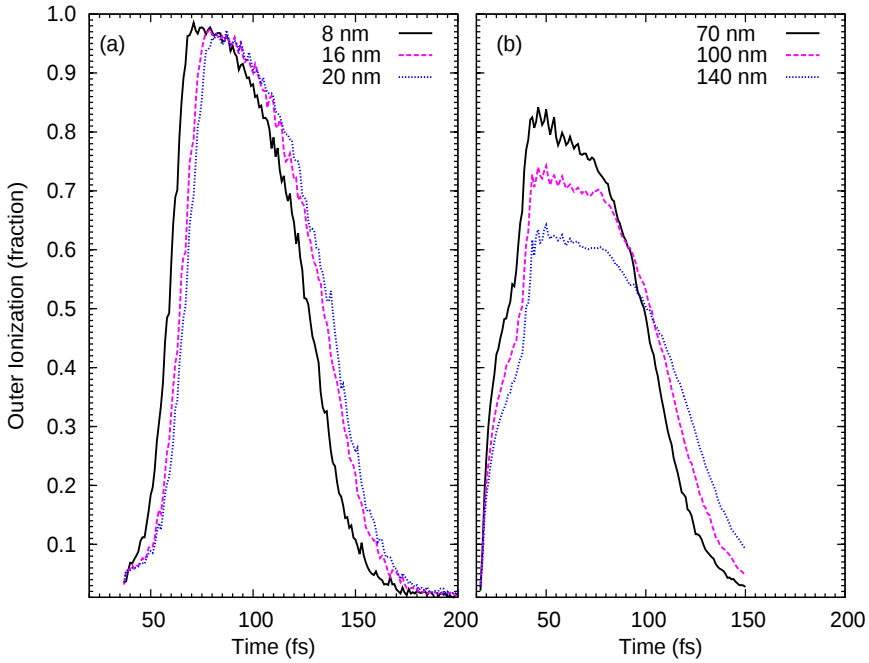

Figure 6.12: *Temporal evolution of fractional outer electrons (outer ionization) for small clusters (a) and for nanodroplets (b). The laser conditions for (a) are same as in Fig. 6.4, while for (b) the laser intensity , pulse duration and wavelength are* 10^{19} *W/cm*^{2}*, 30 fs and 800 nm respectively.*

in our MD model. However, the linear dependence of the absorbed laser energy with cluster radius in cases of nanodroplets is in agreement with the results presented by the Ron et. al. [151].

The observed quadratic and linear dependence of the absorbed energy on cluster size for smaller clusters and nanodroplets can be explained on the basis of the cluster outer ionization. The inner and outer ionization of the cluster is mainly decided by the presence of the electrons inside or outside the cluster. In case of the inner ionization, the electrons are removed from the parent atoms but they still remain confined to the cluster due to the attractive forces of positive ions. The cluster is said to undergo outer ionization when these electrons overcome the attractive forces of residual ions and leave the cluster boundary.

For both the smaller clusters and nanodroplets the time evolution of such outer electrons resulting from outer ionization of the cluster is presented in Fig. 6.12. It can

be seen that initially the fraction of outer electrons increases and after attaining the maximum it decreases. The decrease of outer electron population after achieving a maximum value is due to cluster expansion leading to the capture of outer electrons by it. Furthermore, as can be observed from Fig. 6.12(a) for the cases of smaller clusters (8, 16 and 20 nm) the outer ionization is complete. In these cases, the clusters undergo pure Coulomb explosion due to the complete outer ionization and the average kinetic energy as well as energy absorbed per particle scale quadratically with respect to cluster radius[153]. On the other hand, in case of larger clusters (Fig. 6.12(b)) or nanodroplets (70, 100 and 140 nm) it is observed that cluster never attains the complete outer ionization. Moreover the fraction of outer ionized electrons decreases as we increase the cluster radius further. The incomplete outer ionization of larger clusters leads to linear dependence of absorbed energy on cluster radius.

6.4 Summary

In short, the high intensity laser interaction with large deuterium cluster is investigated using a parallel molecular dynamic code. The deuterium ions from the Coulomb explosion of these large cluster give rise to the generation of neutrons while passing through a deuterium or tritium containing target. For the estimation of neutron yield, the parallel MD code is coupled with a beam energy deposition model. Various laser and cluster parameters like laser intensity, cluster radius and inter-cluster distance are varied to observe their effect on the neutron production from these clusters. It is observed that the neutron yield varies as $\sim R^3$ with R being the cluster radius. The laser intensity plays not that prominent role after a threshold intensity value. Furthermore, it is observed that the inter-cluster distance between the cluster which translates to the number of cluster per unit volume plays very crucial role in determining the energetic of the laser-cluster interaction and so the production of the neutrons.

CHAPTER 7

Conclusions and future directions

The field of laser matter interaction has been completely revolutionized by the invention of high intensity and short duration laser pulses. This field possesses a huge number of applications like x-ray generation, particle acceleration, inertial confinement fusion etc. In this thesis, we have concentrated on a specific target for laser irradiation namely clusters, which are collection of thousands of particles bounded by weak van der Walls forces. We have investigated various issues like absorption of laser energy, anisotropy in the cluster explosion etc. occurring in the cluster nano-plasma with the help of a simulation model. In the following, we briefly summarize our main results of the thesis. Also, we will present some direction for the future work.

7.1 Final summary and conclusions

Starting from the introduction chapter, where we defined clearly the meaning of ultrashort and high intense laser fields and methods of generation of this type of laser pulses. Since the number of atoms in a cluster is limited to few thousands, intermediate to gases and solids, we first described the interaction lasers with isolated atoms and their applications. Further, we mentioned briefly about the laser interaction with solid targets that ultimately relies on the generation of hot dense plasma. To understand that process, we also described about various introductory concepts of plasma physics. Once the description in the two extreme limits was over, we finally introduced our main topic of studies namely laser cluster interaction. A very important characteristics of laser driven clusters is a very strong laser energy absorption which translated into the energetic particle (ion/electrons/photons). Due to the unique nature of this interaction, laser driven clusters found various applications like

particle acceleration, coherent and incoherent x-ray generation, nuclear fusion in deuterium clusters etc. In this chapter, we presented various models like CEM model, nanoplasma model, ionization ignition model etc. to completely describe the various features observed in the LCI. Among those models, the most widely used model is Ditmire's nanoplasma model which considers the cluster plasma as dielectric spherical ball in spatially uniform yet time dependent electric field. The electron density of is assumed to be radially constant throughout the cluster expansion. The expansion of the cluster plasma occurs in the combined action of hydrodynamic pressure of electron gas and Coulomb pressure from the charge buildup in the cluster due to the outer ionization of the cluster. The most astounding result of the nanoplasma model was the the prediction of linear resonance occurring during the expansion of the cluster the electron density that is three times critical density. Although this model was able to explain various features of laser-cluster interaction but it has certain limitations due to the reason that it treats the cluster in statistically continuum fashion. But cluster is a barely a collection of particles that led to development of various particle models like particle in cell (PIC) and molecular dynamics (MD).

In chapter 2, we described our particle-particle simulation model relying on the MD approach that was used further extensively to study the time dependent interaction dynamics of various laser driven clusters. In our model, we assumed a spherical cluster of N ($N = (R_0/R_W)^3$, R_0 and R_W represent the cluster radius and Weigner-Seitz radius of the cluster atom, respectively) particles in the center of a three dimensional computational box of size R_{IC} (R_{IC} is the distance between two clusters). This cluster was irradiated with a spatially uniform but time dependent laser pulse. The ionization of the cluster atoms was due to both tunnelling ionization and collisional ionization. The total force experienced by the charge particles was the sum of forces due to the laser electromagnetic field and Coulomb field due to other charges particles. The charged particles motion was governed according to their relativistic equation of motion. The influence of the other clusters was accommodated by the use of periodic boundary condition (PBC). We validated our model with earlier published theoretical and experimental results so as to use it for further studies. For example, this code was

used to calculate various quantities like average degree of ionization, average kinetic energy, cluster radius etc. for various clusters. These results were is good agreement with the earlier computational studies keeping the same input parameters. We also compared the experimental results of normal anisotropy (more number of ions along laser polarization direction than perpendicular to it) from the cluster explosion with the results of our MD simulations. Not only the maximum energy observed in the experiments was found to match correctly but also, the results of anisotropy were also comparable with the MD results.

Possibly, the most prominent feature of the cluster nanoplasma produced due to the laser irradiation was its energetics that contained both laser energy absorbed by the cluster and final energies of the particles after explosion of cluster. In chapter 3, we investigated about the factors like laser pulse duration and cluster density which influence the energetics of the cluster plasma. In particular, we used MD results of absorbed laser energy and mean kinetic energy of ions from the Ar cluster driven by Gaussian laser pulses with time duration ranging from 10 to 120 fs and revalidated the theory of linear resonance proposed by Ditmire's nanoplasma model. Both of these parameters showed an optimum pulse duration which was an indication of linear resonance occurring during the expansion of the cluster. For super-Gaussian laser pulse, we did not observe this kind of optimum pulse duration. Further, we also found cluster density to be an important parameter, affecting the energetics of cluster nanoplasma. We found that just by increasing the size of the cluster, it was not possible to increase the the mean kinetic energy of ions after explosion. In fact, the shielding of the ions due to electrons of neighbouring cluster was more effective when the smaller value of inter-cluster distance was used for larger sized clusters. Further, we also compared our MD results of distribution of various ionic species with the earlier experimental results which were in good agreement for appropriately chosen inter-cluster distance consistent with the experiments.

In chapter 4, we investigated the anisotropy in the ion emission from the clusters which were irradiated by laser pulses of few cycles. It was explained that both pure coulomb explosion and hydrodynamic expansion led to spherical ion emission, the

anisotropy was the result of intermediate electron population in the cluster. We found normal anisotropy (more number of ions along the direction of laser polarization than perpendicular to it) when the clusters were irradiated by many cycles pulse duration. This situation reversed completely when few cycles laser pulses were used for irradiation. For this case, atypical anisotropy (more number of ions along perpendicular to laser polarization than perpendicular to it) was observed. This reversal of anisotropy was explained on the basis of initial shielding of ions due to oscillation of inner electrons along the direction of laser polarization. Moreover, we calculated explicitly the electric field on the on the periphery of expanding cluster along the two directions namely parallel and perpendicular to laser polarization. In our calculation we found that the electric field was more along the perpendicular direction of laser polarization. The direct calculation of electric field supported the shielding argument given before to explain the observed atypical anisotropy.

As mentioned in the chapter 5, the full description of the electric field for the laser pulses with few cycles pulse duration also required the knowledge of CE phase along with the angular frequency of the carrier wave and amplitude of the electric field. We investigated the effect of CE phase on the ionization dynamics of Xe clusters which were driven by for both few cycles and many cycles laser pulses. We found that the conventional ADK tunnelling formulation to account for the optical field ionization was appropriate for the many cycles laser pulses. But this formula was accordingly modified in few cycles pulse duration limit. With the modified formula, we observed that yield for various ionized species changed when the CE phase of the laser pulse was shifted from 0 to $\pi/2$. No difference was observed for two values of CE phase when the cluster was exposed to many cycles laser pulses. The difference in the temporal variation of electric field for the two values of CE phases that decided the birth of electrons and its further collision with other and parent ions, was the reason for the observed difference in few cycles laser pulse duration limit. For many cycles pulse duration limit, these effects got averaged out no difference was observed.

Possibly the most significant application of laser cluster interaction was the d-d fusion reaction occurring in the deuterium cluster plasma which opened a path to get

a compact table top neutron source. In view of this, we investigated the high intensity laser interaction with large deuterium clusters in chapter 6 that led to generation of high energy deuterium ion as a out come of Coulomb explosion of the cluster. The high energy deuterium ions produced neutrons while they travelled through a deuterium or tritium target coated on a cylindrical vessel. We modified the existing MD code to include a beam energy deposition model so as to determine the neutron yield. With the help of this modified code, we investigated the effects of various factors like cluster radius, laser intensity and cluster density. It was observed that neutron yield scaled as R^3, with R as radius of the cluster. The laser intensity after a certain threshold value did not alter the neutron yield. We also found that cluster density played a significant role in determining the energetics of the cluster plasma and so the production of neutrons.

7.2 Directions for future work

In this thesis, we only concentrated on the nature of laser-cluster coupling the IR laser pulse of wavelength 800 nm produced from Ti:Sapphire laser. With the advent of free-electron laser (FEL), it has become possible to generate comparably intense laser pulse extending from VUV to XUV region. Even these pulse at 12.7 photon energy, $7 \times 10^{13} W/cm^2$ intensity and 100 fs pulse duration, were used to shine the rare-gas clusters[156]. Various interesting were observed in these experiments like no cluster fragments were detected, higher charge states of the ions were found. These results could not be explained on the basis of earlier knowledge of laser-cluster interaction in IR regime. In VUV regime, the fundamental ionization mechanism is photoionization rather than field driven ionization. Also, collective effects like resonance are also not possible due to the high laser frequency. Various theoretical approaches like enhanced inverse bremsstrahlung (IBS) due to strong electron-ion scattering[157], over efficient IBS heating resulting from a high-density nanoplasma produced by local field enhancement of inner ionization by neighbouring[158] and many body heating effects[159], were used to explain these experimental observations. We will also ex-

plore the laser-cluster interaction in the VUV regime in near future.

While investigating the laser cluster interaction in our MD code, we only considered a single cluster size with PBC to account for the all the clusters lying in the focal volume of the laser pulse. It has been experimentally shown that clusters produced from the super-sonic expansion through a nozzle are not single sized clusters, but they follow a long-normal distribution of cluster sizes[102]. Also, one has to also consider the spatial profile of the laser beam in the case when the laser cluster experiments are carried out near the output of the nozzle. In this situation, our approximation where we take spatial profile of the laser beam to be constant, is not valid. It will be interesting to include both the effects of cluster size distribution and spatial profile of laser intensity[160] in our MD code so that our simulation results can be well compared with real experiments.

While discussing the results of CE phase on the ionization dynamics of Xe clusters in few cycles laser pulse duration regime, we approximated the initial tunnel ionization rate appropriately keeping the information of the complete laser electric field. In the conventional ADK formula[26] describing the tunnelling ionization of the cluster atoms, the peak strength of the electric field was replaced by the magnitude of the complete electric field of the laser following the work of Bauer *et al*[132]. This kind of approximation retain partially the information of CE phase in the electric field and thus on the tunnelling ionization rates. To account more accurately the phase dependent effects, a simple closed-form analytic expression for ionization rate as a function of instantaneous laser CE phase was proposed by Yudin and Ivanov[161] in the case of pulse durations approaching towards single laser cycle limit. It will be noteworthy and more accurate to implement this ionization mechanism in our MD code and to see its impact on the ionization results of rare gas cluster driven by laser pulses of few cycles.

Bibliography

[1] U. KELLER. "Recent developments in compact ultrafast lasers". *Nature*, **424**, 831–838 (2003).

[2] RULLIRE, C. *Femtosecond Laser Pulses: Principles and Experiments* (Advanced Texts in Physics (Springer, New York), 2005).

[3] M. D. PERRY AND G. MOUROU. "Terawatt to Petawatt Subpicosecond Lasers". *Science*, **264**, 917–924 (1994).

[4] D. E. SPENCE, P. N. KEAN, AND W. SIBBETT. "60-fsec pulse generation from a self-mode-locked Ti:sapphire laser". *Opt. Lett.*, **16**, 42–44 (1991).

[5] D. STRICKLAND AND G. MOUROU. "Compression of amplified chirped optical pulses". *Optics Communications*, **56**(3), 219 – 221 (1985).

[6] P. MAINE, D. STRICKLAND, P. BADO, ET AL. "Generation of ultrahigh peak power pulses by chirped pulse amplification". *Quantum Electronics, IEEE Journal of*, **24**, 398–403 (1988).

[7] SVELTO, O. *Principles of lasers* (Plenum Press New York, 1989).

[8] M. PICHE. "Beam reshaping and self-mode-locking in nonlinear laser resonators". *Optics Communications*, **86**(2), 156 – 160 (1991).

[9] G. A. MOUROU, C. P. J. BARRY, AND M. D. PERRY. "Ultrahigh-Intensity Lasers: Physics of the Extreme on a Tabletop". *Physics Today*, **51**(1), 22 (1998).

[10] S. BACKUS, C. G. DURFEE III, M. M. MURNANE, ET AL. "High power ultrafast lasers". *Review of scientific instruments*, **69**(3), 1207–1223 (1998).

[11] T. BRABEC AND F. KRAUSZ. "Intense few-cycle laser fields: Frontiers of nonlinear optics". *Rev. Mod. Phys*, **72**, 545 (2000).

[12] M. NISOLI, S. DE SILVESTRI, AND O. SVELTO. "Generation of high energy 10 fs pulses by a new pulse compression technique". *Applied Physics Letters*, **68**(20) (1996).

[13] C. HAURI, W. KORNELIS, F. HELBING, ET AL. "Generation of intense, carrier-envelope phase-locked few-cycle laser pulses through filamentation". *Applied Physics B*, **79**(3), 673–677 (2004).

[14] P. AGOSTINI AND G. PETITE. "Photoelectric effect under strong irradiation". *Contemporary Physics*, **29**(1), 57–77 (1988).

[15] A. EINSTEIN. "Uber einen die Erzeugung und Verwandlung des Lichtes betreffenden heuristischen Gesichtspunkt". *Annalen der Physik*, **17**(6), 132–148 (1905).

[16] M. GOPPERT-MAYER. "Uber Elementarakte mit zwei Quantensprngen". *Ann. Phys.*, **9**(3), 273–294 (1931).

[17] G. VORONAV AND N. DELONE. "Ionization of the Xenon atom by the electric field of ruby laser emission". *JETP Lett.* (1965).

[18] P. AGOSTINI, G. BARJOT, J. BONNAL, ET AL. "Multiphoton ionization of hydrogen and rare gases". *IEEE J. Quantum Electronics*, **4**(10), 667–669 (1968).

[19] M. PROTOPAPAS, C. H. KEITEL, AND P. L. KNIGHT. "Atomic physics with super-high intensity lasers". *Reports on Progress in Physics*, **60**(4), 389 (1997).

[20] P. AGOSTINI, F. FABRE, G. MAINFRAY, ET AL. "Free-Free Transitions Following Six-Photon Ionization of Xenon Atoms". *Phys. Rev. Lett.*, **42**, 1127–1130 (1979).

[21] P. KRUIT, J. KIMMAN, H. G. MULLER, ET AL. "Electron spectra from multiphoton ionization of xenon at 1064, 532, and 355 nm". *Phys. Rev. A*, **28**, 248–255 (1983).

[22] JOACHAIN, C. J. AND KYLSTRA, N. J. AND POTVLIEGE, R. M. *Atoms in Intense Laser Fields* (Cambridge University Press, 2012).

[23] L. V. KELDYSH. "Ionization in the field of a strong electromagnetic wave". *Sov. Phys. JETP*, **20**, 1307–1314 (1965).

[24] A. M. PERELOMOV, V. S. POPOV, AND M. V. TERENTEV. "Ionization of atoms in an alternating electric field". *Sov. Phys. JETP*, **23**, 924–934 (1966).

[25] A. M. PERELOMOV AND POPOV. "Ionization of atoms in an alternating electric field. III". *Sov. Phys. JETP*, **25**, 336–343 (1967).

[26] M. V. AMMOSOV, N. B. DELONE, AND V. P. KRAINOV. "Tunnel ionization of complex atoms and of atomic ions in an alternating electromagnetic field". *Sov. Phys. JETP*, **64**, 1191–1194 (1986).

[27] PIEL, ALEXANDER. *Plasma Physics An Introduction to Laboratory, Space and Fusion Plasmas* (Springer-Verlag Berlin Heidelberg, 2010).

[28] ELIEZER, SHALOM. *The interaction of high-power lasers with plasmas* (Institute of Physics Publishing Bristol and Philadelphia, 2002).

[29] GIBBON, PAUL. *Short pulse laser interaction with matter* (Imperial College Press London, 2005).

[30] MULSER, PETER AND BAUER, DIETER. *High power laser-matter interaction* (Springer-Verlag Berlin Heidelberg, 2010).

[31] F. BRUNEL. "Not-so-resonant, Resonant absorption". *Phys. Rev. Lett.*, **59**, 52–55 (1987).

[32] W. L. KRUER AND K. ESTABROOK. "$J \times B$ heating by very intense laser light". *Phys. Fluids*, **28**, 430–432 (1985).

[33] HUILLIER, A. L AND LOMPRE, L. AND MAINFRAY, G. AND MANUS, C. *Atoms in Intense Laser Fields* (Academic Press Inc., 1992).

[34] Y. NAGATA, K. MIDORIKAWA, S. KUBODERA, ET AL. "Soft-x-ray amplification of the Lyman-α transition by optical-field-induced ionization". *Phys. Rev. Lett.*, **71**, 3774–3777 (1993).

[35] J. D. KMETEC, C. L. GORDON, J. J. MACKLIN, ET AL. "MeV x-ray generation with a femtosecond laser". *Phys. Rev. Lett.*, **68**, 1527–1530 (1992).

[36] A. P. FEWS, P. A. NORREYS, F. N. BEG, ET AL. "Plasma Ion Emission from High Intensity Picosecond Laser Pulse Interactions with Solid Targets". *Phys. Rev. Lett.*, **73**, 1801–1804 (1994).

[37] T. DITMIRE, R. A. SMITH, J. W. G. TISCH, ET AL. "High intensity laser absorption by gases of atomic clusters". *Phys. Rev. Lett.*, **78**, 3121–3124 (Apr. 1997).

[38] T. DITMIRE, J. W. G. TISCH, E. SPRINGATE, ET AL. "High Energy Ion Explosion of Atomic Clusters: Transition from Molecular to Plasma Behavior". *Phys. Rev. Lett.*, **78**, 2732–2735 (1997).

[39] T. DITMIRE, J. W. G. TISCH, E. SPRINGATE, ET AL. "High-energy ions produced in explosions of superheated atomic clusters". *Nature (London)*, **386**, 54–56 (1997).

[40] Y. L. SHAO, T. DITMIRE, J. W. G. TISCH, ET AL. "Multi-keV electron generation in the interaction of intense laser pulses with Xe clusters". *Phys. Rev. Lett.*, **77**, 3343–3346 (1996).

[41] A. MCPHERSON, B. D. THOMPSON, A. B. BORISOV, ET AL. "Multiphoton-induced X-ray emission at 4-5 keV from Xe atoms with multiple core vacancies". *Nature*, **370**, 631–634 (1994).

[42] T. DITMIRE, T. DONNELLY, R. W. FALCONE, ET AL. "Strong X-Ray Emission from High-Temperature Plasmas Produced by Intense Irradiation of Clusters". *Phys. Rev. Lett.*, **75**, 3122–3125 (1995).

[43] T. DITMIRE, T. DONNELLY, A. M. RUBENCHIK, ET AL. "Interaction of intense laser pulses with atomic clusters". *Phys. Rev. A*, **53**, 3379–3402 (1996).

[44] Y. FUKUDA, A. Y. FAENOV, M. TAMPO, ET AL. "Energy Increase in Multi-MeV Ion Acceleration in the Interaction of a Short Pulse Laser with a Cluster-Gas Target". *Phys. Rev. Lett.*, **103**, 165002 (2009).

[45] A. B. BORISOV, X. SONG, F. FRIGENI, ET AL. "Ultrabright multikilovolt coherent tunable x-ray source at 2.712.93 ". *Journal of Physics B: Atomic, Molecular and Optical Physics*, **36**(16), 3433 (2003).

[46] T. DITMIRE, J. ZWEIBACK, V. P. YANOVSKY, ET AL. "Nuclear fusion from explosions of femtosecond laser-heated deuterium clusters". *Nature*, **398**(6727), 489–492 (1999).

[47] V. KUMARAPPAN, K. Y. KIM, AND H. M. MILCHBERG. "Guiding of Intense Laser Pulses in Plasma Waveguides Produced from Efficient, Femtosecond End-Pumped Heating of Clustered Gases". *Phys. Rev. Lett.*, **94**, 205004 (2005).

[48] B. SHIM, G. HAYS, R. ZGADZAJ, ET AL. "Enhanced Harmonic Generation from Expanding Clusters". *Phys. Rev. Lett.*, **98**, 123902 (2007).

[49] O. F. HAGENA AND W. OBERT. "Cluster formation in expanding supersonic jets: effect of pressure, temperature, nozzle size and test gas". *J. Chem. Phys.*, **56**, 1793–1802 (1972).

[50] J. WORMER, V. GUZIELSKI, J. STAPELFELDT, ET AL. "Fluorescence excitation spectroscopy of xenon clusters in the VUV". *Chem. Phys. Lett.*, **159**, 321–326 (1989).

[51] F. DORCHIES, F. BLASCO, T. CAILLAUD, ET AL. "Spatial distribution of cluster size and density in supersonic jets as targets for intense laser pulses". *Phys. Rev. A*, **68**, 23201 (2003).

[52] T. FENNEL, K.-H. MEIWES-BROER, J. TIGGESBÄUMKER, ET AL. "Laser-driven nonlinear cluster dynamics". *Reviews of Modern Physics*, **82**(2), 1793–1842 (2010).

[53] A. MCPHERSON, T. S. LUK, B. D. THOMPSON, ET AL. "Multiphoton induced x-ray emission from Kr clusters on M-shell (∼100 Å) and L-shell (∼6 Å) transitions". *Phys. Rev. Lett.*, **72**, 1810–1813 (1994).

[54] A. MCPHERSON, T. S. LUK, B. D. THOMPSON, ET AL. "Multiphoton-induced X-ray emission and amplification from clusters". **57**(5), 337–347 (1993).

[55] K. BOYER, B. D. THOMPSON, A. MCPHERSON, ET AL. "Evidence for coherent electron motions in multiphoton X-ray production from Kr and Xe clusters". *Journal of Physics B: Atomic, Molecular and Optical Physics*, **27**(18), 4373 (1994).

[56] J. D. JACKSON. *Classical Electrodynamics* (Wiley, New York, 1975).

[57] N. W. ASHCROFT AND N. D. MERMIN. *Solid State Physics* (Saunders College Publishing, Orlando, 1976).

[58] C. ROSE-PETRUCK, K. J. SCHAFER, K. R. WILSON, ET AL. "Ultrafast electron dynamics and inner-shell ionization in laser driven clusters". *Phys. Rev. A*, **55**, 1182–1190 (1997).

[59] H. M. MILCHBERG, S. J. MCNAUGHT AND E. PARRA. "Plasma hydrodynamics of the intense laser-cluster interaction". *Phys. Rev. E*, **64**, 056402 (2001).

[60] J. ZWEIBACK, T. DITMIRE, AND M. D. PERRY. "Femtosecond time-resolved studies of the dynamics of noble-gas cluster explosions". *Phys. Rev. A*, **59**, R3166–R3169 (1999).

[61] J. LIU, R. LI, P. ZHU, ET AL. "Modified hydrodynamic model and its application in the investigation of laser-cluster interactions". *Phys. Rev. A*, **64**, 033426 (2001).

[62] F. MEGI, M. BELKACEM, M. A. BOUCHENE, ET AL. "On the importance of damping phenomena in clusters irradiated by intense laser fields". *Journal of Physics B: Atomic, Molecular and Optical Physics*, **36**(2), 273 (2003).

[63] S. MICHEAU, C. BONTE, F. DORCHIES, ET AL. "Dynamics of rare gas nanoclusters irradiated by short and intense laser pulses". *High Energy Density Physics*, **3**, 191–197 (2007).

[64] P. HILSE, M. MOLL, M. SCHLANGES, ET AL. "Laser-cluster-interaction in a nanoplasma-model with inclusion of lowered ionization energies". **19**, 428–436 (2009).

[65] J. C. STEWART AND K. D. PYATT, JR. "Lowering of Ionization Potentials in Plasmas". *Astrophysical Journal*, **144**, 1203 (1966).

[66] I. LAST AND J. JORTNER. "Quasiresonance ionization of large multicharged clusters in a strong laser field". **60**(3), 2215–2221 (1999).

[67] I. LAST AND J. JORTNER. "Dynamics of the Coulomb explosion of large clusters in a strong laser field". **62**(1) (2000).

[68] K. ISHIKAWA AND T. BLENSKI. "Explosion dynamics of rare-gas clusters in an intense laser field". *Physical Review A*, **62**(6), 063204 (2000).

[69] U. SAALMANN AND J.-M. ROST. "Ionization of Clusters in Intense Laser Pulses through Collective Electron Dynamics." *Physical review letters*, **91**(22), 223401 (2003).

[70] G. M. PETROV, J. DAVIS, A. L. VELIKOVICH, ET AL. "Modeling of clusters in a strong 248-nm laser field by a three-dimensional relativistic molecular dynamic model". *Physical Review E - Statistical, Nonlinear, and Soft Matter Physics*, **71**(3) (2005).

[71] G. M. PETROV, J. DAVIS, A. L. VELIKOVICH, ET AL. "Dynamics of a Xe cluster plasma produced by an intense ultrashort pulse KrF laser". *Physics of Plasmas*, **12**(6), 063103 (2005).

[72] G. M. PETROV AND J. DAVIS. "Modeling of clusters by a molecular dynamics model using a fast tree method". *European Physical Journal D*, **41**(3), 629–639 (2007).

[73] G. M. PETROV AND J. DAVIS. "Interaction of intense ultrashort pulse lasers with clusters". *Physics of Plasmas*, **15**(5), 056705 (2008).

[74] M. ELOY, R. AZAMBUJA, J. T. MENDONÇA, ET AL. "Interaction of ultrashort high-intensity laser pulses with atomic clusters". *Physics of Plasmas (1994-present)*, **8**(3) (2001).

[75] Y. KISHIMOTO, T. MASAKI, AND T. TAJIMA. "High energy ions and nuclear fusion in laser-cluster interaction". *Physics of Plasmas*, **9**(2), 589 (2002).

[76] T. TAGUCHI, T. M. ANTONSEN, AND H. M. MILCHBERG. "Resonant Heating of a Cluster Plasma by Intense Laser Light". *Phys. Rev. Lett.*, **92**, 205003 (2004).

[77] C. JUNGREUTHMAYER, M. GEISSLER, J. ZANGHEILINI, ET AL. "Microscopic analysis of large-cluster explosion in intense laser fields". *Physical Review Letters*, **92**(13), 133401–1 (2004).

[78] W. LOTZ. "An empirical formula for the electron-impact ionization cross-section". *Zeitschrift f??r Physik*, **206**(2), 205–211 (1967).

[79] W. LOTZ. "Electron-impact ionization cross-sections and ionization rate coefficients for atoms and ions from hydrogen to calcium". *Zeitschrift f??r Physik*, **216**(3), 241–247 (1968).

[80] J. BARNES AND P. HUT. "A hierarchical O(N log N) force-calculation algorithm". **324**(6096), 446–449 (1986).

[81] P. MULSER, M. KANAPATHIPILLAI, AND D. HOFFMANN. "Two Very Efficient Nonlinear Laser Absorption Mechanisms in Clusters". *Physical Review Letters*, **95**(10), 103401 (2005).

[82] M. KUNDU AND D. BAUER. "Nonlinear resonance absorption in the laser-cluster interaction". *Physical Review Letters*, **96**(12) (2006).

[83] PRESTON, M. A. *Physics of the nucleus* (Addison-Wesley, Reading, MA, 1962).

[84] W. A. SAUNDERS AND N. DAM. "Liquid drop model of multiply charged metal cluster fission". *Zeitschrift für Physik D Atoms, Molecules and Clusters*, **20**(1), 111–113 (1991).

[85] D. J. WALES AND J. P. K. DOYE. "Global Optimization by Basin-Hopping and the Lowest Energy Structures of Lennard-Jones Clusters Containing up to 110 Atoms". *The Journal of Physical Chemistry A*, **101**(28), 5111–5116 (1997).

[86] C. SIEDSCHLAG AND J. M. ROST. "Electron Release of Rare-Gas Atomic Clusters under an Intense Laser Pulse". *Phys. Rev. Lett.*, **89**, 173401 (2002).

[87] S. LOCH, M. PINDZOLA, AND D. GRIFFIN. "Electron-impact ionization of atomic ions in the Sn and Xe isonuclear sequences". *International Journal of Mass Spectrometry*, **271**(1-3), 68–75 (2008).

[88] G. VORONOV. "A Practical fit formula for ionization rate coefficients of atoms and ions by electron impact : Z= 128". *Atomic Data and Nuclear Data Tables*, **65**(1), 1–35 (1997).

[89] T. TAGUCHI, T. M. ANTONSEN, J. PALASTRO, ET AL. "Particle in cell analysis of a laser-cluster interaction including collision and ionization processes." *Optics express*, **18**(3), 2389–405 (2010).

[90] C. PRIGENT, C. DEISS, E. LAMOUR, ET AL. "Effect of pulse duration on the x-ray emission from Ar clusters in intense laser fields". *Physical Review A*, **78**(5), 053201 (2008).

[91] T. DITMIRE. "Simulation of exploding clusters ionized by high-intensity femtosecond laser pulses". *Physical Review A*, **57**(6), R4094–R4097 (1998).

[92] V. P. KRAINOV AND M. B. SMIRNOV. "Cluster beams in the super-intense femtosecond laser pulse". *Phys. Reports*, **370**, 237–331 (2002).

[93] A. HEIDENREICH, I. LAST, AND J. JORTNER. "Extreme dynamics and energetics of Coulomb explosion of Xe clusters". *Phys. Chem. Chem. Phys.*, **11**(1), 111–124 (2009).

[94] A. HEIDENREICH AND J. JORTNER. "Effects of The Nanoplasma Electrons on Coulomb Explosion of Xenon Clusters". *The Journal of Physical Chemistry C*, **114**(48), 20636–20647 (2010).

[95] V. KUMARAPPAN, M. KRISHNAMURTHY, AND D. MATHUR. "Asymmetric High-Energy Ion Emission from Argon Clusters in Intense Laser Fields". *Physical Review Letters*, **87**(8), 085005 (2001).

[96] M. KRISHNAMURTHY, J. JHA, D. MATHUR, ET AL. "Ion charge state distribution in the laser-induced Coulomb explosion of argon clusters". *Journal of Physics B: Atomic, Molecular and Optical Physics*, **39**(3), 625–632 (2006).

[97] I. KOSTYUKOV AND J.-M. RAX. "Collisional versus collisionless resonant and autoresonant heating in laser-cluster interaction". *Phys. Rev. E*, **67**, 66405–66406 (2003).

[98] M. B. SMIRNOV AND V. P. KRAINOV. "Hot electron generation in laser cluster plasma". *Phys. Plasmas*, **10**, 443–447 (2003).

[99] J. DAVIS, G. M. PETROV, AND A. VELIKOVICH. "Nonlinear energy absorption of rare gas clusters in intense laser field". *Phys. Plasmas*, **14**, 60701–60704 (2007).

[100] C. DEISS, N. ROHRINGER, J. BURGDÖRFER, ET AL. "Laser-Cluster Interaction: X-Ray Production by Short Laser Pulses". *Phys. Rev. Lett.*, **96**, 13203–13204 (2006).

[101] E. SPRINGATE, N. HAY, J. TISCH, ET AL. "Explosion of atomic clusters irradiated by high-intensity laser pulses:Scaling of ion energies with cluster and laser parameters". *Physical Review A*, **61**(6), 063201 (2000).

[102] K. MENDHAM, N. HAY, M. MASON, ET AL. "Cluster-size distribution effects in laser-cluster interaction experiments". *Physical Review A*, **64**(5), 055201 (2001).

[103] K. Y. KIM, V. KUMARAPPAN, AND H. M. MILCHBERG. "Measurement of the average size and density of clusters in a gas jet". *Applied Physics Letters*, **83**(15), 3210 (2003).

[104] O. F. HAGENA. "Cluster ion sources (invited)". *Review of Scientific Instruments*, **63**(4), 2374 (1992).

[105] J. KOU, V. ZHAKHOVSKII, S. SAKABE, ET AL. "Anisotropic Coulomb explosion of C[sub 60] irradiated with a high-intensity femtosecond laser pulse". *The Journal of Chemical Physics*, **112**(11), 5012 (2000).

[106] V. KUMARAPPAN, M. KRISHNAMURTHY, AND D. MATHUR. "Two-dimensional effects in the hydrodynamic expansion of xenon clusters under intense laser irradiation". *Phys. Rev. A*, **66**, 33203–33204 (2002).

[107] D. SYMES, M. HOHENBERGER, A. HENIG, ET AL. "Anisotropic Explosions of Hydrogen Clusters under Intense Femtosecond Laser Irradiation". *Physical Review Letters*, **98**(12), 123401 (2007).

[108] B. N. BREIZMAN, A. V. AREFIEV, AND M. V. FOMYTSKYI. "Nonlinear physics of laser-irradiated microclustersa)". *Physics of Plasmas (1994-present)*, **12**(5), 056706 (2005).

[109] D. MATHUR, F. A. RAJGARA, A. R. HOLKUNDKAR, ET AL. "Strong-field ionization and Coulomb explosion of argon clusters by few-cycle laser pulses". *Physical Review A*, **82**(2), 025201 (2010).

[110] D. MATHUR AND F. A. RAJGARA. "Communication: Ionization and Coulomb explosion of xenon clusters by intense, few-cycle laser pulses." *The Journal of chemical physics*, **133**(6), 061101 (2010).

[111] E. SKOPALOVÁ, Y. C. EL-TAHA, A. ZAÏR, ET AL. "Pulse-Length Dependence of the Anisotropy of Laser-Driven Cluster Explosions: Transition to the Impulsive Regime for Pulses Approaching the Few-Cycle Limit". *Physical Review Letters*, **104**(20), 203401 (2010).

[112] M. KRISHNAMURTHY, D. MATHUR, AND V. KUMARAPPAN. "Anisotropic "charge-flipping" acceleration of highly charged ions from clusters in strong optical fields". *Phys. Rev. A*, **69**, 33202–33205 (2004).

[113] A. R. HOLKUNDKAR, G. MISHRA, AND N. K. GUPTA. "Molecular dynamic simulation for laser-cluster interaction". *Physics of Plasmas*, **18**(5) (2011).

[114] L. XU, C. SPIELMANN, A. POPPE, ET AL. "Route to phase control of ultrashort light pulses." *Optics letters*, **21**(24), 2008–10 (1996).

[115] D. J. JONES, S. A. DIDDAMS, J. K. RANKA, ET AL. "Carrier-Envelope Phase Control of Femtosecond Mode-Locked Lasers and Direct Optical Frequency Synthesis". *Science*, **288**(5466), 635–639 (2000).

[116] A. APOLONSKI, A. POPPE, G. TEMPEA, ET AL. "Controlling the Phase Evolution of Few-Cycle Light Pulses". *Phys. Rev. Lett.*, **85**, 740–743 (2000).

[117] A. BALTUSKA, T. UDEM, M. UIBERACKER, ET AL. "Attosecond control of electronic processes by intense light field". *Nature*, **421**, 611 (2003).

[118] G. G. PAULUS, F. LINDNER, H. WALTHER, ET AL. "Measurement of the Phase of Few-Cycle Laser Pulses". *Phys. Rev. Lett.*, **91**, 253004 (2003).

[119] M. Y. AMUSIA AND M. Y. KUCHIEV. "Multiple Pole in the Electron Hydrogen-Atom Scattering Amplitude". *Phys. Rev. Lett.*, **48**, 1726–1729 (1982).

[120] P. B. CORKUM. "Plasma Perspective on Strong-Field Multiphoton Ionization". *Phys. Rev. Lett.*, **71**, 1994–1997 (1993).

[121] K. J. SCHAFER, B. YANG, L. F. DIMAURO, ET AL. "Above threshold ionization beyond the high harmonic cutoff". *Phys. Rev. Lett.*, **70**, 1599–1602 (1993).

[122] P. J. HO, R. PANFILI, S. L. HAAN, ET AL. "Nonsequential Double Ionization as a Completely Classical Photoelectric Effect". *Phys. Rev. Lett.*, **94**, 093002 (2005).

[123] X. LIU AND C. F. DE MORISSON FARIA. "Nonsequential Double Ionization with Few-Cycle Laser Pulses". *Phys. Rev. Lett.*, **92**, 133006 (2004).

[124] X. LIU, H. ROTTKE, E. EREMINA, ET AL. "Nonsequential Double Ionization at the Single-Optical-Cycle Limit". *Phys. Rev. Lett.*, **93**, 263001 (2004).

[125] H. ROTTKE, X. LIU, E. EREMINA, ET AL. "Non-sequential double ionization in a few-cycle laser pulse: the influence of the carrierenvelope phase". *Journal of Modern Optics*, **53**(1-2), 149–162 (2006).

[126] D. MATHUR, K. DOTA, A. K. DHARMADHIKARI, ET AL. "Carrier-Envelope-Phase Effects in Ultrafast Strong-Field Ionization Dynamics of Multielectron Systems: Xe and CS_2". *Phys. Rev. Lett.*, **110**, 083602 (2013).

[127] V. S. RASTUNKOV AND V. P. KRAINOV. "Phase dependence in the ionization of atoms by intense one-cycle laser pulses within the LandauDykhne approximation". *J. Phys. B: Atom. Mol. Opt. Phy.*, **40**, 2277 (2007).

[128] A. V. GETS AND V. P. KRAINOV. "Interaction of Atomic Clusters with Intense Attosecond Pulses". *Contrib. Plasma Phys.*, **51**, 471 (2011).

[129] A. V. GETS AND V. P. KRAINOV. "Ionization of Atoms by Attosecond Pulses". *Contrib. Plasma Phys.*, **53**, 140 (2013).

[130] M. ARBEITER AND T. FENNEL. "Ionization heating in rare-gas clusters under intense XUV laser pulses". *Phys. Rev. A*, **82**, 013201 (2010).

[131] K. HOFFMANN, B. MURPHY, N. KANDADAI, ET AL. "Rare-gas-cluster explosions under irradiation by intense short XUV pulses". *Phys. Rev. A*, **83**, 043203 (2011).

[132] D. BAUER. "Plasma formation through field ionization in intense lasermatter interaction". *Laser Part. Bemas*, **21**, 489 (2003).

[133] U. SAALMANN AND J. M. ROST. "Rescattering for Extended Atomic Systems". *Phys. Rev. Lett.*, **100**, 133006 (2008).

[134] J. ZWEIBACK, T. COWAN, R. SMITH, ET AL. "Characterization of fusion burn time in exploding deuterium cluster plasmas". *Physical review letters*, **85**(17), 3640–3 (2000).

[135] D. W. HEIKKINEN, C. M. LOGAN, AND J. C. DAVIS. "Rotating Target 14-MeV Neutron Generators". *NUCLEAR SCIENCE AND ENGINEERING*, **106**, 228–233 (1990).

[136] P. W. LISOWSKI, C. D. BOWMAN, G. J. RUSSELL, ET AL. "The Los Alamos National Laboratory Spallation Neutron Sources". *NUCLEAR SCIENCE AND ENGINEERING*, **106**, 208–218 (1990).

[137] M. H. KEY, M. D. CABLE, T. E. COWAN, ET AL. "Hot electron production and heating by hot electrons in fast ignitor research". *Physics of Plasmas*, **5**(5), 1966 (1998).

[138] R. A. LERCHE, D. R. KANIA, S. M. LANE, ET AL. "Neutron emission time measurements for ICF targets". *Review of Scientific Instruments*, **59**(8), 1697 (1988).

[139] J. ZWEIBACK, R. SMITH, T. COWAN, ET AL. "Nuclear fusion driven by coulomb explosions of large deuterium clusters". *Physical review letters*, **84**(12), 2634–7 (2000).

[140] J. ZWEIBACK, T. E. COWAN, J. H. HARTLEY, ET AL. "Detailed study of nuclear fusion from femtosecond laser-driven explosions of deuterium clusters". *Physics of Plasmas*, **9**(7), 3108 (2002).

[141] K. MADISON, P. PATEL, M. ALLEN, ET AL. "Role of laser-pulse duration in the neutron yield of deuterium cluster targets". *Physical Review A*, **70**(5), 053201 (2004).

[142] I. LAST AND J. JORTNER. "Nuclear Fusion induced by Coulomb Explosion of Heteronuclear Clusters". *Physical Review Letters*, **87**(3), 033401 (2001).

[143] I. LAST AND J. JORTNER. "Nuclear fusion driven by Coulomb explosion of homonuclear and heteronuclear deuterium- and tritium-containing clusters". *Physical Review A*, **64**(6), 063201 (2001).

[144] K. W. MADISON, P. K. PATEL, D. PRICE, ET AL. "Fusion neutron and ion emission from deuterium and deuterated methane cluster plasmas". *Physics of Plasmas*, **11**(1), 270 (2004).

[145] J. DAVIS, G. M. PETROV, AND A. L. VELIKOVICH. "Fusion neutron yield from high intensity laser-cluster interaction". *Physics of Plasmas*, **13**(6), 064501 (2006).

[146] G. M. PETROV, J. DAVIS, AND A. L. VELIKOVICH. "Neutron production from high-intensity lasercluster induced fusion reactions". *Plasma Physics and Controlled Fusion*, **48**(12), 1721–1739 (2006).

[147] A. R. HOLKUNDKAR. "Parallel implementation of three-dimensional molecular dynamic simulation for laser-cluster interaction". *Physics of Plasmas*, **20**(11), 113110 (2013).

[148] J. F. ZIEGLER, M. ZIEGLER, AND J. BIERSACK. "SRIM The stopping and range of ions in matter (2010)". *Nuclear Instruments and Methods in Physics Research Section B: Beam Interactions with Materials and Atoms*, **268**(11-12), 1818–1823 (2010).

[149] V. P. KRAINOV, B. M. SMIRNOV, AND M. B. SMIRNOV. "Femtosecond excitation of cluster beams". *Physics-Uspekhi*, **50**(9), 907 (2007).

[150] I. LAST, S. RON, AND J. JORTNER. "Aneutronic H+ˆ{11}B nuclear fusion driven by Coulomb explosion of hydrogen nanodroplets". *Physical Review A*, **83**(4), 043202 (2011).

[151] S. RON, I. LAST, AND J. JORTNER. "Nuclear fusion of deuterons with light nuclei driven by Coulomb explosion of nanodroplets". *Physics of Plasmas*, **19**(11), 112707 (2012).

[152] HUBA, J. D. *NRL Plasma Formulary* (Naval Research Laboratory, Washington, D.C., 2009).

[153] "Electron and nuclear dynamics of molecular clusters in ultraintense laser fields. III. Coulomb explosion of deuterium clusters." *The Journal of chemical physics*, **121**(7), 3030–43 (2004).

[154] H. LI, J. LIU, C. WANG, ET AL. "Coulomb explosion of hydrogen clusters irradiated by an ultrashort intense laser pulse". *Physical Review A*, **74**(2), 023201 (2006).

[155] I. LAST AND J. JORTNER. "Scaling procedure for simulations of extreme ionizations and Coulomb explosion of large clusters". *Physical Review A*, **75**(4), 042507 (2007).

[156] H. WABNITZ, L. BITTNER, A. R. B. DE CASTRO, ET AL. "Multiple ionization of atom clusters by intense soft X-rays from a free-electron laser." *Nature*, **420**(6915), 482–5 (2002).

[157] R. SANTRA AND C. GREENE. "Xenon Clusters in Intense VUV Laser Fields". *Physical Review Letters*, **91**(23), 233401 (2003).

[158] C. SIEDSCHLAG AND J.-M. ROST. "Small Rare-Gas Clusters in Soft X-Ray Pulses". *Physical Review Letters*, **93**(4), 043402 (2004).

[159] C. JUNGREUTHMAYER, L. RAMUNNO, J. ZANGHELLINI, ET AL. "Intense VUV laser cluster interaction in the strong coupling regime". *Journal of Physics B: Atomic, Molecular and Optical Physics*, **38**(16), 3029–3036 (2005).

[160] M. ISLAM, U. SAALMANN, AND J. ROST. "Kinetic energy of ions after Coulomb explosion of clusters induced by an intense laser pulse". *Physical Review A*, **73**(4), 041201 (2006).

[161] G. YUDIN AND M. IVANOV. "Nonadiabatic tunnel ionization: Looking inside a laser cycle". *Physical Review A*, **64**(1), 013409 (2001).